Development of a Rapid Tooling Injection Moulding Process for the Production of Pharmaceutical Oral Solid Dosage Forms with Surface Micro-Features

PhD Thesis

E. Walsh

CMAC

University of Strathclyde

November 13, 2021

This thesis is the result of the author's original research. It has been composed by the author and has not been previously submitted for examination which has led to the award of a degree.

Signed: 

Date: 13/11/2021

For my father, James Anthony Walsh.

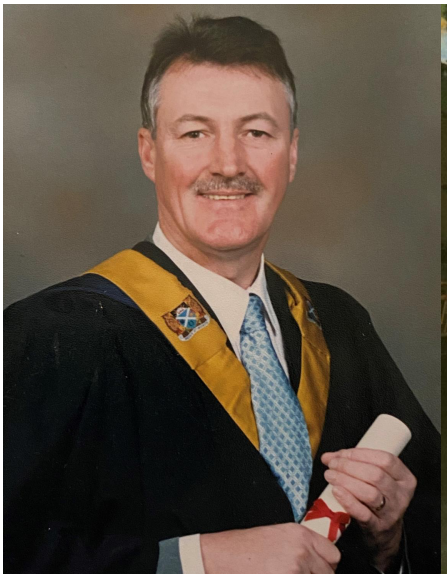

Abstract

The overarching aim of this research was to develop a novel manufacturing process for the production of pharmaceutical dosage forms with accurate and precise surface micro-features.

A novel method for the manufacture of oral solid dosage forms was developed by coupling stereolithography additive manufacture with injection moulding in a process known as Rapid Tooling Injection Moulding (RTIM). An assessment of a number of materials for the stereolithography process was performed, with the essential material properties for success in RTIM determined. From this study, a workflow was generated detailing the critical material properties to use stereolithography in conjunction with injection moulding and how to assess a new material for its suitability.

A number of pharmaceutical polymer-based formulations were trialled in the RTIM process. A better understanding of the limitations of this technique was obtained and a number of oral solid dosage forms comprising surface micro-features were produced. The accuracy and precision of the dosage forms produced was measured, including the surface micro-features. Comparisons are made to similar manufacturing techniques in terms of the accuracy and precision of the dosage forms produced.

Finally, paracetamol loaded polymeric formulations with varying specific surface areas were produced and the resulting drug release profiles captured. The accuracy and precision of the dosage forms produced was measured and the actual specific surface area was calculated. The RTIM process was capable of producing accurate and precise dosage forms in a variety of pharmaceutical polymeric materials. The drug release profiles were able to be modified for some formulations via altering the specific surface area of the tablets indicating that fine-tuning of the drug release profiles can be

obtained using this manufacturing process. From this, a workflow was developed for the alteration of a drug release profile for a given formulation via modification of the specific surface area.

The future applications of the RTIM method described in this research include its use as a direct manufacturing method for low production runs of pharmaceutical tablets. Additionally, the method can be utilised as a development tool to aid in the determination of the required tablet geometry for a desired drug release amongst other applications.

Contents

List of Figures

List of Figures

List of Figures

List of Tables

List of Abbreviations

AM - Additive Manufacture

API - Active Pharmaceutical Ingredient

BCS - Biopharmaceutical Classification System

CAD - Computer Aided Design

FDM - Fused Deposition Modelling

FFF - Fused Filament Fabrication

HDT - Heat Deflection Temperature

HME - Hot Melt Extrusion

IM - Injection Moulding

IPA - Isopropyl Alcohol

LDPE - Low Density Polyethylene

OCT - Optical Coherence Tomography

OSDF - Oral Solid Dosage Form

PAT - Process Analytical Technology

PVT - Pressure-Volume-Temperature

RTIM - Rapid Tooling Injection Moulding

SA - Surface Area

SLA - Stereolithography

SSA - Specific Surface Area

STL - Surface Tesselation Language

μIM - Micro Injection Moulding

Acknowledgements

I would like to thank my supervisor, Dr. Daniel Markl, for his unwavering support and encouragement throughout my PhD journey. Thank you for your patience, understanding and motivation without which this thesis would never have existed. I feel very privileged to have been your first PhD student and will be forever grateful that you took a chance on me. To Prof. Joop ter Horst I want to extend my thanks particularly for always providing such truly valuable feedback on my work. I would also like to thank my research group for reminding me that we are all in this together.

I would like to thank all of my colleagues in CMAC, you truly made my PhD experience a lot less scary and a lot more enjoyable. In particular I want to thank Elke, Moulham, Ecaterina and Alice for helping me with material preparation, test methods and answering endless questions. I really could not have done it without you all! I'd also like to extend my thanks to the PSSRC, being able to collaborate, share my research and learn from others was an invaluable experience for me.

To Natalie, I don't think I can adequately put into words just how thankful I am. You have truly been my rock throughout this journey, being with me every step of the way. We have shared our lows, our highs and knowing that I had someone with me who truly understood how this all felt meant the world to me. Who knows how I would have got this finished without your support, growing trees in our forests and our power hours. You truly are the best PhD partner I could have wished for!

To my family, thank you for your continuous support. You have always encouraged me to follow my dreams and told me that anything is possible. Thank you for helping me to believe in myself.

To Bonnie, thank you for being my writing buddy and for ensuring I take plenty of

breaks. I'm not sure what I would have done without you to keep me company and to always make me laugh!

Finally, to my fiancé Sam. Thank you for sticking by me and always being my biggest supporter. I will be forever grateful for your patience, kindness and understanding but more than anything else for just always being there to listen when things didn't work and then again when they finally did. I love you!

Research Outputs

Peer Reviewed Publications

1. Soundaranathan M., Vivattanaseth P., **Walsh E.**, Pitt K., Johnston B. and Markl D.. Quantification of swelling characteristics of pharmaceutical particles. *International Journal of Pharmaceutics.* **590**, (2020).

2. Maclean, N., **Walsh, E.**, Khadra, I., Mann, J., Williams, H. and Markl, D. Exploring the Performance-Controlling Tablet Disintegration Mechanisms. *International Journal of Pharmaceutics*, **599**, (2021).

3. **Walsh, E.**, ter Horst J. H. and Markl, D. Development of 3D Printed Rapid Tooling for Micro-Injection Moulding. *Chemical Engineering Science*, **235**, (2021).

4. **Walsh, E.**, Prasad E., Halbert G., ter Horst J. H. and Markl, D. Manufacture of Oral Solid Dosage Forms with Micro-structure Features via Rapid Tooling Injection Moulding. *To be determined* (In preparation).

5. **Walsh, E.**, Turner A., Alsuleman M., Prasad E., Maclean N., Halbert, G., ter Horst J. H. and Markl, D. Linking Specific Surface Area to Dissolution for Oral Solid Dosage Forms. *To be determined* (In preparation).

Other Publications

1. Majewski C. and **Walsh E.** Changing Times for UK Additive Manufacturing *UK Manufacturing Review 19/20 - Manufacturing Sectors, Regions, Trailblazers, Technologies.* 193-195 (2019)

Conference Contributions

1. **Walsh E.**, ter Horst J. H. and Markl D. Accuracy Analysis of 3D Printed Injection Moulds for the Manufacturing of Micro-scale Particles. EPSRC CMAC Open Day, 2018. Glasgow, UK.
   Poster Presentation.

2. **Walsh E.**, ter Horst J. H. and Markl D. Developing Engineered Pharmaceutical Polymer-based Particles. 13^{th} Pharmaceutical Solid State Research Cluster Annual Meeting, 2019. Düsseldorf, Germany.
   Oral Presentation.

3. Soundaranathan M., **Walsh E.**, Johnston B. and Markl D. Quantifying the Swelling of Single Particles using a Custom-Built Flow Cell 13^{th} Pharmaceutical Solid State Research Cluster Annual Meeting, 2019. Düsseldorf, Germany.
   Oral Presentation.

4. **Walsh E.**, ter Horst J. H. and Markl D. SLA Additive Manufacture Rapid Tooling in Injection Mouding. EPSRC CMAC Summer School, 2019. Glasgow, UK.
   Poster Presentation.

5. Soundaranathan M., **Walsh E.**, Johnston B. and Markl D. Quantifying the Swelling of Single Particles using a Custom Built Flow Cell. EPSRC CMAC Summer School, 2019. Glasgow, UK.
   Poster Presentation.

6. **Walsh E.**, ter Horst J. H. and Markl D. Utilizing Rapid Tooling to Produce Ideal Particles via Injection Moulding. EPSRC CMAC Summer School, 2019. Glasgow, UK.
   Oral Presentation.

7. **Walsh E.**, ter Horst J. H. and Markl D. Developing Engineered Pharmaceutical Micro-particles. Strathclyde Intiture of Pharmacy and Biomedical Sciences Symposium, 2020. Glasgow, UK.

Poster Presentation.

8. **Walsh E.**, ter Horst J. H. and Markl D. Development of a Structure by Design Pharmaceutical Dosage Form for Controlled Release. EPSRC CMAC Internal Research Day, 2020. Glasgow, UK.
   Poster Presentation.

9. Soundaranathan M., Vivattanaseth, P., **Walsh E.**, Pitt K. and Markl D. Quantifying the Swelling of Single Particles using a Custom-Built Flow Cell. EPSRC CMAC Internal Research Day, 2020. Glasgow, UK.
   Poster Presentation.

10. **Walsh E.**, ter Horst J. H. and Markl D. Manufacturing Tablets with Desired Specific Surface Area. EPSRC CMAC Open Day, 2020. Online.
    Poster Presentation.

11. Soundaranathan M., Vivattanaseth, P.,**Walsh E.**, Pitt K. and Markl D. Quantification of Swelling Characteristics of Pharmaceutical Particles. EPSRC CMAC Open Day, 2020. Online.
    Poster Presentation.

12. **Walsh E.**, ter Horst J. H. and Markl D. Manufacturing Tablets with Desired Specific Surface Area. EPSRC CMAC Open Day, 2020. Online.
    Oral Presentation.

13. **Walsh E.**, ter Horst J. H. and Markl D. Development of 3D Printed Rapid Tooling for Micro-Injection Moulding. 14^{th} Pharmaceutical Solid State Research Cluster Annual Meeting, 2020. Online.
    Oral Presentation.

14. Soundaranathan M., Vivattanaseth P.,**Walsh E.**, Pitt K. and Markl D. Quantification of Single Particle Swelling. 14^{th} Pharmaceutical Solid State Research Cluster Annual Meeting, 2020. Online.
    Oral Presentation.

15. Maclean N., **Walsh E.**, Soundaranathan M., Khadra I., Abbot A., Mead H., Williams H., Mann J. and Markl D. Exploring the Performance and Stability-Controlling Tablet Disintegration Mechanisms. PBP World Meeting, 2021. Online.
    Poster Presentation.

16. **Walsh E.**, Turner. A, Prasad E., Alsuleman M., Halbert G., ter Horst J. and Markl D. Manufacturing Tablets with Desired Specific Surface Area. CMAC Mini Symposia, 2021. Online.
    Poster Presentation.

17. **Walsh E.**, Turner. A, Prasad E., Alsuleman M., Halbert, G., ter Horst J. and Markl D. Manufacturing Tablets with Desired Specific Surface Area. CMAC Mini Symposia, 2021. Online.
    Oral Presentation.

18. **Walsh E.**, Turner. A, Prasad E., Alsuleman M., Halbert, G., ter Horst J. and Markl D. Fine Tuning Dissolution Profiles via Surface Micro-Features. 15th Pharmaceutical Solid State Research Cluster Annual Meeting, 2021. Online.
    Oral Presentation.

Supervisory Roles

1. Kyriakidou L. Hot Melt Extrusion Formulation Development for Injection Moulding. Submitted in partial fulfilment for the degree of Master of Science in Advanced Pharmaceutical Manufacturing, 2019. University of Strathclyde, UK.
   Secondary Supervisor

2. Habashy M. M. Understanding the Link Between Polymer Rheology and Injection Moulding. Submitted in partial fulfilment for the degree of Master of Science in Advanced Pharmaceutical Manufacturing, 2019. University of Strathclyde, UK.
   Secondary Supervisor

3. Alshehri I. Modelling of Release-by-Design Tablets. Submitted in partial fulfilment for the degree of Master of Science in Advanced Pharmaceutical Manufacturing, 2020. University of Strathclyde, UK.
   Secondary Supervisor

Prizes

1. **Walsh E.**, Maclean N. and Markl D. 'Shaping the Future of Medicines'. Images of Research, 2020. University of Strathclyde, UK.
   Highly Commended Photo Entry

2. **Walsh E.**, ter Horst J. H. and Markl D. Development of a Structure by Design Pharmaceutical Dosage Form for Controlled Release. EPSRC CMAC Internal Research Day, 2020. Glasgow, UK.
   1st Place Poster Prize

3. **Walsh E.**, ter Horst J. H. and Markl D. Manufacturing Tablets with Desired Specific Surface Area. EPSRC CMAC Open Day, 2020. Online.
   2nd Place Poster Prize

4. **Walsh E.**, ter Horst J. H. and Markl D. Development of 3D Printed Rapid Tooling for Micro-Injection Moulding. 14th Pharmaceutical Solid State Research Cluster, 2020. Online.
   Highly Commended Oral Presentation

Research Outputs

Chapter 1

Introduction

1.1 General Introduction

Over the last 200 years the world of pharmaceuticals has been totally transformed, moving from botanical concoctions to highly sophisticated and hugely researched chemical and biological entities (Arden et al., 2021). Improvements to both quality of life and life expectancy have been realised in this time, in part due to these advancements in the pharmaceutical industry (Khanna, 2012). Our modern pharmaceutical industry has demonstrated significant and continued growth, with the market growing from a value of approximately $390 billion USD to $1.27 trillion USD from 2001 to 2020 (Mikulic, 2020). This growth is expected to continue, with forecast Compound Annual Growth Rates for the global market of 13.74% between 2020 and 2027 (Mikulic, 2020). Projected growth suggests that in 2024, sales from the USA alone will be in the region of $633 billion USD (Mikulic, 2021). In the UK market, the pharmaceutical industry contributes significantly to the economic wealth having a gross value of £13.7 billion in 2016 (The Association of the British Pharmaceutical Industry, 2021).

It is common for the highest revenue producing drugs to be approved for use in multiple chronic conditions or cancers (Mikulic, 2020). Oncologics accounted for approximately $100 billion USD in 2018, making them the leading therapeutic class in terms of sales revenue. Following this are analgesics and pain therapy medicines and then anti-diabetics (Mikulic, 2020). In addition to the revenue provided to the economy

from the sales of pharmaceuticals, the financial investment of the industry in research and development (R&D) is also significant, with £115 billion each year being spent on such activities (The Association of the British Pharmaceutical Industry, 2021). Compared to any other industry, pharmaceuticals are more dependent on R&D with some companies investing approximately 20% of their sales directly back into R&D (Mikulic, 2017). Some examples of this heavy investment can be seen by the likes of AstraZeneca who in 2020 invested $133 million USD in the expansion of their manufacturing site in Australia (Grand View Research, 2020).

While the continued growth within the pharmaceutical industry can be easily captured by looking at these financial outputs, the evolution of the industry cannot. Compared to other fields where manufacturing plays a critical role, the pharmaceutical industry is lagging behind (Politis and Rekkas, 2011). This is in part due to the highly regulated nature of the industry and the need for monitoring to ensure reproducible quality (Stegemann, 2016). Pharmaceutical manufacture has traditionally been based on batch-production, where a number of individual unit operations are performed in series with intermediate product testing. This approach to manufacturing was effective for high volume production, and typically companies would have specialised large-scale facilities for such manufacturing processes (Stegemann, 2016). These batch processes carry with them a high degree of operational complexity, and a high throughput is required to justify the operation of such large and expensive equipment. Alongside this, this batch approach does not offer a great deal of flexibility, with limitations on how such systems can be modified (Bähner and Huusom, 2019). The traditional approach to manufacturing for pharmaceuticals is not bomb-proof either with costs associated with manufacturing being approximately double that of R&D. On top of this, delays of up to 2 years in getting drug products to the market associated with manufacturing challenges are not uncommon and have serious knock-on effects on the total revenue that the drug can produce while under patent (Politis and Rekkas, 2011). Manufacturing defects also accounted for 75% of all drug product recalls in the USA between 2000 and 2004 which clearly demonstrates that these processes are not without issue (Politis and Rekkas, 2011). Advances in manufacturing technologies provide a basis for the

shift from this traditional, large-scale batch production for high volume pharmaceutics to micro-batch, highly flexible manufacturing facilities which are needed as we shift towards the future landscape of medicines. The key drivers for this shift are improvements in quality, reduction in waste and increased flexibility and agility in the manufacturing approach (Politis and Rekkas, 2011). In similar manufacturing industries such as the chemical and petrochemical industries, continuous production processes are favoured over batch production. While these industries do not face the same degree of regulation and monitoring, this is a strong indicator of the economic superiority that arises from a step away from traditional batch production (Bähner and Huusom, 2019).

Within the pharmaceutical market, oral solid dosage forms, including tablets and capsules, are the preferred drug delivery method for the majority of patients. As a result, they hold the vast majority of the market share at 80% (Eggenreich et al., 2016). Of this, tablets alone accounted for 25.4% of the market share in 2019 (Grand View Research, 2020), with the popularity for the oral administration route set to continue. This dominance is in part due to the affordability, ease of manufacture and widespread patient acceptance for oral dosage forms (Grand View Research, 2020). Enhancements to drug delivery systems such as modified release formulations and targeted drug delivery systems have further expanded the market occupancy for oral administration (Grand View Research, 2020).

1.2 Challenges for the Pharmaceutical Industry

Janet Woodcock from the FDA's Centre for Drug Evaluation and Research views the future of the pharmaceutical industry as being 'a maximally efficient, agile, flexible, manufacturing sector' (Department of Health and Human Services and Administration, 2007). This outlook highlights some of the critical parameters which will be necessary for the current pharmaceutical industry to be able to pivot in response to the current challenges they face.

While innovation has always been at the core of the pharmaceutical industry, reductions in productivity, increasing costs for R&D and a diminishing drug pipeline cannot be ignored (Khanna, 2012). This is in part due to a shift away from large scale block-

buster drugs and towards more specialised medicines (Khanna, 2012). Additionally, the costs associated with drug development are rising. It is estimated that the expenditure associated with taking a new drug from conceptualisation to the market is now in the region of $2 million USD (Khanna, 2012). The previous approach that the industry applied to R&D is no longer suitable, with the discovery of new blockbuster drugs few and far between, a focus on the smaller market size drugs must be adopted. This transition from traditional large scale batch production to low volume, micro-batch production has resulted in a demand for novel manufacturing technologies (Kapoor et al., 2021). Many of these novel and emerging technologies are inherently more flexible than the traditional manufacuting techniques and therefore offer greater agility (Kapoor et al., 2021). A greater degree of flexibility in an approach to manufacturing would provide both economic benefits and be better able to serve patient needs (Kapoor et al., 2021).

A more agile approach to manufacture will produce a better equipped industry to adapt to the changing frontier of health care. We live in a time where our population is both ageing and growing. The census estimates that 12.9% of the US population were aged over 65 in 2009, with evidence that this number is set to continue growing (Khanna, 2012). This is further supported by looking at UK census data, which details that in 2019, 18.5% of the population was over 65, with this predicted to grow to 23.9% by 2039 (Office For National Statistics, 2021). This evolving patient demographic puts changing demands on the pharmaceutical industry. In addition to this, multi-morbidity and poly-pharmacy are becoming a part of everyday life now for much of the population (Florence and Lee, 2011; Trivedi et al., 2018). In response to this changing demographic, personalised medicine is on the rise, with current on the market medicines already demonstrating clearly the need for a more personalised approach. Codeine for example was found to be the most commonly prescribed opiate in a recent study in the USA, with there having been a 5-fold increase in the rate of prescription from 2006 - 2017 (Jani et al., 2020). The number of patients receiving such a prescription was found to be 2,456 in every 10,000 patients per year (Jani et al., 2020). A portion of the population are unable to convert codeine into the active drug form in their bodies due to genomic variations (Lurcott, 1999). For these individuals, codeine

offers no analgesia and it is not the only drug which fails to be effective due to the genomics of the patient (Lurcott, 1999). By ignoring this clear need for personalised medicines, we are failing these individuals. While it is clear from this example that personalised medicine requires increased use of biomarkers and diagnostics (Harvey et al., 2012), pharmaceutical manufacture also has a role to play (Florence and Lee, 2011). While there are well-documented challenges with the prescribing of opiates, other drug classes also demonstrate this need for personalisation (Jani et al., 2020). Cardiovascular disease is the leading global killer and multiple medications are typically prescribed in conjunction (Lloyd-Jones et al., 2006). This combination of medications typically posses different formulatory requirements, with differing chemistries and drug release requirements. Personalised medicine can offer a benefit in these situations through the creation of 'Polypills' - where multiple active pharmaceutical ingredients can be carefully co-formulated (Khaled et al., 2015). Development of more agile manufacturing platforms will be key for the implementation of personalised medicines. The ability to design and develop effective, reproducible manufacturing processes will become even more critical as batch sizes decrease and complexity of dosing and physical structure increases (Sarkis et al., 2021). Oral solid dosage forms are manufactured on mass with distinct pre-determined drug loadings. These drug loadings are typically selected during the early stages of clinical trials and are chosen based on demonstrating a therapeutic effect on the highest proportion of the trialled population (Alomari et al., 2015; Cohen, 2001). This does not always produce available dosages which are suitable for all, with fluoxetine demonstrating this fact. A 20 mg dose was selected for this drug as it demonstrated efficacy on 64% of the target population, while the lower 5 mg dose was only found to be therapeutic on 54% (Cohen, 2001). What was not considered in this was that for that 54% who found benefits with the lower dose, fewer side effects were reported and the drop-out rates were lower than those for the higher dose (Cohen, 2001). Limitations on the manufacturing of dosages for clinical trials leads to a 'one-size-fits-all' approach to dosing, which is not always in the best interests of the patient (Trivedi et al., 2018; Prendergast and Burdick, 2020). Flexibility in manufacture would allow for a wider range of dosages to be produced for clinical trials in a more

time and cost efficient manner. This would not only reduce the lead time and expenses associated with this phase of clinical trials, but could also result in a more inclusive understanding of therapeutic dosages for a given drug (Trivedi et al., 2018). Current work arounds for unsuitable tablet dosages are to split tablets, however this negatively impacts the integrity of the medication and can result in vastly different drug release profiles from the designed drug delivery. This difference in drug release can result in premature drug release, or ineffective release, both delivering sub-optimal therapeutic effect for the patient (Trivedi et al., 2018). Personalisation for dose becomes even more important when we consider paediatric and geriatric patients where physiological and metabolic changes are associated with ageing (Alomari et al., 2015). Knowing that our patient demographic is evolving, it is clear why development in precise and personalised dosing is required. This need for personalisation demonstrates a need to shift from mass manufacture to mass customisation - with the patient at the core (Siiskonen et al., 2020).

Development of a drug delivery system which is able to deliver a fine-tuned approach to drug release will help pave the way towards the potential of personalised and precision medicines (Bruschi, 2015). By having a deliberate, design-based approach to drug release a number of benefits for patients can be unlocked (Bruschi, 2015). Work has already begun in the design of precision medicines to deliver a desired drug release profile, demonstrating the importance of the physical structure of the dosage form (Siepmann et al., 2000; Goyanes et al., 2015a).

In the last 10 years, this vision of a more patient-centric model of health care and therefore of drug product development has gained substantial notice (Jamróz et al., 2018). In order to take the steps necessary to further evolve our approach to drug product development, a number of technologies will play a critical role including pharmacogenomics, pharmacometabolomics and therapeutically tailored medicines (Trivedi et al., 2018). At the forefront of therapeutically tailored medicines, novel manufacturing technologies can provide a route for the design of precision medicines, flexible dosing and the ability to design the dosage with the patient in mind (Trivedi et al., 2018). While this shift to a more personalised approach is still considered to be fairly

novel, backing by high ranking officials such as former president of the USA Barack Obama in his Precision Medicines Initiative have affirmed its right of place. Estimates suggest that the market for precision medicines alone is set to reach $87 billion USD by 2023 (Prendergast and Burdick, 2020), further supporting the benefits that can come from this move. The transition away from large batch production to small batch, or even continuous, manufacturing is set to be the next major global challenge for the pharmaceutical industry (Walker and Albadarin, 2018). One of the main benefits to a continuous process is the ability to employ real-time release testing via the employment of process analytical technologies to reduce the total time of manufacture and quality assurance. Micro-batch production allows for a far more economical production process for formulations where much smaller quantities are required. This offers benefits both in terms of cost savings, but also to the environment by using smaller, less energetically expensive equipment and reducing waste. While these alternative approaches to large scale batch manufacture differ greatly in their approach, they will both form a critical part of the future manufacturing landscape. Micro-batch production will be better suited to smaller, more precise manufacture where continuous manufacture will be able to produce larger batch sizes in a far more economical and environmentally friendly manner.

1.3 Micro-Batch Pharmaceutical Manufacture

In order to facilitate this move, the current manufacturing toolset needs to evolve. Manufacturing of these novel drug delivery systems with the current pharmaceutical technologies is challenging. Despite innovation being a cornerstone of the pharmaceutical industry, innovation in the manufacturing sector has not been a strength. One of the main barriers to development in this area has been the regulatory framework, which is essential for pharmaceuticals. In recent years, partly due to the increased pressures for the industry to evolve, interest in manufacturing development has been on the rise. One of the key drivers for this is the need for a greater degree of flexibility (Rantanen and Khinast, 2015).

A new approach to pharmaceutical development, where the design of a dosage form

is driven by the desired application and being best suited to the patients, will require new thinking and approaches. While some approaches that are used in much larger scale manufacture can be down-scaled, the economic and sustainability implications of this cannot be ignored. Additionally, a process which is successful at a large scale may not be successful at a lower scale without alterations to the manufacturing process so it is often not as simple as just making less. The basis of these processes are typically not well understood in comparison to other industrial processes, they lack agility and changes to manufacturing scale are challenging (Lee et al., 2015). Recent advances in technology offer new manufacturing avenues for the pharmaceutical industry to explore, promising greater agility alongside economic and sustainability profits (Lee et al., 2015).

1.3.1 Traditional Manufacture Techniques

Some examples of more traditional manufacture techniques would be tableting and capsule filling, which are both used in large scale batch production and can also be utilised in continuous processes. While tableting is the dominant form for oral solid dosage forms, using this technique for the production of micro-batches is not as simple as just down-scaling. Tableting is a complex process which typically involves formulations with many excipients. Some of these excipients are present solely to aid in the compaction process, where the resultant strength of the compacted tablet is critical (Wagner et al., 2018). In an ideal world, a formulation that is to be made into tablets would undergo direct compression however this is not always possible. Additional pre-processing steps are frequently required such as wet or dry granulation (Markl et al., 2018b). These additional steps mean that a number of processes need to be reconfigured for a reduction in manufacture scale, further increasing the complexity of this manoeuvre. Capsule filling is often used for formulations which cannot be processed via compaction as it is able to work with formulations with poor flowability (Wagner et al., 2018). These capsule formulations are typically less complicated and make the inclusion of drugs and excipients which are difficult to process via compaction far simpler. Capsule filling as a process is more time-consuming than tableting and as such a lower throughput and a higher cost is to be expected. In addition, capsules typically have a shorter shelf-life

compared to tablets. The use of either of these techniques on a micro-scale is possible, but there are significant economic and sustainability costs associated with this and it will require investment in new, appropriately scaled equipment to ensure quality standards are maintained.

While both of these techniques have truly earned their place in the manufacturing landscape, they do not offer the degree of flexibility that will be required for the medicines of the future. For example, neither technique is particularly well suited for the fine-tuning of drug release for example, due to a lack of control of the microstructure within the dosage form. This creates a space in the landscape for more novel manufacturing techniques which can provide a greater control of the both the internal and external geometry of the dosage form amongst other applications.

1.3.2 Additive Manufacture

Introduction

In recent years, the implementation of more novel manufacturing technologies for the production of pharmaceutical tablets is growing. One such technique is additive manufacturing (AM). AM is primarily a rapid prototyping technology (Prasad and Smyth, 2016), and may be more recognisable by its subset 3D printing, which has been a growing technology in recent years. In the literature, AM is additionally referred to by a number of synonyms including, but not limited to, rapid prototyping, layered manufacturing, solid freeform fabrication and 3D fabbing however additive manufacturing is typically the preferred term for engineers (Ligon et al., 2017). AM has been defined by the international standard organization as being a generalised term covering: 'technologies that based on a geometrical representation creates physical objects by successive addition of material' (International Standards Organisation, 2015). The building of the object is achieved by depositing material in a layer-by-layer basis, and this is what distinguishes AM from other manufacturing technologies. AM has been gaining attention in the pharmaceutical field due to the opportunities to make tailor-made and personalised medicines (Jamróz et al., 2018).

To create an object via AM, a digital design of the desired object must be created.

This design, referred to as a computer aided design (CAD), can then be converted into a surface tessellation language (STL) file (Wang et al., 2017). An STL file describes the triangulated surface geometry of a three-dimensional object (Jamróz et al., 2017). This STL file is then used to produce the slicing required to build the object which can be deciphered by the 3D printer to allow it to produce the object designed. Some AM techniques require the addition of supports for the designed object, particularly for any areas of overhang in the design. Often there is software associated with the printer which will generate any necessary supports for the design.

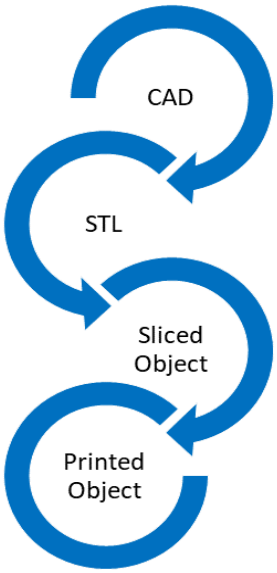

Figure 1.1: Flowchart demonstrating the process to produce an object via additive manufacturing.

AM evolved from the description of a layer-by-layer solidification of powder through the use of a high energy beam by Pierre A. L. Ciraud in the early 1970s (Jamróz et al., 2018). Patents covering AM began to appear in the early 1980s, with the first AM technology commercialised by Chuck Hull (Jamróz et al., 2018). Despite the relatively early commercialisation of this technology, the rapid and significant uptake of patents (predominantly by Massachusetts Institute of Technology) meant that the technology

was inaccessible by many for a period of time. Interest in AM has been rising over the last 30 years, with significant growth in the last 5-10 years. Many patents covering the methods of AM expired between 2013 and 2015, presenting the potential for more accessible AM (Ligon et al., 2017). It was not until 2009 that the first desktop 3D printers were readily available for purchase and use, making this technology accessible not only to other researchers, but to industry and also to the public (Finnes, 2015).

Accessibility of the technology has only improved since the expiry of these patents, with desktop style 3D printers now being commercially available for less than $500 USD (Ligon et al., 2017). Despite the skyrocketing interest and ever-increasing accessibility of the technology, it is still considered by some to be a rapid prototyping technology only and not a scalable manufacturing technique (Prasad and Smyth, 2016).

However, data suggests that despite concerns that AM may not be a scalable manufacturing technique, industrial belief in the technology is present (Ligon et al., 2017). One big driver for the adoption of AM is clear in the pharmaceutical industry, where the production of an oral solid dosage form (tablet) is a multi-step process. Utilising AM allows the significant reduction in production steps as illustrated in Figure 1.2. This reduction in processing steps materialises to being a massive cost saving for the companies who choose to employ AM as a manufacturing technology. In addition to this, benefits in terms of sustainability can also be realised due to improved resource efficiency.

While the principle of AM is to build an object in a layer-by-layer fashion, this can be achieved through a number of different methods. The first commercialised technology in AM was stereolithography (SLA) (Liaw and Guvendiren, 2017). Since then, a number of different technologies have been developed which all utilise different methods for adding and solidifying the consecutive layers to produce the designed object. Due to the increasing number of methods within AM, a number of terms were defined the ASTM International Committee F42 on Additive Manufacturing Technology in 2009. These terms were intended to distinguish AM from both formative and subtractive manufacture and also to classify the different AM processes (Ligon et al., 2017). This can be observed in Figure 1.3.

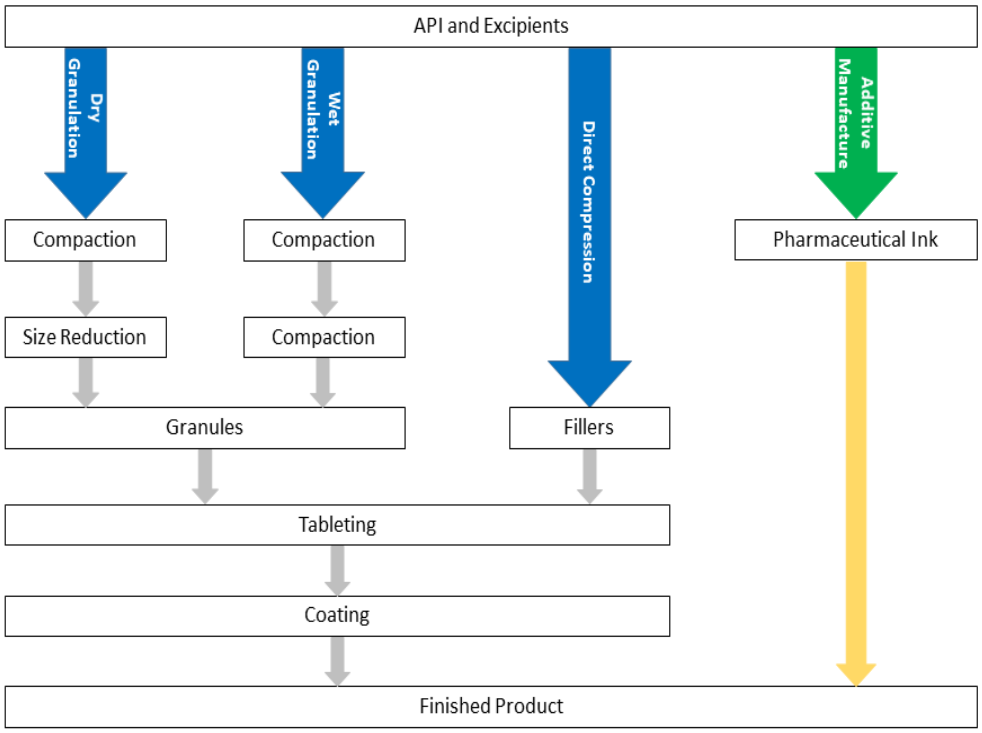

Figure 1.2: Schematic detailing steps of common pharmaceutical manufacturing processes and AM (adapted from Alhnan et al. (2016)).

An alternative grouping is to organise the AM technologies by their mechanism of action, as depicted in Figure 1.4.

Although this introduction aims to provide a general overview of AM technologies, the rapid adoption of this technology and its ever-growing interest have resulted in a massive increase in the literature published on the topic. As a result, this introduction will cover an overview of the AM technique which is most commonly applied for the direct fabrication of objects. Additionally, due to the nature of this research, a focus on AM for pharmaceutical applications is to be expected. For readers seeking additional detail on AM, the book entitled Additive Manufacturing Technologies (Rashid, 2018) is recommended. The reader interested in materials associated with AM is referred to the articles by Ligon et al. (2017) and Ngo et al. (2018).

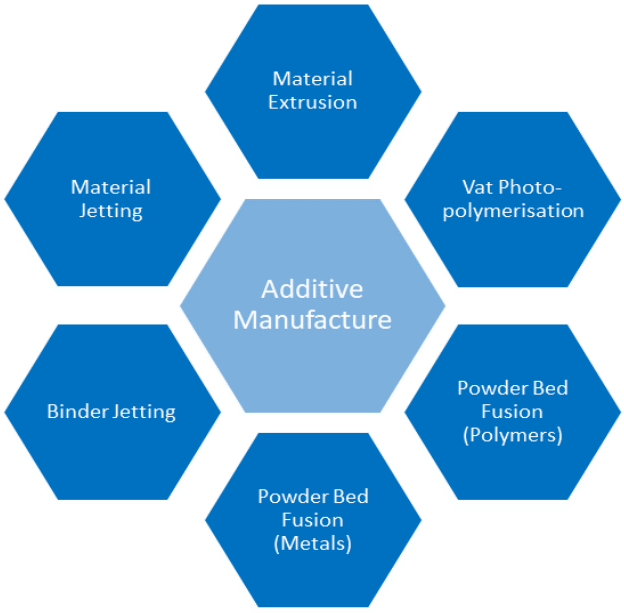

Figure 1.3: A selection of the classified AM processes according to the ASTM International Committee F42 on Additive Manufacturing Technology.

Material Extrusion Additive Manufacture

Of the various AM techniques, material extrusion is the most popular technique for pharmaceutical applications. Within the classification of material extrusion there are a number of sub-categories. Whilst all of these sub-categories follow the same basic principle of extrusion, they work through different means or use different material classes. From the material extrusion classification, fused deposition modelling (FDM) is by far the most common and widely used technique (Ngo et al., 2018). Other notable techniques which employ the principle of material extrusion are 3D dispensing and direct ink writing. 3D Dispensing operates via an almost identical process as FDM, however it is highly versatile and has a significantly wider range of compatible materials. 3D Dispensing is able to print with polymers, ceramics and even metals (Ligon et al., 2017). Direct ink writing is a notable technique mainly for its application in bio-printing (Liaw and Guvendiren, 2017). Other techniques which fall under the umbrella of material extrusion include fluid dosing and deposition and 3D plotting (Ligon et al., 2017). In this introduction the method of focus for material extrusion is FDM as it is

Figure 1.4: A selection of the AM techniques, with an example for each, adapted from (Jamróz et al., 2018).

the most common technique for pharmaceutical applications.

FDM is also referred to in the literature as fused filament fabrication (FFF), with both terminologies being synonymous (Ligon et al., 2017). FDM creates objects by extruding a filament of a molten or semi-molten thermoplastic polymer (Ngo et al., 2018), pastes, polymer solutions or polymer dispersions (Ligon et al., 2017). It is not only the most common material extrusion technique, but it is also the most common technique from all of the AM subtypes. Currently this technology accounts for the largest number of 3D printers globally (Varotsis, 2019).

The objects produced by FDM are made from the successive layering of a material softened by heating (Ngo et al., 2018). A semi-liquid material is extruded through a moveable nozzle or orifice, acting as the print head, which can be pneumatically controlled (Ligon et al., 2017). This nozzle extrudes the thermoplastic material to produce the two dimensional slice of the object by moving in both the $x-$ and $y-$ directions (Ligon et al., 2017). The material cools and solidifies post-extrusion. The

print head can then move up to create the next layer, or the build platform will move down (Ligon et al., 2017).

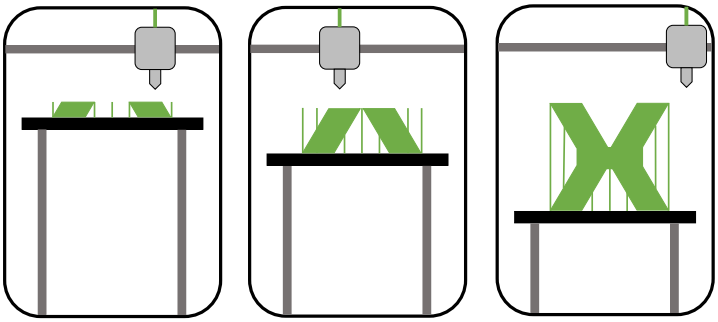

Figure 1.5: Depiction of material extrusion based additive manufacture.

The vast majority of commercial FDM printers allow many of the printing parameters to be adjusted to suit the material being used or the geometry of the object being printed. Typically, the temperature of the nozzle can be controlled, and in some cases the build platform itself can be temperature controlled also. The height of the layers printed, and the speed of the fans used to cool the extruded material can also be adjusted in many FDM printers. These parameters will have a significant influence on the success of a print and ultimately the quality of the object produced. Hence, a printer which allows control of these parameters will be able to be used with a much wider variety of materials and for more complex object geometries (Varotsis, 2019). The processing temperature selected when printing via FDM is usually 1°C higher than the solidification temperature of the thermoplastic material being extruded (Nale and Kalbande, 2016), although it may be higher than this to achieve a preferable melt rheology. A number of FDM printers have now been developed with capability to print from multiple print heads (Ligon et al., 2017). This opens up the possibility of printing with multiple materials, which has been utilised to produce objects with one material, and the supporting material for that object in another material which is soluble in a solvent for example. This greatly improves the process of removing the support material from the completed object and provides an overall superior finish to the printed object.

Resolution is a key variable between AM techniques that massively impacts the quality of the object printed (Ngo et al., 2018). When quoting the resolution for a 3D printer, particularly from the vendor, the $z-$resolution is archetypally used. The $z-$resolution is more easily understood to be the layer height, or the step-change between layers on the $z-$axis of the printer. While this value is often quoted as the sole resolution indicator for a 3D printer, the $x-$ and $y-$ axes also play a role in the overall resolution of the printer. In the case of FDM, the diameter of the filament will directly impact the $x-y-$resolution. FDM printers typically possess z-resolutions in the 50-400 μm range (Rashid, 2018; Varotsis, 2019). A lower number in the resolution will typically result in a better quality finish on the printed object. As the $z-$resolution represents the thickness of each layer, a smaller number for the $z-$resolution results in more layers being printed to make the object. This typically results in a smoother finish, particularly in objects which are curved. The caveat to this is that the smaller layer height results in a significantly longer print time. For example, for two identical objects printed at a resolution of 50 μm and 200 μm, the 50 μm object would take 4 times longer to produce.

While the semi-liquid state of the thermoplastic filament is truly at the core of FDM, it is also the reason behind one of the major vulnerabilities of the objects printed by this method. The cooling and solidifying of the thermoplastic are wholly necessary for the success of this technique, but this inevitably results in some degree of contraction from the material. The issue arises when different parts of the printed layer experience different cooling rates. This differential cooling causes layers to effectively pull up the layer underneath, producing objects that are dimensionally warped (Varotsis, 2019). The extent of object warpage can be minimised through intelligent digital design of the object, avoiding large flat portions and also thin protruding components. Filament material is also important here, with polymers having a higher glass transition temperature tending to be more vulnerable (Varotsis, 2019). Due to the solidification of the thermoplastic material of one layer before the extrusion of the successive layer, interlayer binding is minimal. This results in anisotropic objects, with the strength of the $x-y-$axes being significantly stronger than the $z-$axis. This is thought to be

the main cause of the mechanical weakness associated with object printed via FDM (Ngo et al., 2018). For this reason, it is important to consider the orientation that the object is printed in to optimise the strength of the object for its particular application. Other intrinsic issues with objects printed via this technique are a high degree of surface roughness, due to the resolution limitations of the layer height, and high porosity within the object produced (Ligon et al., 2017).

One of the major benefits of FDM is its cost-effectiveness, with desktop printers being commercially available for less than £350 and minimal material costs (for commodity materials) FDM has earned its place as the most popular and accessible form of AM. Its ability to quickly produce low-cost plastic objects puts traditional time-scales for rapid prototyping to shame. FDM is suitable for use with an extensive list of materials, making it suitable to almost every application. The intrinsic anisotropy of the objects produced should be considered when assessing the suitability of this technique for the desired application. Additionally, FDM does require a careful balance of filament properties, polymer melt rheology and processing parameters and the success of this technique is closely related to the complexity of the CAD (Ligon et al., 2017).

Literature has documented trials of FDM being used in the production of pharmaceutical dosage forms and devices, and with the first 3D printed dosage form receiving Food and Drug Administration (FDA) approval being produced there are signs that the landscape of pharmaceutical manufacture is evolving. The release and approval of this drug, Spiritam (levetiracetam), demonstrates the potential to overcome challenges with approval for drug manufacturing via novel techniques (Vithani et al., 2019). Alongside this, there have been a growing number of publications demonstrating the use of FDM for pharmaceutical applications including the production of tablets and devices (Goyanes et al., 2017; Melocchi et al., 2015; Kollamaram et al., 2018; Goyanes et al., 2015b; Sadia et al., 2016; Genina et al., 2016; Skowyra et al., 2015; Pietrzak et al., 2015; Beck et al., 2017).

1.3.3 Injection Moulding

Introduction

A further technology which has been implemented for the small scale production of pharmaceuticals is injection moulding (IM). IM is a widely applied manufacturing technique in the plastics industry (Bartlett, 2017; Quinten et al., 2009b). IM is the primary technique employed for the production of the majority of the plastic products in the world currently (Formlabs, 2016a). This manufacturing technique is employed on a massive scale to produce complex objects from thermoplastics. The technique relies on a combination of heat and pressure to fill a mould cavity with the thermoplastic material (Quinten et al., 2009b). The popularity of IM is easily comprehensible due to its versatility and time efficiency (Zema et al., 2012). During the IM process, the thermoplastic material is softened by heating. This softened material is then injected into a mould cavity under high pressure. The thermoplastic material then cools in the mould cavity causing it to solidify in the specific shape of the mould (Quinten et al., 2009c; Zema et al., 2012). A simplified schematic of the IM process can be seen in Figure 1.6.

IM has been largely used in the manufacture of packaging for both the pharmaceutical and the cosmetics industries. More recently it has been utilised for the production of biomedical devices such as scaffolds (Zema et al., 2012). IM was first employed as a pharmaceutical manufacturing technique in 1964 by Speiser for the creation of oral solid dosage forms (Quinten et al., 2009b; Zema et al., 2012). With IM being a highly versatile technique, it opens up a number of opportunities to produce oral solid dosage forms of defined shape or size (Zema et al., 2012). An additional benefit of using IM for the manufacture of pharmaceuticals is that the processing conditions, being high pressure and temperature, help to reduce microbial contamination (Zema et al., 2012). Additionally, interactions between the drug molecule and the polymer can be achieved leading to solid solutions or solid dispersions (Zema et al., 2012). These solid dispersions or solid solutions can increase the dissolution of the drug and can aid the bioavailability (Quinten et al., 2009b).

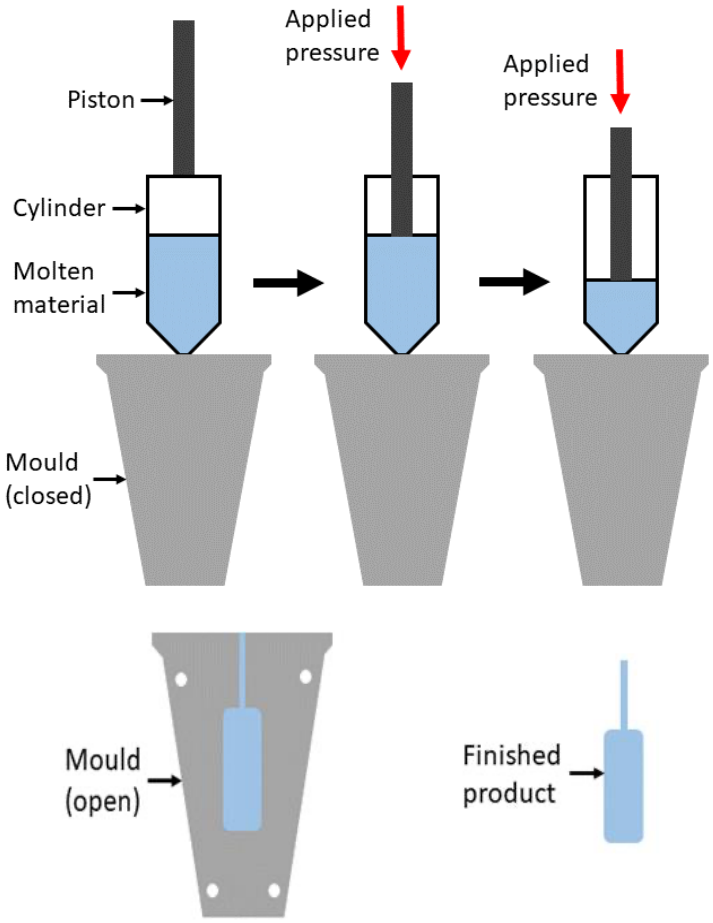

Figure 1.6: Schematic of the Injection Moulding process.

Micro-Injection Moulding

IM as a manufacturing technique is often split into a number of different sub-categories. These sub-categories relate to the designed dimensions of the object being produced and any significant process alterations. The traditional macro IM process is used to produce objects where all of the designed dimensions are larger than the micro-scale. Micro-IM (μIM) is used when an object contains either a mass of a few milligrams, a feature with dimensions in the micrometre scale or objects where dimensional tolerances are in the micrometre range (but there is no dimensional limit) (Giboz et al., 2007; Packianather et al., 2015).

The μIM process was first employed over 30 years ago and its popularity has con-

tinued to increase due to the growing importance of microsystem technologies (Annicchiarico and Alcock, 2014; Zhao et al., 2003). While it is possible to make small plastic components via the traditional IM approach, the object rejection rate is typically high at between 30-50%. Moving to a specific μIM process reduces this rejection rate (Zhao et al., 2003). The basic process and the factors which affect it are universal across all forms of IM, however the impact of each factor varies significantly as you move to different sub-categories of IM. Moving from macro-IM to μIM is not as simple as scaling down the process, each part of the process requires reassessment (Giboz et al., 2007). In μIM moulds, the aspect ratio (which is defined as being the thickness over the lateral dimension) is typically greater than 1. As a result, the thickness of the object being produced is not insignificant with respect to the other designed dimensions. This brings in an additional complication not seen in macro-IM (Giboz et al., 2007). Heckele and Schomburg (2004) suggested that macro-IM processes can be adapted to be effective μIM processes using a variotherm process (Heckele and Schomburg, 2004).

Process Parameters

The process and materials utilised must be completely understood, and the process must be optimised if repeatable, high-quality parts are to be produced in any IM process (Tosello et al., 2010). There are over 200 process parameters that need to be established and controlled (Eggenreich et al., 2016). The process parameters considered to be of the highest importance or of having the highest influence over the IM process as a whole are generally agreed as being the mould temperature, cylinder or melt temperature, injection pressure, injection speed, injection time and the holding pressure and time (Giboz et al., 2007; Mohan et al., 2017; Packianather et al., 2015; Sha et al., 2007). These parameters are considered to have the highest impact on the melt flow properties of the injected material (Packianather et al., 2015).

While the process parameters between macro-IM and μIM are the same, some of these process parameters are of even more critical importance in μIM (Packianather et al., 2015). The mould temperature tends to be significantly different when using the same injection material in the macro-IM and μIM techniques (Giboz et al., 2007).

Setting the cylinder and mould temperatures high improves the melt flow properties, particularly in micro-cavities (Zhang and Gilchrist, 2012). This can however increase the likelihood of defects appearing on the moulded objects (Packianather et al., 2015). Using higher temperatures can also lead to degradation of the polymer being injected and of any drug embedded into that polymer. The polymer/drug will experience very high shear rates and also a significant thermal gradient during the μIM process (Zhang and Gilchrist, 2012). Higher temperatures also require a significantly longer cooling time, which increases the total time required to complete one injection cycle (Sha et al., 2007). The use of higher pressures can also lead to degradation of both the polymer and the drug (Packianather et al., 2015).

In μIM, the high aspect ratio results in accelerated cooling of the injection material (Giboz et al., 2007; Zhang and Gilchrist, 2012). This causes issues with incomplete filling of the mould cavity due to the viscosity of the injection material increasing as the material cools (Fischer et al., 2017). This is minimised by implementing a higher mould temperature or by increasing the cylinder temperature to extend the time that the material is in the molten state (Giboz et al., 2007). One method for minimising the issues caused by the rapid cooling is to set the mould temperature higher than the crystallisation temperature of the thermoplastic material being injected. Dynamic tempering can be implemented to improve this further, which involves the material in the mould cavity being held isothermally to maximise cavity filling (Fischer et al., 2017). For μIM, the mould temperature is considered to be a major factor in the success of the injection and it allows for the reduction of both the injection time and the injection pressure (Giboz et al., 2007).

A high injection speed is typically favoured in μIM as it is thought to increase mould filling via decreasing the viscosity of the injection material (Giboz et al., 2007). The rheological behaviour of the molten or softened injection polymer will be directly affected by any changes to the shear flow, elongation flow and also to the temperature (Mohan et al., 2017). All of these factors impact the materials viscosity and the unwinding relaxation behaviour of the polymers (Mohan et al., 2017). There are differences in which process parameters are reported as being the most important for

μIM. Some suggest that the melt temperature, mould temperature and the injection speed have the largest impact on the filling of micro-cavities (Lucchetta et al., 2014; Sha et al., 2007). It is reported by Wimberger-Friedl (2000) and Shen and Wu (2002); Shen et al. (2002) that having a mould temperature above the T_g of the injection material is the most important factor for μIM. Whereas Sha et al. (2007) suggests that other researchers have found the injection speed, cylinder temperature and holding pressure to be more influential than the mould temperature (Sha et al., 2007). This disagreement on which factors have the most impact on μIM has likely arisen due to the experiments being carried out with different injection moulding machines, different mould geometries and with different injection materials. Generally, it is accepted that an increase in mould temperature will increase the fill of micro-cavities by extending the time that the material remains molten and therefore mobile (Valette et al., 2017). Ultimately, the success of μIM is dependent on these process parameters but also the injection material, the mould geometry and the material that the mould is made of (Valette et al., 2017). Optimisation of the processing parameters is considered to be one of the most important steps in IM (Mohan et al., 2017).

Materials for Injection Moulding

Most commonly, the materials that are used in IM are thermoplastics. In the pharmaceutical field, thermoplastic polymer carriers can be combined with drug molecules and these can be used in the IM process. A thermoplastic material is a polymer which, when heated, undergoes a thermal transition into a molten or softened state (Zema et al., 2012). The thermal transition that the polymer undergoes will differ depending on whether the polymer is amorphous or crystalline in nature. Amorphous polymers soften upon sufficient application of heat and exhibit poor lubricity. Crystalline polymers will melt upon sufficient application of heat and exhibit good lubricity (Zema et al., 2012). The characteristics of the objects moulded from these polymers also differ. Objects moulded from amorphous polymer will typically experience limited and isotropic shrinkage, where those moulded from crystalline polymers experience significant and anisotropic shrinkage. Generally, objects from amorphous materials have a

higher impact strength and are typically translucent, where with a crystalline material the impact strength is low and an opaque appearance is expected however there are exceptions to these generalisations(Zema et al., 2012).

Thermoplastics are a particularly large collection of materials which all have unique thermal, mechanical and electrical characteristics and therefore they do not all behave identically (Giboz et al., 2007; Heckele and Schomburg, 2004). The differing material properties of these thermoplastic materials therefore need to be understood to utilise them effectively in an IM process. Pressure-volume-temperature (PVT) behaviour, polymer structure and morphology and material crystallinity are all material properties that will have a major impact on the IM process (Annicchiarico and Alcock, 2014). The PVT behaviour of the thermoplastic is intrinsically linked to the shrinkage behaviour of the material. There is a marked difference in the PVT behaviour of amorphous and crystalline polymers which explains the differences observed in shrinkage occurrence in moulded objects (Annicchiarico and Alcock, 2014). When in the melt condition, both amorphous and crystalline polymers demonstrate a linear dependency of the specific volume from the temperature. A difference however is observed when the materials are in the solid state. Due to the crystallinity in crystalline or semi-crystalline polymers, the specific volume decreases at an exponential rate relative to decreasing temperature. Amorphous materials do not demonstrate any change in behaviour moving from the melt state to the solid state, retaining the linear dependency of specific volume and temperature (Annicchiarico and Alcock, 2014). Shrinkage can also be impacted by the morphology of the polymeric material (Annicchiarico and Alcock, 2014). The level of crystallinity will also impact shrinkage as crystallisation continues to occur below the melting point and above the glass transition temperature (Annicchiarico and Alcock, 2014). The more crystalline the polymer is, the more shrinkage should be expected. This is due to the increased packing that is associated with crystalline polymer, below the melting point the polymer will tightly pack and will occupy less space, resulting in shrinkage. The rheological behaviour of the polymer when molten or softened is particularly important in any kind of IM. Rheological characterisation of molten polymers is a commonly used analysis in process monitoring, quality control, process design and

also in modelling and simulation (Zhang and Gilchrist, 2012). Rheology is the study of material deformation under force Satin and Bílik (2016). To understand the rheological behaviour of a material you can either observe how the material deforms under a given force, or determine the force required to achieve the desired deformation (Satin and Bílik, 2016). When studying material rheology, the first property to consider is whether the material acts as a Newtonian or a non-Newtonian fluid. The rheological behaviour of Newtonian fluids (linear elastic materials) is far simpler to understand and a general equation can be used to describe how these materials will react to deformation (Satin and Bílik, 2016). A constitutive equation or rheological equation of state can therefore be produced for Newtonian fluids which describes their flow (Satin and Bílik, 2016). Not all materials behave in this way and understanding the rheology of non-Newtonian fluids is far more complex. Molten thermoplastics are examples of non-Newtonian fluids and as such, they are rheologically complex and can exhibit interesting rheological properties (Satin and Bílik, 2016). One of the major differences observed between Newtonian and non-Newtonian fluids is their viscosity. Viscosity is defined as shear stress divided by shear rate. For Newtonian fluids, viscosity is independent of time and only temperature, pressure and molecular properties of the material itself impact the speed shear deformation (Satin and Bílik, 2016). For Non-Newtonian fluids, the viscosity changes as a function of strain rate and the behaviour of these substances can be described as either viscoplastic or dilatant (Satin and Bílik, 2016). A number of process parameters involved in IM will therefore impact the viscosity of the thermoplastic material such as shear stress, shear rate, temperature and pressure. Non-newtonian injection materials demonstrate significant changes to their melt viscosity with relatively small variation in the shear rate making the prediction of process parameters difficult. This change in melt viscosity is due to the entanglement and disentanglement of polymer chains when the external forces of the injection moulding process are applied (shear) (Kashyap and Datta, 2015). Additionally, there is some evidence which suggests that the viscosity of molten thermoplastics is lower in the micro-channels of a μIM mould than is measured using a capillary rheometer (Zhang and Gilchrist, 2012).

Material for IM (and the filament used in FDM also) is often prepared via hot melt

extrusion (HME). HME is a technique used to combine materials to achieve sufficient mixing through the use of heating and shear stress. The viscosity of the molten mixtures is also important in the HME process. It must be low enough to not exceed the torque capability of the extruder but also must be sufficient to allow proper mixing (Verstraete et al., 2016a). HME processing is typically possible with complex viscosity values between 1,000 and 10,000 Pa s (Verstraete et al., 2016a). It is a fair assumption that a formulation that is processable by HME should also be processable by macro-IM, however a lower viscosity may be required for μIM techniques. The torque experienced in the extrusion process can be reduced by increasing the barrel temperatures, allowing for formulations with high drug loadings (up to 80% w/w) to be successfully extruded (Verstraete et al., 2016a). Molten plastics demonstrate pseudo-plastic behaviour at high temperatures, with their viscosity decreasing with increased shear rate (Giboz et al., 2007). Polymers which demonstrate good melt flow properties are typically preferred for μIM. These materials typically have a low viscosity and include polypropylene (PP), polyethylene (PE), polyether ether ketone (PEEK) and cyclic olefin copolymer (COC) (Packianather et al., 2015). When adding an active pharmaceutical ingredient (API) into a polymer for IM, a plasticising effect is observed (Eggenreich et al., 2016) which will reduce the melt viscosity of the polymer.

Object Defects in Injection Moulding

Differences between the designed mould shape and the shape of the object produced are often observed with IM, due to shrinkage and warpage experienced by the object during the process (Mohan et al., 2017). The temperature, pressure distribution and a variety of other process parameters of the IM process cause this shrinkage and warpage. This is due to the creation of local shrinkage and differences in the internal stress experienced by different areas of the object being moulded (Mohan et al., 2017). The extent of shrinkage experienced varies massively and this variation is largely down to the different injection materials being used. For both amorphous and crystalline materials, the volume of the molten material varies in a linear fashion relative to the temperature of the melt (Bould et al., 2015). Crystalline thermoplastics will result

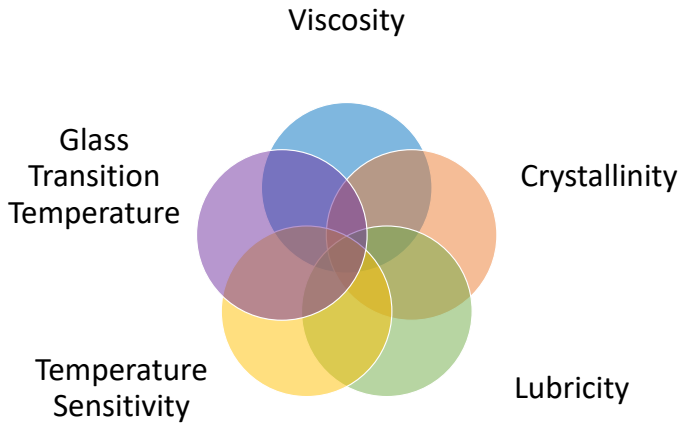

Figure 1.7: A summary of some of the critical polymer properties which must be considered for injection moulding.

in a greater degree of shrinkage than amorphous thermoplastics (Bould et al., 2015). When using thermoplastics, shrinkage is not an avoidable phenomenon (Mohan et al., 2017). Shrinkage can occur isotropically or anisotropically, with anisotropic shrinkage leading to the additional deformation known as warpage. If shrinkage is completely uniform, then no warpage will occur (Bould et al., 2015). Warpage can be caused by different cooling rates being experienced by different object surfaces, differential shrinkage and introduction impacts (Mohan et al., 2017). This increased shrinkage and warpage associated with crystalline character of thermoplastics typically results in reduced ductility of the moulded part when compared to that made from an amorphous thermoplastic (Bartlett et al., 2017). Injection material selection plays a significant role in determining the extent of warpage. Materials with low stiffness may experience warpage to a larger extent due to having a lower resistance to distortion. A material with higher stiffness will experience this less and therefore could experience less warpage overall (Bould et al., 2015). The compression of the air originally in the mould cavity prior to the injection of the molten material was believed to be the cause for some object defects. This was disproved by Sha et al who confirmed that the air present

in the mould cavity was not responsible for any defects observed (Sha et al., 2007). Another common defect in moulded objects is flash. This occurs when the injected material is forced out with the confines of the designed mould space and sits between the two mould halves. This can occur if the mould is overfilled or if the parting plane between the mould halves is not perfectly flat and aligned (Formlabs, 2016a).

While both FDM printing and IM have been employed in the direct fabrication of pharmaceutical dosage forms, both of these techniques have drawbacks. Primarily, issues around accuracy and precision and material flexibility impose limitations on the usefulness of FDM in the pharmaceutical sector. For IM, a lack of flexibility to modify the physical structure of the tablet poses issues.

1.3.4 Rapid Tooling Injection Moulding

Introduction

More recently, IM has been used in combination with AM technologies. This coupling of techniques is referred to as rapid tooling injection moulding (RTIM). It is common for moulding tools used in μIM to typically comprise a mould insert with the desired micro-structure and a tool for the insert to sit in (Heckele and Schomburg, 2004). A mould insert must be manufactured in such a way that it can create these precise micro-structures. The material in which the mould is composed of must be sufficiently hard and ductile in order to survive the IM process (Heckele and Schomburg, 2004). Developments in AM technology and capabilities have opened the door for rapid tooling in IM as an alternative to traditional metal moulds (tools) (Rani et al., 2018). Traditional metal mould making is a time-consuming process which is both cost and skill exhaustive (Rani et al., 2018). Rapid tooling is defined as being the use of AM techniques for the manufacture of moulds directly (direct tooling) or to create a pattern which is then used to manufacture a mould (indirect tooling) (Mendible et al., 2017; Qayyum et al., 2017; Rani et al., 2018). With AM techniques now utilising photopolymers to print objects with high resolution, the potential for this technique to be used to manufacture moulds for μIM is apparent (Mohan et al., 2017). AM techniques such as stereolithography and polyjet printing have been utilised to manufacture rapid tooling

moulds for IM (Bartlett et al., 2017). In order for these materials to be suitable for use in μIM, there must be sufficient resistance to both the temperature and pressure experienced during the injection process (Bartlett et al., 2017). These photopolymer-based AM techniques were selected due to the material properties of the photoresins used. Moulds created from these photoresins are expected to have high thermal resistance and superior surface quality making them ideal for rapid tooling (Bartlett et al., 2017), 2017). Evidence suggests moulds created through stereolithography can survive up to 500 injection shots (Rahmati and Dickens, 2007). The integration of rapid tooling and IM reduces the overall cost and the lead-time that comes with using traditional metal moulds (Formlabs, 2016a; Mendible et al., 2017) with the lead-time able to be reduced by as much as 50% (Levy et al., 1999). This coupling of technologies makes low production runs economically feasible and also allows for a more agile approach to research (Formlabs, 2016a; Mendible et al., 2017).

Comparison to Traditional Injection Moulding

When using rapid tooled moulds, the difference in thermal conductance must be considered. For a traditional steel mould, the thermal conductivity is typically in the range of 20 – 80 W/mK whereas an unfilled rapid tooled mould is expected to be 0.5 W/mK. This significant difference in thermal conductivity has practical implications for the IM process as the rate of both heating and cooling will be slower. This will increase the overall cycle time of the IM process and in increased cooling time can impact the shrinkage of the moulded object (Kovács et al., 2015; Mendible et al., 2017). Rapid tooled moulds are typically far more fragile than traditional steel moulds and the difference in the strength of these materials results in mould fractures and eventually failure in the rapid tooled moulds after relatively few injections compared to the capabilities of the steel mould (Van den Broeck, 2017). The poor thermal conductance also makes modelling the behaviour of rapid tooled moulds far more difficult than for steel moulds (Mendible et al., 2017). For RTIM, process parameter alterations may also be required due to the different material properties of a rapid tooled mould compared to a traditional tooled steel mould. The mould temperature and the injection pressure in

particular must be modified to make the process suitable for use with a rapid tooled mould insert (Tuteski and Kočov, 2018).

Studies have demonstrated that similar mechanical properties can be achieved for these photopolymer moulds as is observed in the traditional metal moulds used in IM. One mechanical property where a difference between the photopolymer and metal moulds can be observed is in the ductility of the object being moulded (Bartlett et al., 2017). Objects produced from photopolymer moulds typically exhibit significantly lower ductility compared to those produced from a metal mould (Bartlett et al., 2017). One other significant difference between the rapid tooled moulds and metal moulds is the intrinsic strength of the mould itself (Bartlett et al., 2017). The rapid tooled moulds are not as strong or robust as a metal mould which can lead to significantly more mould failures when using a rapid tooling mould (Ribeiro et al., 2004).

Moulds can be produced from thermosetting epoxy resins via stereolithography (SLA) AM. Moulds made of these materials are suitable for use in IM as with increasing temperature, the tensile strength of the mould material decreases while its resistance to impact increases. The mould temperature is therefore a delicate balance between resistance to impact and the tensile strength of the mould (Rahmati and Dickens, 2007). The injection pressure used is particularly important with rapid tooling μIM as if the injection pressure is higher than the strength of the rapid tooled mould, failure of the mould can occur (Rahmati and Dickens, 2007). SLA is particularly useful for producing moulds which have features in the micro-scale due to its high resolution capabilities and the smooth finish of the objects it produces (Formlabs, 2016a). Moulds produced by SLA will typically undergo a post-curing step to polymerise any uncured material and to achieve the final mechanical properties of the resin (Ribeiro et al., 2004). This post-curing step often includes application of both heat and UV light. The UV light initiates a radical initiation step causing a photoinitiator molecule in the resin to split forming two radical species while the higher temperature increases the mobility of the free radical species which can then induce further polymerisation increasing the polymer chain cross-linking (Colton and Blair, 1999). This cross-linking is critical for the material to possess its final mechanical properties, such as the T_g and ductility of

the material (Ribeiro et al., 2004). Polymers with a high degree of cross-linking tend to have a higher dimensional stability when placed under a load, high mechanical strength and typically will have a higher T_g than polymers with less cross-linking. Lower cross-linking in polymers results in a higher degree of elasticity in the material (Ribeiro et al., 2004). There is some disagreement amongst the wider research community as to whether this post-curing step is beneficial for rapid tooling applications. It has been suggested that in the case of some photopolymer resins, post-curing leaves the mould too brittle for it to be used in IM (Ribeiro et al., 2004). Salmoria et al. (2002) found that a thermal post-cure process caused an increase in both the Youngs Modulus and the ultimate tensile strength (UTS) whereas others have reported that the post-curing process had no significant impact on either of these material properties (Ribeiro et al., 2004). Additionally, there is evidence to suggest that the flexural modulus is also increased following the post-curing process (Jacobs, P. F., 1993).

Previous research found that mould failure could occur during both the injection step and the ejection step (Ribeiro et al., 2004). This failure can take the form of a catastrophic crack or break in the mould surface but can also be the incremental chipping away of some sections of the mould surface (Ribeiro et al., 2004). Ultimately, all of these failures can be accredited to the material properties of the resins that the moulds are manufactured from (Ribeiro et al., 2004). The mechanical properties of the resins can alter over time due to the light-sensitive nature of the resins themselves. Additionally, increases in mould temperature will result in a decrease in ultimate tensile strength leading to mould weakness and brittleness (Ribeiro et al., 2004). Cracks in these moulds tend to occur where the stress concentration is highest on the mould e.g. sharp corners and weak points between printed layers. The mechanism of failure for rapid tooled moulds can be considered to be a function of the mould materials toughness when held at elevated temperatures (Rahmati and Dickens, 2007). The failure of these moulds can occur at both high and low temperatures. At low temperatures, the ability of the mould to resist impact is low and this can lead to mould damage. At high temperatures, the tensile strength of the mould decreases and as the temperature rises above the T_g, the material strength drops (Rahmati and Dickens, 2007). The most

likely cause of fractures and damage of moulds is due to the flexural stress of the IM process being higher than the flexural capability of the material (Rahmati and Dickens, 2007). Effectively, the material is not able to flex or bend sufficiently to handle the process, so it breaks instead. This type of failure is far more likely than failure due to shear stress, particularly when the mould temperature is greater than 40°C (Rahmati and Dickens, 2007). The geometry of the mould will also have a large impact on its ability to withstand damage (Rahmati and Dickens, 1997).

Despite these known issues associated with rapid tooled moulds, there have been examples demonstrating that moulds of this kind can be used in excess of 500 injection shots with no damage to the mould (Rahmati and Dickens, 1997).

Stereolithography Additive Manufacture

The preferred method of AM for generating these mould inserts is SLA. In SLA, an object is created from the selective curing of a photosensitive polymer resin on a layer-by-layer basis. SLA is famed for being the first of the AM technologies, with the first patent covering SLA being filed in 1986 (Liaw and Guvendiren, 2017; Ngo et al., 2018; Varotsis, 2019). SLA is typically the most cost effective way to produce plastic objects with high resolution and smooth surfaces (Varotsis, 2019).

SLA uses UV light to polymerise resin oligomer or monomer solutions via a radicalised chain reaction (Ngo et al., 2018). The UV laser is controlled by a pair of mirrors within a galvanometer. The slice information is presented in the form of a set of co-ordinates, defining the tilt angle of the two mirrors, which guide the position of the laser beam along the plane (Ligon et al., 2017). SLA printers come in two variants, right-side up and inverted. As indicated by the names, the difference between the two is the orientation of the build platform. For right-side up SLA, the object is built on to a build platform immersed in the resin bath. For inverted SLA, the build platform is suspended upside down above the resin bath (see Figure 1.8 for a depiction of Inverted SLA). The inverted system is more common in desktop SLA printers, with the right-side up approach being preferred in industrial machines. For the purpose of this introduction, inverted SLA will be described as this is the technique utilised in this

thesis.

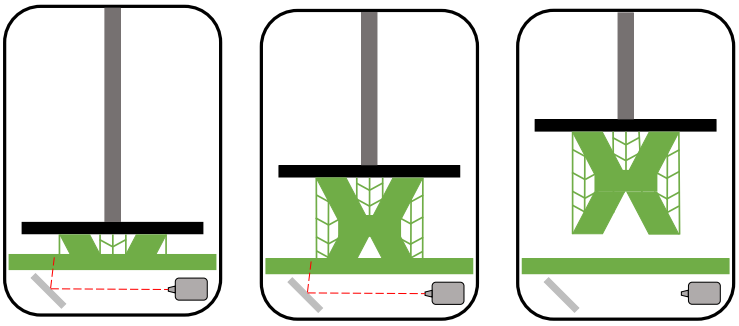

Figure 1.8: Depiction of inverted SLA based additive manufacture.

The build platform lowers, leaving a distance of one layer height between the bottom of the resin tank and the build platform. The UV laser then maps out the layer being created, initiating the radicalised chain reaction and solidifying the liquid resin. When the layer is complete, the build platform moves up one layer height and a sweeper blade ensures the resin tank is adequately coated to create the next layer. This process repeats until the object is complete. The finished object then requires post processing to clean the excess resin from it and to achieve the materials mechanical properties (Jamróz et al., 2018; Varotsis, 2019).

The process which causes the liquid resin to solidify is called photopolymerisation. Initiator molecules within the photopolymer resin are activated by the UV light, causing bond fission and creating radicals. These radicals then propagate and cause oligomers and monomers within the resin to bond together, creating longer chains. As these chains become longer, the polymer takes on a more solid form. Inhibitor molecules terminate the radical species, ending the polymerisation reaction.

SLA is considered to be one of the most precise AM methods (Jamróz et al., 2017), with SLA being capable of producing objects with twice the resolution of FDM (Finnes, 2015). The typical layer height for an SLA printer ranges between 10 – 100 μm (Ngo et al., 2018; Varotsis, 2019). Most SLA printers have capability to alter this layer height to suit the needs of the particular print. For prints with complex or curved geometries, a layer height of around 25 μm should be used to best capture these features. For prints

where there are no complex features, 100 μm should be used to reduce the print time, cost and also the number of layers required (which in turn reduces the probability of a print failure) (Varotsis, 2019). The layer height is also impacted by the energy of the UV light source and the exposure time (Ngo et al., 2018). The minimum resolution of the light source and the path planning operations influence the $x-y-$resolution (Ligon et al., 2017). The accuracy of the step-motor (which moves the build platform) influences the $z-$resolution (Ligon et al., 2017). The $x-y-$resolution is determined by the spot size of the focussed laser beam, which provides SLA its high spatial resolution (Ligon et al., 2017). The absorption and curing characteristics of the material selected also impacts the resolution (Ligon et al., 2017). This is strongly dependent on the monomer used and the presence of initiator and/or inhibitor molecules.

When an object has finished printing in SLA, it is still considered to be in a green state and requires post processing to complete the polymerisation process and achieve the mechanical properties expected for the printed material. Objects also require printing support material, which must be removed after the polymerisation process has completed. The surface quality of SLA printed parts is excellent, due to the high resolution capabilities of this technique. Curling of objects can occur due to shrinkage of the resin when it is solidified and can be minimised through careful design of both the object being printed and the printing parameters. Due to the photosensitive nature of the materials used in SLA printing, exposure to UV can result in degradation of the mechanical properties of the material over time. Parts produced by SLA have good inter-layer bonding due to this green state and the continuation of polymerisation after the printing process has been completed. This results in almost isotropic mechanical properties such as tensile strength, however the elongation at break of SLA parts tends to suffer as a result (Varotsis, 2019). When the printing process is completed, the object must be washed (typically in isopropyl alcohol). This step is required to remove any un-cured resin from the object. Following washing, the object must be allowed to dry completely before the post-curing process can begin. Post-curing with both UV light and heat is required to achieve the mechanical properties expected for the material (Liaw and Guvendiren, 2017). The length of time that the object must be post-cured

for is dependent on the material used. Following post-curing, the support material can be removed from the object and if required, it can then be sanded or polished to achieve the desired finish.

In order for a material to be suitable for use in SLA, the polymer resin should be a liquid which rapidly solidifies upon illumination with light. These materials tend to be glassy, rigid and brittle (Melchels et al., 2010). The materials used in SLA printing are mainly acrylic or epoxy-based resins (Ngo et al., 2018). The price for these resins varies massively depending on the expected application of the material, with standard materials being as little as £35 per litre and more speciality materials being as much as £400 per litre. Speciality resins are available for a number of different applications, including those with increased temperature resistance, durable resins and even dental resins (Varotsis, 2019). The material options for SLA are improving over time, expanding the possibilities for this technology.

1.4 Environmental Impact

In light of the current climate crisis we face, it cannot go unmentioned that new manufacturing methods give rise to the opportunity for consideration and change. The manufacturing methods discussed in this thesis involve the use of synthetic polymers. Our world is facing its largest battle yet against climate change, and the manufacturing sector also has a role to play both in making our processes more environmentally friendly and energetically economical. The United Nations published their 17 Sustainable Development Goals, capturing the main challenges facing our world. Goal 12 focuses on responsible consumption and production (United Nations, 2015). It is clear that the pharmaceutical manufacturing industry needs to step up and play its part in working towards achieving this goal. The use of polymers in pharmaceutical formulations therefore must be considered. The polymers used in this thesis are considered to be biodegradable, meaning their degradation should not result in waste that cannot be broken down. It is the responsibility of all of us involved in pharmaceutical research and industry to be considerate of the materials we use and the impact they will have on our planet. Future polymers may provide superior properties in terms of processability

for example, but we must primarily ensure they are safe for patients and safe for our planet.

1.5 Summary

Looking at the bigger picture, our healthcare systems are evolving and we are reaching a critical point where our ability to provide cradle-to-grave healthcare for patients is being challenged. Changes in the demographic of our patients, increase in multi-morbidity within patients and the huge price tags associated with novel treatments are crippling our ability to provide the best care. Whilst there are very good reasons for the extremely high costs of bringing a new drug to the market, this inherently erects barriers in the path of bringing a new medicine to the patient, and ultimately it is the patients who lose out.

In the pharmaceutical field, the drivers behind the interest in novel manufacturing technologies will only continue to apply pressure. The future of medicines will heavily feature personalised and precision medicines. In addition to this, more and more of the newly discovered drug molecules in the pipeline will be considered to be low solubility. This poses formulatory challenges which a technique such as RTIM could help to overcome. RTIM could also provide a quicker and less expensive option for the production of dosage forms for clinical trials. The employment of RTIM either as a direct manufacture technique for very low production runs or as a development tool for a higher production run promises benefits both in terms of economics and sustainability.

Chapter 2

Aims and Objectives

The principle objective of this thesis is to develop a manufacturing process and development tool for the production of pharmaceutical oral solid dosage forms (OSDFs) with surface micro-features via the rapid tooling injection moulding (RTIM) process. The aim is for this manufacture technique to be suitable for micro-batch pharmaceutical production and for this to be a more time and cost-effective process. The RTIM process couples the additive manufacture technology stereolithography (SLA) and injection moulding (IM). While both of these techniques are currently used in the production of pharmaceutical OSDFs, limitations are present for both such as material constraints and restrictions on the physical geometries of the dosage forms that can be produced. This research aims to demonstrate that through the coupling of the technologies, the limitations on formulation space and OSDF geometry can be overcome. The aims of this research are to develop a robust manufacture technique which is capable of producing OSDFs which are accurate and precise to a digital design. This work also aims to alter the drug release of the dosage forms via changes in the physical structure to demonstrate a controlled release functionality. The overall objectives are broken down into specific aims and objectives which are:

- To examine the accuracy and precision of SLA and its suitability for use as a rapid tooling technique for RTIM. A number of different parameters will be assessed, including the thermal uptake of a variety of SLA materials and the suitability of different SLA materials in conjunction with the RTIM process. A scaling factor

to ensure the physical printed object is accurate to the digital design will be determined as will the material properties which are deemed critical for success in the RTIM process.

- To assess the accuracy and precision of the RTIM process with a variety of polymer-based formulations. A number of pharmaceutical polymer-based formulations will be trialled in the RTIM process to assess their suitability to be used in the technique and to better understand the limitations on the formulation space for RTIM. The variability of the OSDFs produced will be analysed and the physical OSDFs compared to the digital design. The surface area, volume and specific surface area in particular will be calculated and this will allow comparison to both the digital design and also comparison between polymer-based formulations.

- To determine the impact that modification of the OSDF specific surface area has on the drug release profiles. Three OSDF geometries will be produced, with varying specific surface area. Comparisons will be made then on the dissolution profiles produced from these different geometries. Three paracetamol-based formulations will be trialled to assess the impact that different drug release mechanisms have on the this. The accuracy and precision of the drug-loaded OSDFs produced by RTIM will also be assessed to determine if the addition of an active pharmaceutical ingredient to the formulation has any impact in this regard.

Chapter 3

Development of 3D Printed Rapid Tooling for Micro-Injection Moulding

3.1 Chapter Summary

The use of additive manufacturing techniques in conjunction with injection moulding is becoming increasingly popular, with financial and time benefits to coupling the techniques. This chapter demonstrates a systematic development process of 3D printed rapid tooled moulds using stereolithography. A high flexural modulus and elongation were found to increase the likelihood of success of a mould material in the injection moulding process. Success is defined as the mould surviving the process and being capable of producing the desired object successfully. Stereolithography was found to produce high quality moulds when a diagonal print orientation and a scaling factor of 109.3% is employed. The presented technique and systematic workflow is highly suitable for the production of moulds with detailed micro-features. This is of particular interest for rapid tooling for micro-injection moulding for the manufacture of pharmaceuticals and medical devices, where the micro-structure directly impacts the performance of the products. The contents of this chapter have been published (see page xx), however

some sections have been adapted to expand on some of the key concepts. All work and writing in my own unless stated otherwise.

3.2 Introduction

Injection moulding (IM) is a widely applied manufacturing technique for the production of plastic products (Bartlett et al., 2017; Quinten et al., 2009b) due to its versatility and time efficiency (Zema et al., 2012). It is employed on a massive scale to produce complex objects by applying heat and pressure to fill a mould with a thermoplastic material (Quinten et al., 2009b). During the IM process, the thermoplastic material is softened by heating. This softened material is then injected into a mould cavity under high pressure. The thermoplastic material then cools in the mould cavity causing it to solidify in the specific shape of the mould (Quinten et al., 2009c; Zema et al., 2012) as illustrated in Figure 3.1.

With IM being a highly versatile technique, it opens up a number of opportunities to

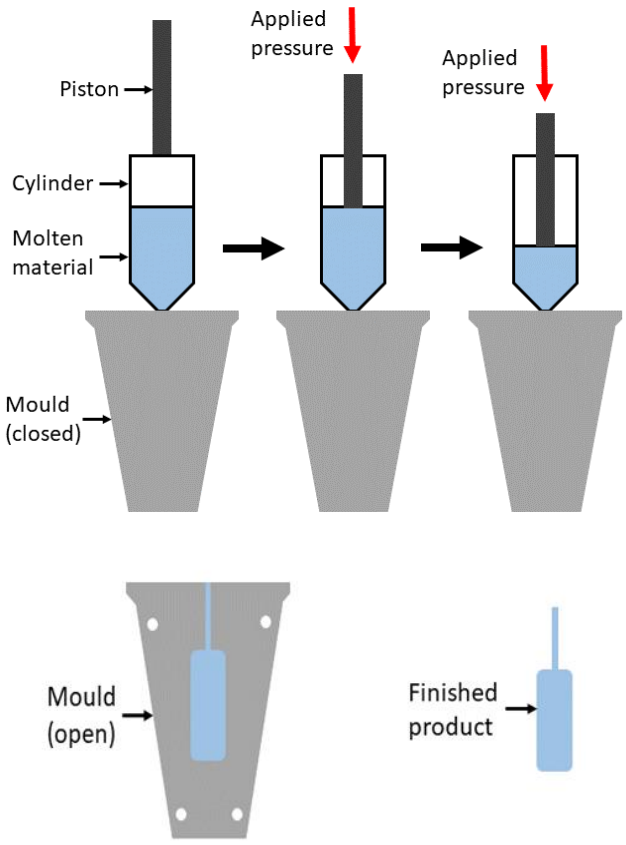

Figure 3.1: Basic schematic of the IM process.

produce functional materials of defined shape and size, which is particularly impactful for the manufacture of pharmaceutical and biomedical devices such as oral solid dosage forms (Quinten et al., 2009b) and scaffolds (Zema et al., 2012). It has the additional benefit for pharmaceutical and medical products that the processing environment helps to reduce microbial contamination (Zema et al., 2012). The performance of many functional materials is driven by how they are organised at the micro- to millimetre scale. Having the ability to create a particular microstructure thus enables the control of the performance of such materials. IM is capable of realising a desired microstructure for thermoplastic materials. This requires, however, a transition from macro-IM to micro-IM (µIM), which is not as simple as scaling down the process, each part of the process must be reassessed (Giboz et al., 2007).

The µIM process was first employed over 30 years ago and its popularity has continued to increase due to the growing importance of microsystem technologies (Annicchiarico and Alcock, 2014; Zhao et al., 2003). While it is possible to make small plastic components via macro-IM, the object rejection rate is typically high at between 30–50%. Moving to a specific µIM process reduces this rejection rate due to improvements in control of metering and increased homogeneity in the component produced (Zhao et al., 2003). The process and the factors which affect it are universal across all forms of IM, however the impact of each factor varies significantly as you move to smaller objects and feature sizes. For µIM moulds, the aspect ratio – which is defined as being the thickness over the lateral dimension – is typically >1 (Giboz et al., 2007). Creating a smaller object will inherently result in smaller channels for the injected material to flow through. The rheology of the injected material thus becomes critical to the success of the IM process.

Moulding tools used in µIM will typically comprise a mould insert with the desired microstructure and a tool for the insert to sit in (Heckele and Schomburg, 2004). A mould insert must be manufactured in such a way that it can create these precise microstructures and the material in which the mould is composed of must be sufficiently hard and ductile to survive the IM process (Heckele and Schomburg, 2004). Recent developments in additive manufacturing (AM) technologies and capabilities have opened

the door for rapid tooling in IM (RTIM) as an alternative to traditional metal moulds (tools) (Rani et al., 2018). Rapid tooling is defined as using AM techniques for the manufacture of moulds directly (direct tooling) or to create a pattern which is then used to manufacture a mould (indirect tooling) (Mendible et al., 2017; Qayyum et al., 2017; Rani et al., 2018).

There are a number of benefits to using RTIM in place of the traditional tooled steel moulds. The use of AM allows the implementation of an iterative learning cycling. The time required to redesign, print and test an AM mould is approximately 24 h compared to several weeks for conventional tooled steel moulds. AM is also significantly more cost-effective than the use of conventional tooled steel moulds (Rani et al., 2018). With AM techniques now utilising photoresins to print objects with high resolution, the potential for this technique to be used to manufacture moulds for µIM is possible (Mohan et al., 2017). In order to make these materials suitable for RTIM, there must be sufficient resistance to both the temperature and pressure experienced during the IM process (Bartlett et al., 2017). The most common AM technique for RTIM is stereolithography (SLA) due to the advantageous material properties of the photoresins used in SLA compared to other AM techniques. Printed moulds created from these photoresins are expected to have high thermal resistance and superior surface quality making them ideal for rapid tooling (Bartlett et al., 2017). It is also suggested that printed moulds created through SLA are capable of surviving up to 500 injection shots (Rahmati and Dickens, 2007).

There are a number of key challenges when implementing RTIM. For a traditional steel mould, the thermal conductivity is typically in the range of 20–80 W/mK whereas an unfilled printed mould is expected to be 0.5 W/mK (Kovács et al., 2015). This significant difference in thermal conductivity has practical implications for the IM process as the rate of both heating and cooling will be slower. This will increase the overall cycle time of the IM process and prolong the cooling process which can in turn cause shrinkage of the moulded object (Kovács et al., 2015; Mendible et al., 2017). Furthermore, printed moulds are typically far more fragile than traditional steel moulds and the difference in the strength of these materials results in mould fractures and

eventually failure in the printed moulds after relatively few injections compared to the capabilities of the steel mould (Van den Broeck, 2017). Additionally, the technique used to produce these printed moulds must be able to produce high quality prints with high accuracy and precision to ensure each moulded object is identical to the digital design. Implementing a systematic approach to assess these challenges will improve the overall process for RTIM.

This work presents a systematic approach to develop a RTIM process using rapid tooling produced via SLA. A methodical process of selecting the tooling material (photoresin), identifying process parameters and assessing the accuracy and precision of micro-scale tooling features is discussed and summarised in a workflow. The selection of the tooling materials includes an analysis of four photoresins in terms of its thermal conductance, mechanical properties and its ability to withstand the temperature and pressure requirements of the RTIM process.

3.3 Materials and Methods

3.3.1 Materials

Stereolithography

A number of compatible photoresins from Formlabs (Massachusetts, USA) were investigated, namely two standard (clear/FC and grey/FG) and one engineering (high temperature/FHT) resins as summarised in Table 3.1. Both standard resins (FC and FG) are identical, with the only differences being the addition of dyes. The data provided in the material data sheets is identical for all Formlabs standard resins and as such data gathered using the FC and FG resin can be used interchangeably. The thermal, mechanical and IM testing was thus only performed for FC, whereas the accuracy and precising testing was performed for FG as the grey material provided a better contrast in the microscope images (see Section 3.3.2 for more details). The FHT resin is from the Engineering Resin family and is designed for high thermal stability. The exact composition of these resins is considered proprietary, however it can be deduced from the material safety data sheets that both the standard and engineering resins

from Formlabs are primarily methacrylate based. One observable difference between the data sheets for the standard resins (FC and FG) and the engineering (FHT) is the replacement of some methyacrylate with acrylate. Both resin families also contain a photoinitiator molecule of undisclosed nature and level. It is likely that this is a species that is easily radicalised upon illumination with UV light (Formlabs, 2016b, 2017).

Additional photoresins were obtained from 3D Resyns (Barcelona, Spain), namely IM-UHR (version 1) and IM-UHT (version 2). Both of these resins are designed for use in conjunction with IM and as such have high thermal stability. No declaration of the composition of these resins is made.

Table 3.1: Summary table of selected resins including the heat deflection temperature (HDT) from the supplier data sheets (Formlabs, 2016b, 2017; Segurola, 2019).

Resin Code	Manufacturer	Supplier Resin Name	HDT at 0.45 MPa	HDT at 1.8 MPa
FC	Formlabs	Clear v4	73.1°C	58.4°C
FG	Formlabs	Grey v4	73.1°C	58.4°C
FHT	Formlabs	High Temp v2	238°C	101°C
RUHR	3D Resyns	IM-UHR-v1	250°C	No information available
RUHT	3D Resyns	IM-UHT-v2	170°C	No information available

The heat deflection temperature (HDT) of these materials is marketed as being the marker of success for these materials when it comes to high temperature applications. The HDT indicates the temperature at which a material begins to deform under a given load. It is thus expected that a material having a high HDT will be better suited to high temperature applications such as RTIM.

Rapid Tooling Injection Moulding

Low-density polyethylene (LDPE) was purchased from Sigma-Aldrich (Missouri, USA). LDPE was selected as previous studies in the literature had shown success in using LDPE with printed moulds (Qayyum et al., 2017; Van den Broeck, 2017).

3.3.2 Methods

Stereolithography 3D Printing

SLA 3D printing is an AM technology which builds three-dimensional objects in a layer-by-layer fashion. In this study, SLA is used to produce customised printed mould inserts for use in IM (see Figure 3.2a). SLA 3D printing uses a UV laser to polymerise a liquid photoresin resulting in the solidification of the resin. The printer used in this work is the Form 2 (Formlabs, Massachusetts, USA), which uses a laser with a wavelength of 405 nm. The 3D object is designed digitally via computer-aided design (CAD) and is converted into a surface tessellation language (STL) file. This STL file is then opened in the Preform software (Formlabs, USA). This software converts the STL file into the sliced object to be printed. In the Preform software, the object to be printed is oriented to achieve the best printing results and necessary build supports are applied. The print material and desired resolution are selected on the software and when the file is ready to be printed, the file generated from the software is then sent to the printer.

The printer resolution is split into the planar $x - y$-axes (140 µm) and the z-axis (25 µm). These are controlled by different mechanisms, and hence have different resolution capabilities. The $x-y$-resolution is governed by the spot size of the UV laser used, while the z-resolution is governed by the step-motor controlling the layer height.

Upon completion of the print, the object was washed in isopropyl alcohol (IPA) to remove excess resin. This was achieved using the automated FormWash (Formlabs, Massachusetts, USA). Following this, the object requires post-processing in the form of UV and thermal curing (Table 3.2). The washing and curing requirements vary for different print materials and these steps are required to achieve the desired material properties of the resins. The UV cure is done for all materials using the FormCure (Formlabs, Massachusetts, USA) with light at a wavelength at 405 nm. FHT, RUHR and RUHT also required an additional thermal cure in a lab-grade oven (details of this can be found as thermal cure in Table 3.2).

Different designs of the printed objects were required to conduct the various assess-

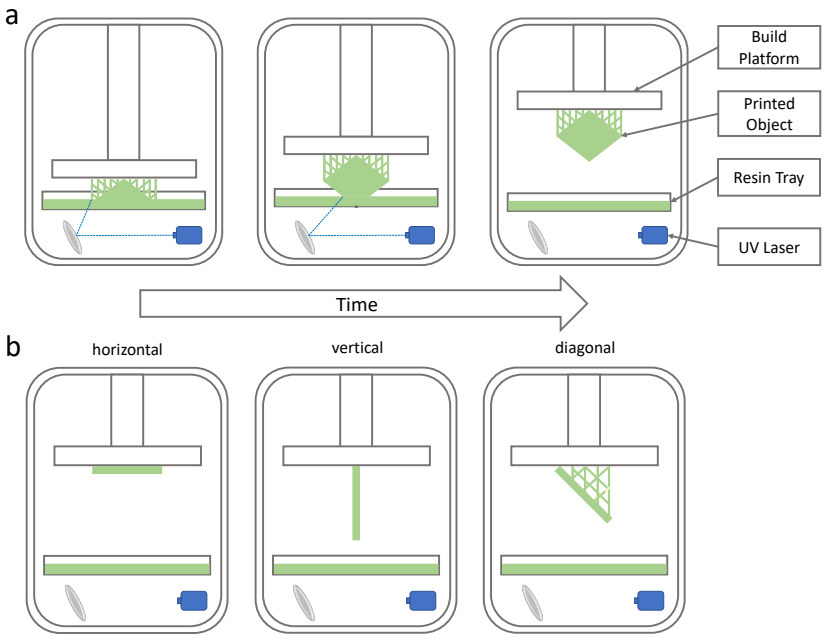

Figure 3.2: Schematic of the SLA printing process and orientations of the print. a) Printing process. b) Print orientation detailing horizontal, vertical and diagonal (45°) print orientation.

Table 3.2: Summary of post-processing requirements of the resins used.

Resin code	Wash time	UV cure	Thermal cure
FC	20 min	60 min at 60°C	N/A
FHT	10 min	120 min at 80°C	180 min at 80°C
RUHR	10 min	60 min at 60°C	1^{st} - 120 min at 80°C 2^{nd} - 180 min at 160°C
RUHT	10 min	60 min at 60°C	1^{st} - 120 min at 80°C 2^{nd} - 180 min at 160°C

ments of the photoresins including thermal testing, mechanical testing, accuracy and precision testing and RTIM testing. The designs are presented in Figure 3.3 and are discussed in more detail in the sections following.

Mechanical Testing of 3D Printed Moulds

A three-point bend test was conducted for the four different printing materials. This test was conducted on a Texture Analyser TA-XT (Stable Micro Systems, UK) fitted with a miniature three-point bend rig. The three-point bend tests were performed with

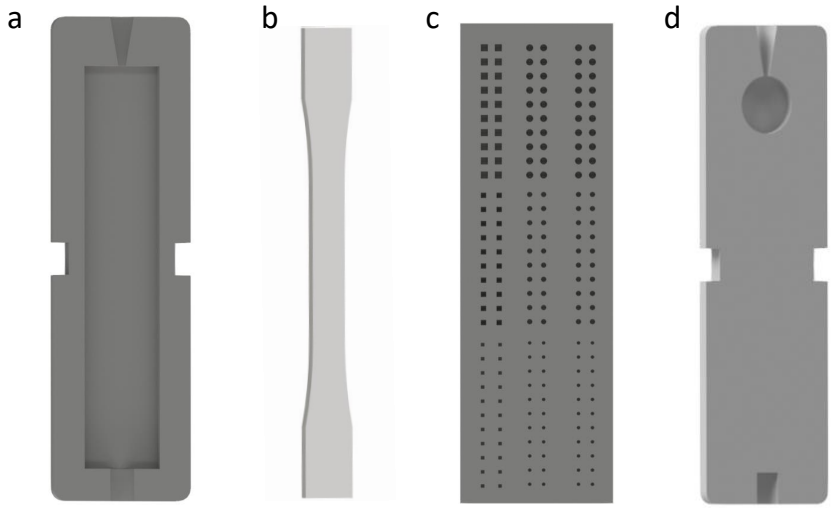

Figure 3.3: Printed mould designs used for the testing. a) thermal testing, b) mechanical testing, c) accuracy and precision testing and d) IM testing.

the following settings: gap size of 80 mm, pre-test speed of 0.5 mm/s, test speed of 0.02 mm/s, a distance travelled by the loading pin of 4.5 mm, trigger force of 0.049 N and data acquisition rate of 22 points/s. Samples were printed in the dog-bone shape as per the ASTM D638 standard (Figure 3.3 sub-figure b) (ASTM International, 2016). A total of five samples for each material were tested according to the ASTM standard requirements. Digital callipers were used to measure the length and width of the samples before they were positioned centrally on the lower support beams. Data analysis was performed with Exponent software (version 6.1.12.0, Stable Micro Systems, UK). Stress-strain graphs were analysed, and the flexural modulus, E_f, was calculated for each material using

$$E_f = \frac{L^3 m}{4bd^3} \tag{3.1}$$

with L as the support span and m as the gradient of the initial straight-line section of the load deflection on the graph. b and d are the width of the test beam and the thickness of the object tested, respectively.

Thermal Testing of 3D Printed Moulds

The heat transfer of printed moulds (Figure 3.3a) from different photoresins was tested using a hotplate and a thermocouple. Blank measurements were taken by placing the thermocouple directly onto the hotplate. The hotplate was set to 200°C and temperature measurements were taken every second. When the temperature reading had equilibrated, the hotplate was turned off and the cooling profile was also recorded at the rate of one temperature recording per second. This process was repeated with the different photoresins by placing the thermocouple on top of the printed mould, which was placed on top of the hotplate.

Accuracy and Precision of 3D Printed Objects

Three factors were varied to investigate the print capabilities (Figure 3.3d):

- Print orientation: horizontal, vertical and diagonal (see Figure 3.2b).
- Particle shape: cubes, spheres and cylinders.
- Particle feature size: 500 µm, 750 µm and 1000 µm (for cubes side length was measured and for both spheres and cylinders the diameter is measured).

Objects were designed to include features of various shapes and sizes and were also printed in three different print orientations. For each shape and a specific size and print orientation, a total of 300 measurements were taken (20 internal replicates on each printed mould and 15 printed moulds for each orientation).

The designed dimensions of these features were then compared to the actual printed dimensions to better understand the impact of these factors on the accuracy and precision of the 3D printer. Measurements were taken using a Leica M165 microscope (image size 1024 x 768 pixels with a pixel size of 8.5 µm) and its associated digital measurement tools. Accuracy and precision of the prints was performed for the FG material as this grey material resulted in high contrast of the features in the microscope images facilitating the measurement of the feature dimensions.

Rapid Tooling Injection Moulding

In order to compare the materials for IM, a series of experiments were conducted to determine the maximum temperature and injection pressure that printed moulds made from each material could withstand. IM experiments were conducted for each SLA resin using LDPE as the melt material. This work used the design shown in Figure 3.3d. An ideal printed mould would be able to withstand both high pressure and high temperature and this is even more important for µIM.

Identical printed mould inserts (Figure 3.4a) were produced from the FC, FHT, RUHR and RUHT materials. Printed mould inserts were inserted into a tooled steel housing as depicted in Figure 3.4. The printed mould inserts are then contained in the tooled steel mould halves and this the steel mould is placed in the HAAKE® MiniJet Pro Piston Injection Moulding System (Thermo Fisher Scientific, Massachusetts) which is an upright pressurised injection moulder.

The maximum temperature that the printed mould material was able to withstand without failure was measured by repeating experiments with equal pressure (10 bar) with increasing temperature values starting at 70°C in 10°C increments. Failure under

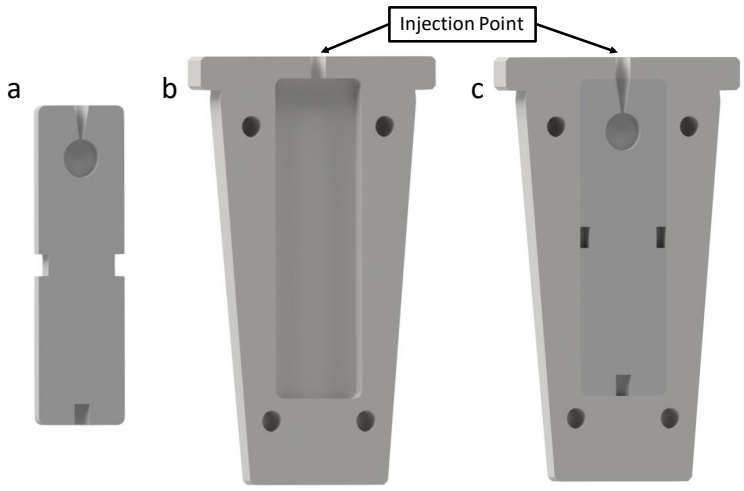

Figure 3.4: Schematic of the tooled steel mould with a printed mould insert produced via SLA 3D printing with a) printed mould insert b) tooled steel mould and c) printed mould insert in tooled steel mould. Depicted in each sub-figure is one half of the mould. The final mould is comprised of two halves.

temperature was taken to be the appearance of fractures on the printed mould surface, fusion of the two printed mould halves or changes in the dimensions of the printed mould resulting in poor fit within the metal mould. The maximum pressure that the printed mould material was able to withstand without failure was measured by repeating experiments with equal temperature (100°C) with increasing pressure values starting at 10 bar in 10 bar increments. Failure under pressure was taken to be the appearance of fractures on the printed mould surface, fusion of the two printed mould halves or breakage of the printed mould. The cylinder temperature, injection time, hold pressure and hold time were kept constant at 160°C, 15 s, 10 bar and 5 s, respectively, for both sets of experiments.

3.4 Results

3.4.1 Mechanical Testing

The results of the three point bend test are reported in Figure 3.5. FC has a significantly higher flexural modulus compared to all other materials tested. This is not unexpected as this material has the highest elongation value on its material data sheet. FHT is found to be significantly higher than both RUHR and RUHT even though the elongation values of all three of these materials are very similar.

Due to the nature of the three point bend test, print quality and in particular the isotropic nature which is typically expected of SLA prints would be a major factor in the performance of these materials. The lower values of flexural modulus obtained for RUHR and RUHT compared to FHT are thus attributed to a lower print quality and an inherent anisotropy.

3.4.2 Thermal Testing

The heat transfer of the printed mould inserts was analysed to better understand how the printed mould would perform in an injection moulder. These materials are compared to the heat uptake of the metal hot plate.

The heat uptake of the materials was recorded, and the time taken to reach 100°C,

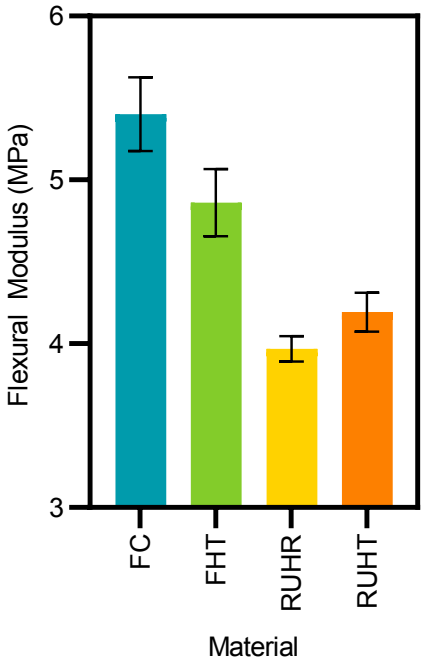

Figure 3.5: Calculated flexural modulus of the different SLA materials. Error bars represent the standard deviation of five measurements.

the rate of heating and the maximum temperature achieved were calculated and summarised in Table 3.3.

Table 3.3: Thermal testing data of the SLA resins in comparison to metal.

Material	Metal	FC	FHT	RUHR	RUHT
Time to reach 100°C	62.67 s	251.33 s	157.00 s	169.33 s	191.66 s
Heating rate (to 100°C)	0.0160 s^{-1}	0.0040 s^{-1}	0.0064 s^{-1}	0.0059 s^{-1}	0.0052 s^{-1}
Max. temp achieved	213°C	136°C	152°C	157°C	142°C

Unsurprisingly, the heat transfer for all of the photoresin materials is significantly lower than that of the metal due to their poor thermal conductivity. It is, however, critical to quantify the difference between the various materials and the metal. The FC material demonstrated the lowest thermal conductivity, achieving a final temperature of only 136°C. A further observation is that it took over 3.5 times longer for the FC material to achieve a temperature of 100°C than for the metal. The FHT moulds showed an improved thermal conductivity when compared to FC. While the FHT material

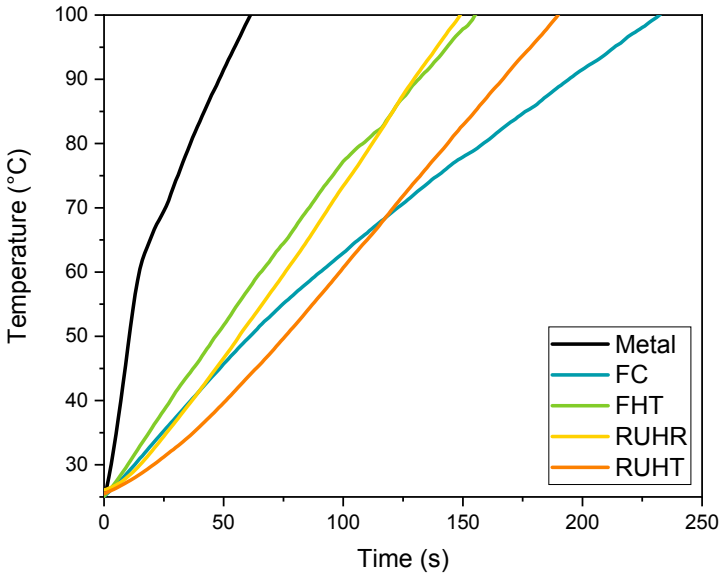

Figure 3.6: The heat uptake of the various photoresins tested from 25-100°C. Metal here refers to the metal hot plate used as a reference.

offers an improvement on the FC material, there is still a significant deficit in thermal conductivity between printed mould materials and the metal. The RUHR material behaved very similarly to the FHT and the RUHT material performed in the middle ground of the FC and FHT materials. Another interesting observation is that the rate of cooling for all of the materials trialled was very similar and was in line with the cooling of the metal hot plate (see Figure 3.7) .

3.4.3 Accuracy and Precision Study of SLA 3D Printing

Microscope images were taken to assess the accuracy and precision of the feature sizes and also the overall quality of the printed moulds (Figure 3.8). The print orientation is found to have a significant impact on the print quality. In the case of the horizontal prints, the resolution control is entirely dependent on the $x - y$-axes which is limited by the laser spot size (140 µm for the printer used in this work). The edges and corners of the cubes are not well defined, which is attributed to the inability of the rounded

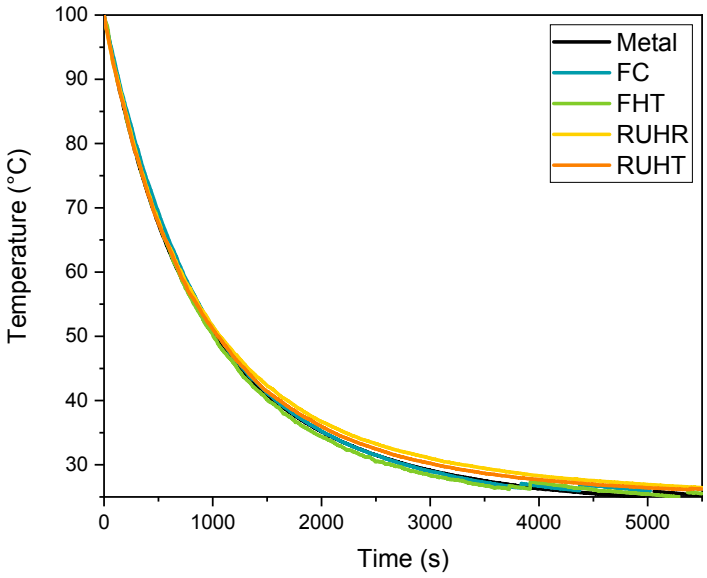

Figure 3.7: The cooling rates of the various photoresins tested from 100-25°C

laser beam to produce defined corners at this resolution (see Figure 3.8b, d and f).

For the vertical prints, sloping is observed on one side of the feature across all shapes. This is attributed to the mechanism by which the printer produces the parts. As the step-motor moves to create the next layer, excess resin pools in the printed engravings and is cured from the residual UV exposure leading to this sloped effect.

The diagonal prints showed no print quality issues and as such the diagonal orientation is recommended for further printing. Neither the feature shape nor the designed feature size has any significant impact on the accuracy or precision of the feature sizes. The print orientation however is found to considerably affect the accuracy of the feature size (Figure 3.9).

This loss of accuracy was only observed for prints from a diagonal orientation, which are dependent on both the $x-y$-axes and the z-axis resolution limits. The reduced accuracy for the diagonal print orientation can be clearly observed in Figure 3.10. The error bars for all print orientations can also be observed, demonstrating the high precision across all print orientations and micro-feature geometries.

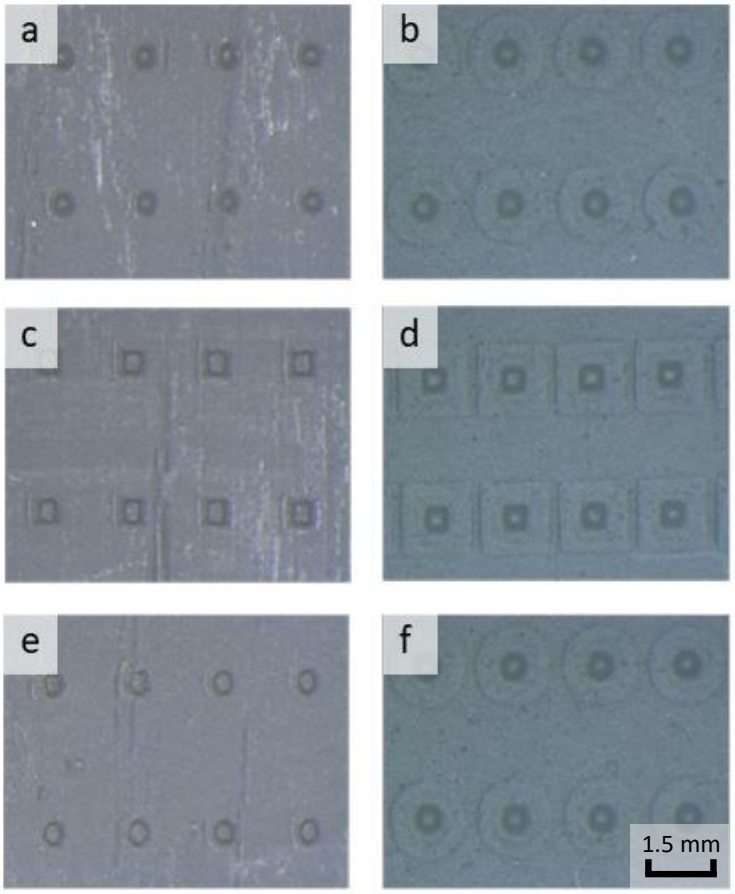

Figure 3.8: Top down microscope images of 3D prints. On the left are prints from diagonal orientation and horizontal on the right. (a,b), (c,d) and (e,f) represent the spheres, cubes and cylinders, respectively. The scale bar indicated in (f) applies to all sub-figures. Visible here are what a good quality print should look like in subfigure a, c and e. In subfigures b, d and f the limitations of the laser point size can be observed for the horizontal print orientation. Expected feature size is 0.5 mm.

Despite the accuracy issues associated with the diagonal prints, the highest print quality can be achieved with this orientation which is essential for this type of work. A scaling factor of 109.30% $\pm$ 1.74 was applied to the digital design and the parts were reprinted in a diagonal orientation (Figure 3.9). The accuracy and precision after the scaling factor had been applied was greatly improved, bringing the diagonal print orientation back in line with the horizontal and vertical orientations but with the additional benefit of better feature quality.

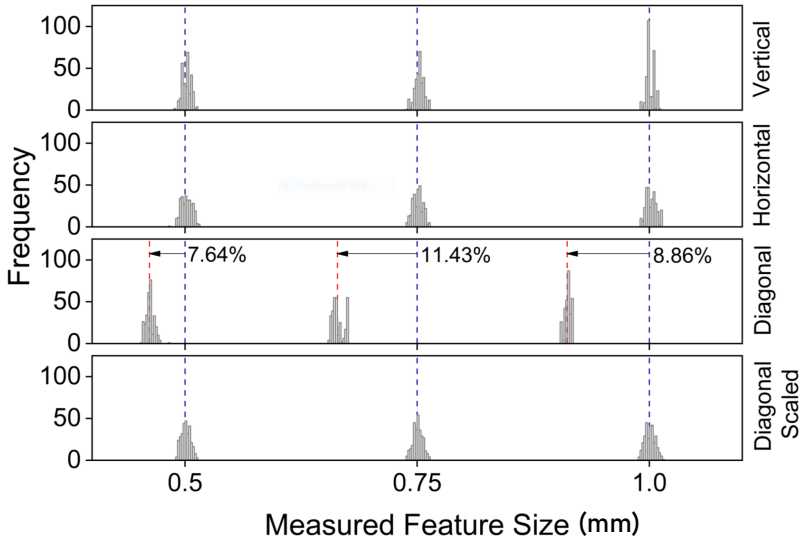

Figure 3.9: Histogram plot demonstrating the accuracy and precision of printed features for all print orientations including the scaled diagonal. A total of 300 measurements were taken for each feature size.

3.4.4 Rapid Tooling Injection Moulding

Materials were trialled in the RTIM set-up to assess their performance under the temperature and pressure loads. The maximum temperature and pressure that the printed moulds could withstand without failure were recorded. The link between the maximum temperature a material can withstand in the RTIM process and the materials HDT was investigated (Table 3.4).

Table 3.4: Data from IM tests to establish the maximum temperature and pressure that the printed mould materials can withstand before failure

Resin Code	Max. Temperature	Max. Pressure
FC	180°C	200 bar
FHT	190°C	10 bar
RUHR	180°C	10 bar
RUHT	160°C	10 bar

While the FHT material was capable of withstanding the highest temperature in the RTIM process at 190°C, the HDT of this material was significantly higher at 238°C.

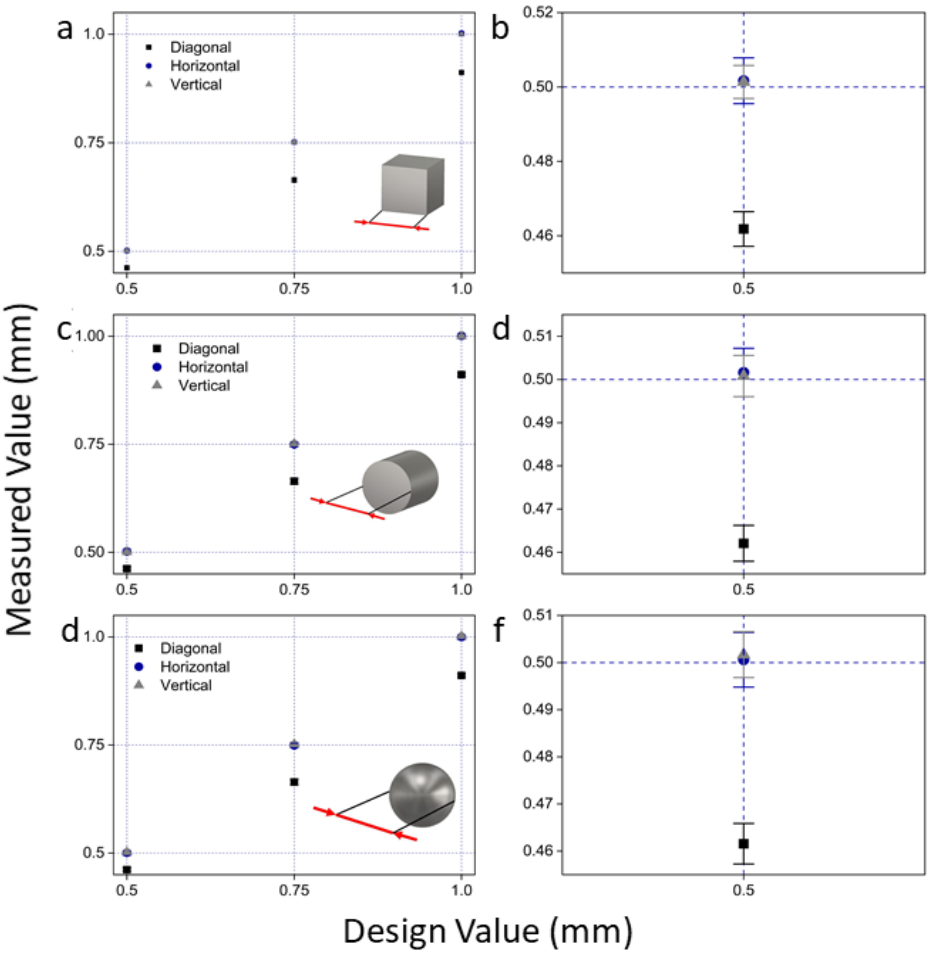

Figure 3.10: Precision and accuracy of printed features split by three different feature shapes. (a,b), (c,d) and (e,f) represent the cubes, cylinders and spheres, respectively. b, d and e demonstrate a close up of the 0.5 mm feature sizes including error bars.

It is worth noting that the HDT of a material is quoted under a given load, 0.45 MPa and 1.8 MPa in this case. The RTIM testing was conducted at a pressure of 10 bar which equates to 1 MPa and as such it is not unexpected that the maximum temperature measured in the RTIM study was found to fall between these two HDT values. It should also be noted the testing conditions are very different between the RTIM testing and the ASTM standard test for measuring the HDT (ASTM International, 2001). Taking the maximum temperature value for the RTIM experiments and plotting this alongside both HDT values from the material data sheets suggests a highly linear relationship ($R^2 = 0.9958$) between the load the material is under and what temperature it can withstand (Figure 3.11).

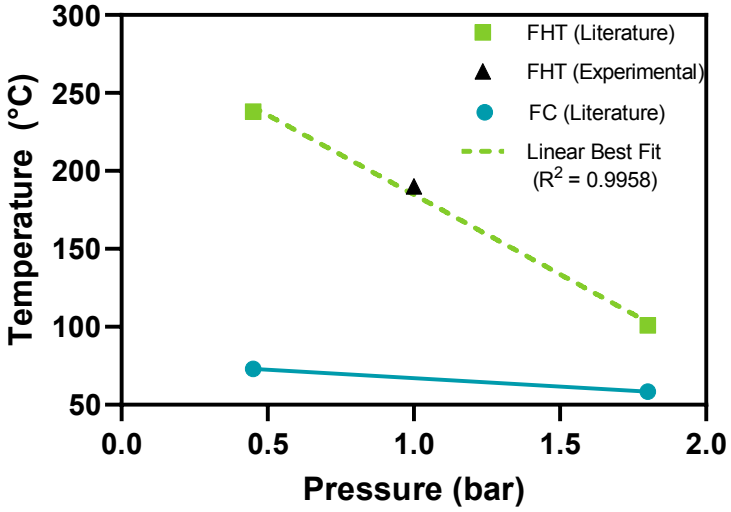

Figure 3.11: Pressure and HDT for FHT and FC using both literature and experimental data taken from Table 3.1.

This relationship is not observed for the FC material. The maximum temperature achieved in the RTIM experiments was in fact significantly higher than either HDT value. This suggests that the material is chemically different from the FHT material. It is expected that the additives in the resins which produce high HDT values ultimately result in more brittle materials making them extremely sensitive to changes in load. Based on the limited information available in the material safety data sheets for these materials, the inclusion of acrylate in the FHT resin is expected to be the cause

of these changes (Formlabs, 2016b, 2017). There is some suggestion that the inclusion of alkyl chains on the acrylate monomers increases the flexibility of the polymer produced. Additionally, increasing chain length of this alkyl component appears to further increase the flexibility (Polymer Properties Database, 2020). With the FHT resins having acrylate in place of methacrylate to some degree, this could explain the decreased flexibility and increased brittleness experienced with this polymer. It is hypothesised that this acrylate is also responsible for the higher HDT value documented for the FHT resin.

The FC material is not expected to contain such additives, and this would explain why this material performs much better than expected under load. Additionally, looking solely at the two data points provided on the material data sheets for the FC resin, the gradient of the slope is significantly lower than that for the FHT resin indicating that the FHT resin is more vulnerable to pressure (Figure 3.11).

3.5 Discussion

A number of assessments must be made in order to select a photoresin that is suitable for the desired RTIM application and identify critical process parameters such as a scaling factor for the digital design as well as heating time and pressure/temperature settings for IM. The proposed assessments and its sequence is summarised in a workflow (Figure 3.12). The aim of this workflow is to minimise the work required to rule out unsuccessful materials by systematically assessing print quality as well as mechanical, thermal and RTIM characteristics. The goal of the workflow is to achieve a robust process in which the mould material survives the RTIM process and the object produced meets the design specification. This workflow is discussed in the following based on the testing results as summarised in the radar chart in Figure 3.13. A description of each property and its significance in selecting a suitable material is provided in Table 3.5.

In Stage 1 of the workflow, prior information, such as elongation, tensile strength and HDT, should be collected to support the decisions in the later stages. The basic assumption that all materials assessed can be used successfully in SLA printing is made

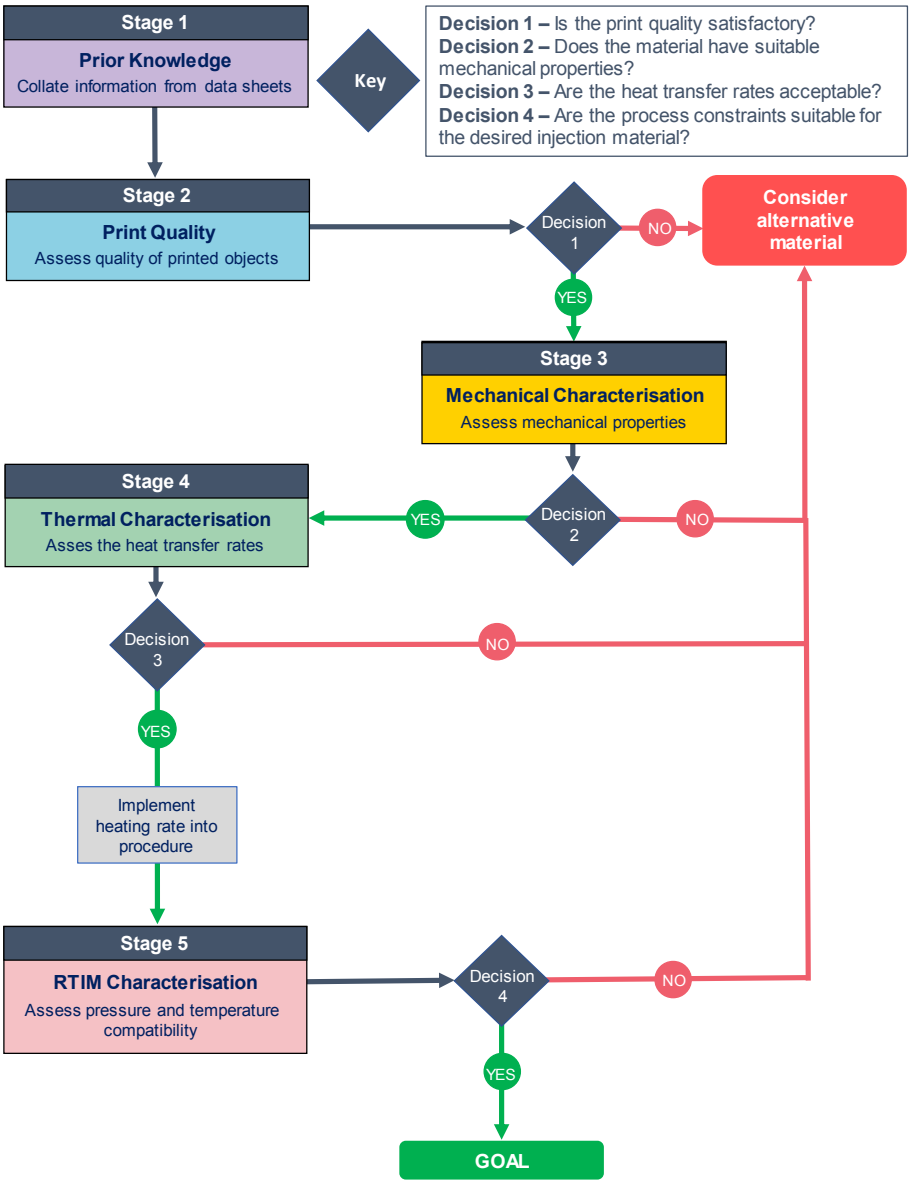

Figure 3.12: Systematic process for assessing SLA photoresins for their suitability in the RTIM process. The grey boxes indicate critical process parameters determined in the preceding stage.

in this workflow.

The mechanical characterisation (Stage 2) includes the assessment of the flexural modulus, elongation and tensile strength. The mechanical properties of the printed moulds are largely dependent on the photoresins (Figure 3.13). The tensile strength of

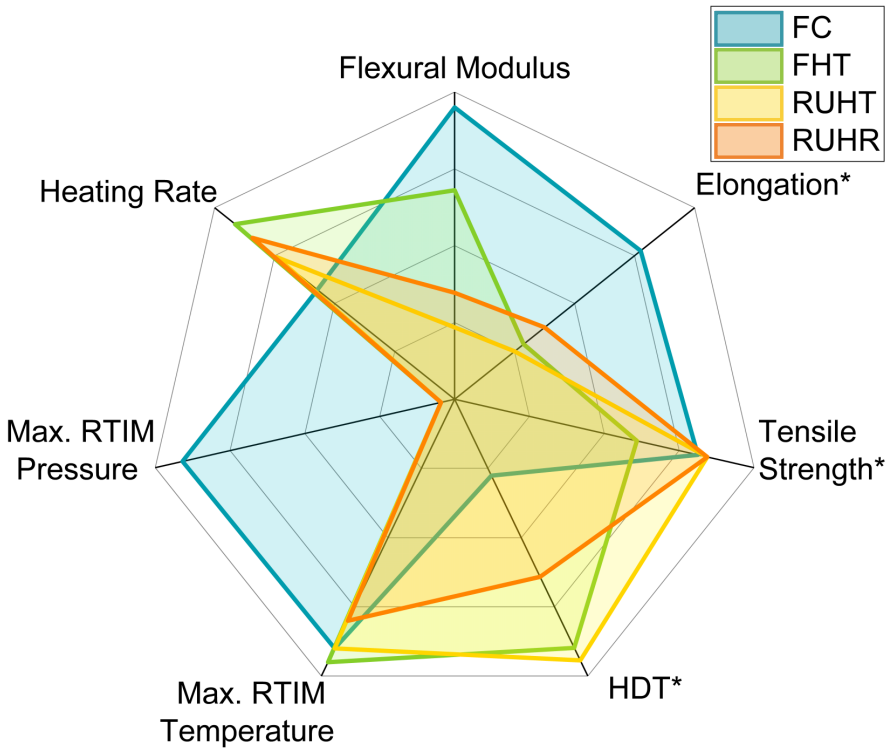

Figure 3.13: Radar chart showing a variety of material and thermal properties of printed moulds. The ranges displayed are as follows: heat deflection temperature: 0–255°C, elongation: 0–8%, tensile strength: 0–80 MPa, max. RTIM pressure: 0–250 bar, max. RTIM temperature: 0–200°C and heating rate: 0–0.008 s^{-1}. A description of each material property is given in Table 3.5. *taken from material data sheet or literature source (Formlabs, 2016b, 2017; Segurola, 2019).

the material is of interest as this is typically used as a universal measure of a materials strength. The tensile strengths of the materials tested in this work vary only marginally, which would suggest that they will all perform similarly in applications which require material strength. The flexural modulus was calculated for each material, and this data was largely in agreement with the elongation data from the literature. It is hypothesised that the flexural capabilities of a photoresin are critical for success in RTIM as a material which is able to flex in response to stress will have a much higher survival rate than a more brittle material. When assessing whether a material has suitable mechanical properties for Decision 1, all mechanical properties discussed should be considered with particular weighting on the flexural modulus and elongation. Printed moulds achieving a flexural modulus greater than 5 MPa have an increased likelihood of success in the

RTIM process.

Information on the heating of these printed mould materials is gathered in Stage 3 and used to assess two thermal aspects: 1) to determine whether the printed mould insert is able to reach a minimum required temperature for moulding, and 2) how much longer these inserts will require to reach the desired temperature in the IM process. The metal mould (containing the printed mould inserts) is placed in a holder which has a surrounding heating jacket. This heating jacket will then heat the metal mould by conduction. The heat transfer between the heating jacket and the metal mould is very efficient as both materials are metallic. The heat is then transferred to the printed mould inserts via conduction from the metal mould. This process takes significantly longer and the information on the heating rates of the different printing materials can then be considered in the form of a time delay to allow the printed mould inserts to reach the desired temperature. In addition, the IM mould insert must reach the required set temperature in order to perform a successful injection of the thermoplastic material. The material of the mould insert thus must be able to reach a minimum temperature required (Decision 3). The minimum temperature required will be linked to the molten material that is to be used in the IM process and therefore will be specific to the desired application.

Stage 4 involves the assessment of a number of factors including the accuracy and precision of feature size of printed moulds. Print setup such as orientation must be considered, and any scaling factors required should be employed. Decision 3 involves consideration of whether the relative standard deviation in the feature size measurements is acceptable for the desired application. For most pharmaceutical applications, the values achieved for the FC resin following the application of the scaling factor are acceptable (standard deviation of 0.77%).

Ultimately in order for a photoresin to be successfully utilised in RTIM, it must be able to withstand the temperatures and pressures associated with the process. The impact of a photoresin being unable to withstand higher pressures and temperatures would mean great limitations on the injection materials that can be used in conjunction with that photoresin.

Typically, HDT is used as the sole indicator of success for a photoresin used in high temperature applications. The HDT is dependent on both the temperature and the pressure that the material is exposed to. The value quoted is the maximum temperature a material can withstand before deforming under a specified load. It is therefore expected that a material having a high HDT will be better suited to high temperature applications such as RTIM.

While the test for HDT is a standardised method, it does not necessarily replicate the stress placed on a material undergoing RTIM. Stage 5 therefore determines the maximum RTIM temperature value, which is a more representative indication of how the photoresin will perform under the stress of RTIM. Comparing the HDT values of these materials with the maximum RTIM temperatures demonstrates the importance of using applicable testing methods as critical differences are observed between the materials. Looking solely at HDT, one would favour the FHT and RUHT materials while FC would be avoided due to its low HDT value. The maximum RTIM temperature data however suggests that there is no deficit for the FC material in-application. This would indicate that the HDT alone is not the critical parameter for determining what temperatures a photoresin will be able to withstand in the RTIM process. A further observation is the trade-off between HDT and elongation. To increase the HDT of a material, the elongation suffers which results in highly brittle materials.

As most molten materials for IM are typically highly viscous, this limits the application of the RTIM process if high temperatures and pressures cannot be applied. The maximum pressure that each material was able to withstand is linked to the brittleness of the printed mould material. All of the materials which aim to maximise HDT at the expense of elongation and flexural modulus were only able to withstand the minimum pressure value of 10 bar (FHT, RUHR and RUHT). FC was able to withstand up to 200 bar of pressure before failure. This supports the hypothesis that an additive included in the FHT, RUHR and RUHT resins which aims to increase HDT value ultimately results in increased brittleness and weakness under load. However, the findings of the RTIM testing (Section 3.4.4) demonstrate that there is a significant difference in the pressure the materials are able to withstand in the RTIM process, with FC being

able to withstand 20-fold the pressure of FHT, FUHT and FUHR.

Decision 4 establishes whether the pressure and temperature capabilities of the printed moulds are sufficient for use in conjunction with the desired molten material for IM. This is directly related to the properties of the molten material and is therefore very specific to the application.

The significance of each assessment stage depends on the desired application, e.g. where µm-features are required in the printed mould design Stage 4 will be of critical importance. A number of critical decision points are marked and the thresholds for these will again be highly dependent on the indented application. The order of the assessment stages is however designed to rule out potential issues with the most significant of these issues being identified first so as to minimise the work associated with a photoresin which is deemed unsuitable.

In summary, the FC resin is significantly different in both its characteristics and performance to the other resins tested. The FHT, RUHT and RUHR resins create very similar profiles on the radar chart suggesting that the chemical make-up of the polymers is highly similar. The higher flexural modulus and maximum RTIM pressure makes the FC material more suitable for the RTIM with µm features. However, it should be noted that the lower heating rate requires a longer cycle time for the IM process using the FC material compared to the other resins tested which has implications for the economics of the process.

3.6 Conclusion

A systematic workflow was developed for assessing a photoresin and identifying critical process parameters for use in RTIM. This process is designed to minimise the work required to determine whether a photoresin is suitable for the required application and to inform the printing and IM moulding setup. The recommended material of those examined in this work is FC considering mechanical, thermal and IM characteristics. It demonstrates higher resistance to the high temperatures and pressures required for the RTIM process despite having a lower HDT compared to other materials tested. Further to this, when looking for an appropriate material for RTIM, the HDT should

Table 3.5: Mechanical and thermal testing parameters including definitions and significance from both literature and experimentation.

Property	Definition	Literature vs Experimental Data	Significance in RTIM
Tensile strength	The resistance of a material to breakage under applied tension	Literature*	The tensile strength is critical for RTIM as this indicates how strong the material is. Given that the high pressures exerted on the printed mould inserts, increased strength is favourable.
Elongation	The percentage of length increase when under stress prior to breakage	Literature*	The elongation of the material is representative of the material. In RTIM, some flexibility is desirable as this helps with part removal and printed mould survival
Heat deflection temperature	The temperature at which a material deforms under a specified load	Literature*	As both pressure and temperature are key process parameters for the RTIM process, the HDT is believed to be a critical parameter however the findings from this study suggest that it does not link well to performance in RTIM.
Heating rate	The rate of thermal conduction of the material	Experimental	Allows for understanding of heat transfer through printed mould inserts which is factored into the method for IM.
Max. RTIM pressure	The maximum pressure the material could withstand without failure in the IM process at a set temperature	Experimental	More viscous injection materials typically require higher injection pressures.
Max. RTIM temperature	The maximum temperature the material could withstand without failure in the IM process at a set pressure	Experimental	A higher melt temperature is required for certain polymers and can be used to reduce material viscosity and improve the IM process.
Flexural modulus	A measure of stiffness in the initial stage of a bending test	Experimental	An increased flexural modulus will result in a more flexible material and therefore a material which is less likely to experience failure in the RTIM process.

not be considered as the lead metric. In its place should be elongation and flexural modulus as these were found to be more indicative of success in the RTIM process.

SLA was found to be a suitable technique for the production of printed mould inserts for use in RTIM as the print quality, accuracy and precision of the printed objects were of a high standard. The use of rapid tooling allows for the reduction in costs and lead time associated with traditional IM and this makes RTIM a suitable method when using iterative design.

Authorship Declaration

Erin Walsh: Conceptualisation, Methodology, Validation, Formal analysis, Data curation, Writing - original draft, Writing - review and editing, Visualisation.
Joop H. ter Horst: Conceptualisation, Writing - review and editing, Supervision.
Daniel Markl: Conceptualisation, Methodology, Resources, Writing - review and editing, Visualisation, Supervision, Project Administration, Funding acquisition.

Chapter 4

Manufacture of Oral Solid Dosage Forms with Micro-Structure Features via Rapid Tooling Injection Moulding

4.1 Chapter Summary

With advancements in the pharmaceutical industry pushing towards more tailored medicines, novel approaches to tablet manufacture are in high demand. This study demonstrates the use of rapid tooling injection moulding (RTIM) as a tablet manufacture process. Eleven polymeric formulations were trialled to produce three different tablet geometries. The surface area of these designs was altered while the volume was maintained, resulting in three different specific surface areas. Mass variability of the tablets produced was found to be low (<2% for all materials tested) and well within pharmacopoeia limits. For the majority of the formulations tested the dimensions of the tablets produced were true to the digital design. The RTIM process has demonstrated its ability to produce tablets of defined specific surface area which is of particular interest for the modification of drug release profiles. All work and writing is my own unless stated otherwise.

4.2 Introduction

The interest in manufacturing micro-scale batches of pharmaceutical products continues to heighten with the growth of the personalised medicine and clinical trials markets. The development and manufacture of products for small patient populations using traditional large scale industrial production processes is currently not cost effective and hence hinders the progress in this area. Novel technologies to manufacture micro-scale batches in a sustainable manner are needed. One such technique is additive manufacturing (AM), commonly referred to as 3D printing. This technique is able to produce tablets with complex geometries allowing formulators to adjust the dose and modify the drug release profiles by varying the specific surface area of the dosage form (Goyanes et al., 2015a; Karasulu and Ertan, 2002). Another manufacturing technology with potential to produce micro-scale batches is injection moulding (IM) coupled with hot melt extrusion (HME). IM is a widely applied manufacturing technique in the plastics industry and has been utilised in the pharmaceutical industry to produce oral solid dosage forms (Bartlett et al., 2017; Quinten et al., 2009b; Zema et al., 2012). The manufacturing benefits of using IM to make pharmaceutical drug products include reduced microbial contamination alongside greater freedom in defining the size and shape of the dosage form (Zema et al., 2012). In addition, IM allows the production of solid dispersions and solutions which can increase the rate of release of the drug and hence improve bioavailability (Quinten et al., 2009b). This aspect is critically important for current and future medicines as approximately 70% of new drug candidates in the development pipeline show poor solubility (Loftsson and Brewster, 2010).

The IM process utilises heat to encourage a thermoplastic material to adopt the desired geometry. Thermoplastics are a particularly large collection of materials with unique thermal, mechanical and electrical characteristics (Giboz et al., 2007; Heckele and Schomburg, 2004). The differing material properties of these thermoplastic materials therefore need to be understood to utilise them effectively in an IM-based process. Pressure-volume-temperature behaviour, polymer structure, morphology and material crystallinity are all material properties that will have a major impact on the IM pro-

cess (Annicchiarico and Alcock, 2014). A number of process parameters involved in IM impact the viscosity of the thermoplastic material such as shear stress, shear rate, temperature and pressure. Non-newtonian injection materials demonstrate significant changes to their melt viscosity with relatively small variation in the shear rate making the prediction of process parameters difficult. This change in melt viscosity is due to the entanglement and disentanglement of polymer chains when the external forces of the injection moulding process are applied (shear) (Kashyap and Datta, 2015).

Beside the solubility of the drug substance, the drug release of oral solid dosage forms made through IM is influenced by the formulation and the specific surface area (SSA) (Goyanes et al., 2015a; Robles Martinez et al., 2018; Quinten et al., 2009a). The SSA can be modified by adjusting the surface area of the tablet while keeping the volume constant. Alterations to the SSA can be achieved by designing micro-features into the surface of the tablet, which can be achieved using μIM. μIM is used when an object contains either a mass of a few milligrams, μm-scale features or objects where dimensional tolerances are in the μm range (but there is no dimensional limit) (Giboz et al., 2007; Packianather et al., 2015). While it is possible to make small plastic components via IM, the object rejection rate is typically high at between 30-50%. Moving to a specific μIM process reduces this rejection rate (Zhao et al., 2003). The process and the factors which affect it are universal across all forms of IM, however the impact of each factor varies significantly as you move to different sub-categories of IM. Moving from IM to μIM is not as simple as scaling down the process, with each part of the process requiring reassessment (Giboz et al., 2007). For example, there is some evidence which suggests that the viscosity of molten thermoplastics is lower in the micro-channels of a μIM mould than is measured using a capillary rheometer (Zhang and Gilchrist, 2012). The rheological behaviour of the polymer when molten or softened is particularly important in the μIM process. Molten thermoplastics are examples of non-Newtonian fluids and their viscosity is a key factor in their performance in μIM.

The injection material is typically prepared through a HME process and it is also the method of choice for μIM. HME is used to achieve molecular mixing by heating the material and applying shear stress. Similarly to IM, the viscosity of the molten mixtures

is important in HME. It must be low enough to not exceed the torque capability of the extruder but sufficiently high to allow proper mixing (Verstraete et al., 2016b). HME processing is generally possible with complex viscosity values between 1,000 and 10,000 Pa s (Verstraete et al., 2016b). Typically, a formulation that is processable by HME should also be processable by traditional IM, however a lower viscosity may be required for μIM techniques. Polymers which demonstrate good melt flow properties are typically preferred for µIM. These materials commonly have a low viscosity and include polypropylene (PP), polyethylene (PE), polyether ether ketone (PEEK) and cyclic olefin copolymer (COC) (Packianather et al., 2015). Pharmaceutical grade polymers have not been investigated with regards to their compatibility and performance in a μIM process.

The IM process (standard and micro) requires an appropriate mould that defines the shape of the final product. Traditional metal mould making is a time-consuming process which is both cost and skill exhaustive (Rani et al., 2018). In most cases this limits the optimisation of moulds, which is a crucial step in identifying a suitable product structure with micro-features that meets the performance specifications. Requirements on the fabrication of the mould and its material include the ability to create precise micro-structures and it must be sufficiently hard and ductile to survive the injection moulding process (Heckele and Schomburg, 2004). Developments in additive manufacturing have opened the door for rapid tooling in IM as an alternative to traditional metal moulds (Rani et al., 2018). Rapid tooling is defined as being the use of additive manufacturing techniques for the manufacture of moulds directly (direct tooling) or to create a pattern which is then used to manufacture a mould (indirect tooling) (Mendible et al., 2017; Qayyum et al., 2017; Rani et al., 2018). With additive manufacturing techniques now utilising photopolymers to print objects with high resolution, the potential for this technique to be used to manufacture moulds for μIM is apparent (Mohan et al., 2017). In order for these materials to be suitable for use in µIM, there must be sufficient resistance to both the temperature and pressure experienced during the injection process (Bartlett et al., 2017). Photopolymer-based additive manufacture techniques were selected due to the material properties of the

photoresins used, i.e. photoresins are expected to have high thermal resistance and superior surface quality making them a good choice for rapid tooling (Bartlett et al., 2017). Previous work by Walsh et al. (2021b) demonstrated that stereolithography (SLA) can produce mould inserts suitable for use in conjunction with IM and suggests printing recommendations for this purpose. The integration of rapid tooling and injection moulding reduces the overall cost and the lead-time that comes with using traditional metal moulds (Formlabs, 2016a; Mendible et al., 2017). The coupling of these technologies makes low production runs economically feasible and also allows for a more agile approach to research (Formlabs, 2016a; Mendible et al., 2017).

Rapid tooling μIM (RTIM) has the same criteria as μIM, but this technique has a process alteration which involves the use of additive manufacture to produce the specific mould being used. Moulding tools used in micro-injection moulding will typically comprise a mould insert with the desired micro-structure and a tool for the insert to sit in (Heckele and Schomburg, 2004). While RTIM for the manufacture of dosage forms has not been investigated to the same extent as standard IM, this technique is very promising particularly in the field of precision medicines and small batch production. RTIM allows for a rapid, iterative design process to establish the desired geometry. The use of rapid tooling in this way results in both economic and time benefits either as a direct manufacture technique for low production runs of <500 parts or as a development tool (Rahmati and Dickens, 2007).

The objectives of this work are to develop a process for producing oral solid dosage forms with micro-features designed to control SSA using the RTIM technique. Three different geometries of dosage forms were produced using ten different pharmaceutical grade polymers which are typically used in HME, IM and additive manufacture and one reference material. The processability of these materials was assessed as was the accuracy and precision of the process in reference to the digital design of the tablets.

4.3 Materials and Methods

4.3.1 Materials

Stereolithography Additive Manufacture

The photoresin used in this work is Clear v4 from Formlabs (Massachusetts, USA) based on the findings from (Walsh et al., 2021b). Isopropyl alcohol (Sigma Aldrich, USA) is used to wash the moulds post-printing.

Rapid Tooling Injection Moulding

A number of raw materials were used in this work as detailed in Table 5.1. The acronym for each material will be used throughout this manuscript to refer to a particular material.

Table 4.1: List of raw materials, their supplier details and their acronyms as used in this study.

Material	Supplier	Acronym
Affinisol HPMC HME 15LV	The Dow Chemical Company, USA	AFF
Eudragit E PO	Evonik, Germany	EPO
Klucel EF	Ashland, USA	KEF
Klucel ELF	Ashland, USA	KELF
Klucel LF	Ashland, USA	KLF
Low-density Polyethylene	Sigma Aldrich, USA	LDPE
Polyethylene	Sigma Aldrich, USA	PE
Polyethylene Glycol 4000	Sigma Aldrich, USA	PEG
Parteck MXP PVA 4-88	Sigma Aldrich, USA	PVA
Soluplus®	BASF, Germany	SOL
Sorbitol Emprove Parteck SI 150	Merck, USA	SOR
Stearic Acid	Sigma Aldrich, USA	SA

The majority of the formulations used in this work required preparation via HME to ensure molecular level mixing prior to feeding the material into the RTIM system. A series of formulations comprised solely of polymers or polymers with plasticising agents were produced and are detailed in Table 5.2.

Table 4.2: List of polymer-based formulations, their preparation method and their acronyms that will be used in this chapter. Composition ratios are given in brackets by weight. No preparation was required for LDPE as the polymer was purchased in a pelletised form.

Primary Polymer	**Plasticiser**	**Preparation Method**	**Acronym**
Affinisol	-	HME	AFF
Affinisol (85%)	Polyethylene Glycol (15%)	HME	AFF/PEG 85/15
Affinisol (85%)	Stearic acid (15%)	HME	AFF/SA 85/15
Affinisol (85%)	Polyethylene (15%)	HME	AFF/PE 85/15
Eudragit EPO (85%)	Polyethylene Glycol (15%)	HME	EPO/PEG 85/15
Klucel EF	-	HME	KEF
Klucel ELF	-	HME	KELF
Klucel LF	-	HME	KLF
Parteck MXP PVA 4-88	-	HME	PVA
Soluplus (85%)	Sorbitol (15%)	HME	SOL/SOR 85/15
LDPE	-	N/A	LDPE

4.3.2 Methods

Stereolithography Additive Manufacture

Mould inserts were printed, as previously reported, using the Form 2 (Formlabs, Massachusetts) stereolithography (SLA) printer (Walsh et al., 2021b). The moulds are printed at a 45° angle from the build platform. On completion of printing, the moulds were washed in isopropyl alcohol in an agitated wash bath for a period of 10 minutes before being left to dry completely. The moulds were then removed from the build platform and placed in the FormCure (Formlabs, Massachusetts) for 60 minutes at 60°C. Supporting material was removed and any surface roughness on the rear of the mould surface was lightly sanded.

Design of Tablet Geometries

Three different mould insert designs were produced for this study (see Figure 4.1) to modify the tablet geometry. Conical frustum shaped 'pins' (Figure 4.2c) were added to the designs in increasing number ($n = 2, 6$ or 10 for the three tablet geometries). In order to maintain the tablet mass across all three designs for a formulation, the volume

of the three designs was kept constant. The diameter of the tablet was adjusted to account for the reduction in volume resulting from the introduction of the pins. The thickness of each tablet was kept constant for all three designs as were the dimensions of each pin.

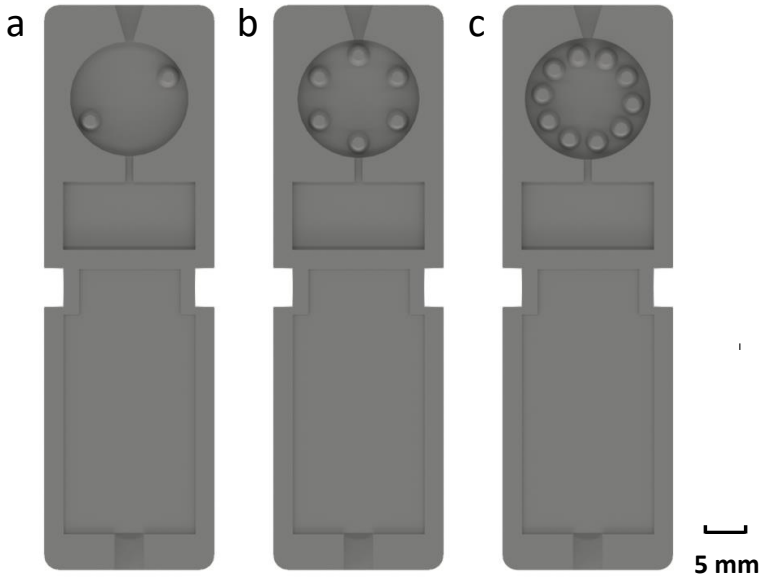

Figure 4.1: The three mould designs used in this study. a) 2 Pin b) 6 Pin c) 10 Pin.

The basic design of the tablet geometries comprised a cylindrical tablet with the conical frustum pins cut into the top surface (Figure 4.2).

The surface area of the tablets was calculated using the following equations:

$$A_{pin} = \pi \left[{r_{pin1}}^2 + (r_{pin1} + r_{pin2}) \sqrt{(r_{pin1} - r_{pin2})^2 + {h_{pin}}^2} \right] \tag{4.1}$$

Where A_{pin} is the surface area of the pin, r_{pin1} is the top radius of the pin, r_{pin2} is the bottom radius of the pin and h_{pin} is the depth of the pin.

$$A_{pinbase} = \pi {r_{pin2}}^2 \tag{4.2}$$

Where $A_{pinbase}$ is the surface area of the base of the pin and r_{pin2} is the bottom radius of the pin.

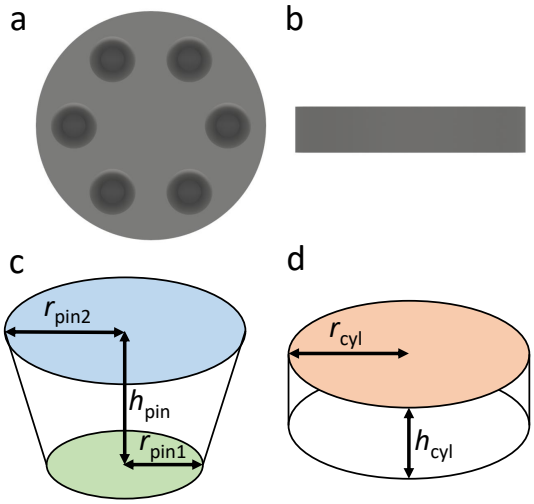

Figure 4.2: Schematic of tablet design features. a) A top and b) side view of a tablet produced from the 6 Pin design; c) design of an individual pin; d) design of the basic cylindrical tablet structure.

$$A_{cyl} = 2\pi r h_{cyl} + 2\pi {r_{cyl}}^2 \tag{4.3}$$

Where A_{cyl} is the surface area of the cylinder, h_{cyl} is the height of the cylinder and r_{cyl} is the radius of the cylinder.

Equations 4.1, 4.2 and 4.3 were combined such that:

$$\begin{aligned} A_{tab} =& 2\pi r h_{cyl} + 2\pi r_{cyl}^2 + \\ & n\pi \left[{r_{pin1}}^2 - {r_{pin2}}^2 + (r_{pin1} + r_{pin2}) \sqrt{(r_{pin1} - r_{pin2})^2 + h_{pin}^2} \right] \end{aligned} \tag{4.4}$$

Where A_{tab} is the tablet surface area, r_{cyl} is the radius of the cylinder h_{cyl} is the height of the cylinder, n is the number of pins, r_{pin1} is the top radius of the pin, r_{pin2} is the bottom radius of the pin and h_{pin} is the depth of the pin.

The volume of the tablets was calculated using the following equations:

$$V_{pin} = \frac{1}{3}\pi h_{pin} \left({r_{pin1}}^2 + {r_{pin2}}^2 + r_{pin1} r_{pin2} \right) \tag{4.5}$$

Where V_{pin} is the volume of a pin, h_{pin} is the depth of a pin, r_{pin1} is the top radius

of the pin and r_{pin2} is the bottom radius of the pin.

$$V_{cyl} = 2\pi {r_{cyl}}^2 h_{cyl} \tag{4.6}$$

Where V_{cyl} is the volume of the cylinder, r_{cyl} is the radius of the cylinder and h_{cyl} is the thickness of the cylinder.

Equations 4.5 and 4.6 were combined such that:

$$V_{tab} = 2\pi {r_{cyl}}^2 h_{cyl} - \left(\frac{1}{3}\pi n h_{pin}\left({r_{pin1}}^2 + {r_{pin2}}^2 + r_{pin1}r_{pin2}\right)\right) \tag{4.7}$$

Where V_{tab} is the tablet volume, r_{cyl} is the radius of the cylinder, h_{cyl} is the thickness of the cylinder, n is the number of pins, h_{pin} is the depth of the pin, r_{pin1} is the top radius of the pin and r_{pin2} is the bottom radius of the pin.

The specific surface area was calculated using:

$$SSA_{tab} = \frac{A_{tab}}{V_{tab}} \tag{4.8}$$

Where $SSA_(tab)$ is the specific surface area of a tablet, A_{tab} is the surface area of the tablet and V_{tab} is the volume of the tablet.

While the introduction of pins on the surface of the tablets increases the surface area of the dosage form, it also decreases the volume. In order to compensate for this volumetric deficit, the radius of the cylindrical component of the dosage forms is increased. To determine the radius required to ensure constant volume across the dosage forms, the following equation is used:

$$r_{cyl} = \sqrt{\frac{n\pi h_{pin}{r_{pin1}}^2 + n\pi h_{pin}r_{pin1}r_{pin2} + n\pi h_{pin}{r_{pin2}}^2 + 3V_{tab}}{6\pi h_{cyl}}} \tag{4.9}$$

Where r_{cyl} is the radius of the cylinder, n is the number of pins, h_{pin} is the depth of the pin, r_{pin1} is the top radius of the pin, r_{pin2}, V_{tab} is the volume of the tablet and h_{cyl} is the height of the cylinder.

Full details of the tablet dimensions produced from these designs can be found in

Table 5.3.

Table 4.3: Summary table of tablet dimensions.

Design Feature	**2 Pin Design**	**6 Pin Design**	**10 Pin Design**
Diameter (mm)	15.23	15.69	16.12
Thickness (mm)	3	3	3
Volume (mm^3)	530.03	529.82	529.80
Surface Area (mm^2)	527.48	592.76	658.08
Number of Pins	2	6	10
Pin Depth (mm)	2	2	2
Pin Radius 1 (mm)	1.5	1.5	1.5
Pin Radius 2 (mm)	0.75	0.75	0.75
Specific Surface Area (mm^{-1})	1.00	1.12	1.24

Error Propagation

All measurements have associated uncertainties, and these are not equal across differing measurements. Acknowledgement of these uncertainties and the correct combination of these is essential to produce accurate and reliable results. The propagation of errors is employed where equations are applied and the variables within that function have their own individual uncertainties. In any case where an equation contains more than one variable, error propagation is the only way to accurately determine the uncertainty of the calculated value.

In principle, the below relationship is employed to determine the relationship between the individual variables and their uncertainties and the overall uncertainty of the calculated value.

$$\sigma_x = \sqrt{\left(\frac{\delta x}{\delta a}\right)^2 \sigma_a^2 + \left(\frac{\delta x}{\delta b}\right)^2 \sigma_b^2 + \left(\frac{\delta x}{\delta c}\right)^2 \sigma_c^2} \tag{4.10}$$

Where σ_x represents the uncertainty of the calculated value, δx is the calculated value of the equation, δa, δb and δc are the measured variables and σa, σb and σc are the uncertainties of the measured variables.

In order to propagate the errors for any value calculated using Equation 4.4, the

following derivations were calculated and applied to Equation 4.16.

$$\frac{\delta A_{tab}}{\delta h_{cyl}} = 2\pi r_{cyl} \tag{4.11}$$

$$\frac{\delta A_{tab}}{\delta h_{pin}} = \frac{n\pi h_{pin}\left(r_{pin1}+r_{pin2}\right)}{\sqrt{\left(r_{pin1}-r_{pin2}\right)^2+{h_{pin}}^2}} \tag{4.12}$$

$$\frac{\delta A_{tab}}{\delta r_{cyl}} = 2\pi(2r_{cyl}+h_{cyl}) \tag{4.13}$$

$$\frac{\delta A_{tab}}{\delta r_{pin1}} = n\pi[\sqrt{\left(r_{pin1}-r_{pin2}\right)^2+{h_{pin}}^2}+\frac{\left(r_{pin1}-r_{pin2}\right)\left(r_{pin1}+r_{pin2}\right)}{\sqrt{\left(r_{pin1}-r_{pin2}\right)^2+{h_{pin}}^2}}+2r_{pin1}] \tag{4.14}$$

$$\frac{\delta A_{tab}}{\delta r_{pin2}} = n\pi[\sqrt{\left(r_{pin1}-r_{pin2}\right)^2+{h_{pin}}^2}+\frac{\left(r_{pin1}-r_{pin2}\right)\left(r_{pin1}+r_{pin2}\right)}{\sqrt{\left(r_{pin1}-r_{pin2}\right)^2+{h_{pin}}^2}}-2r_{pin2}] \tag{4.15}$$

$$\begin{aligned}\sigma_{A,tab} = \Bigg[&\left(\frac{\delta V_{tab}}{\delta h_{cyl}}\right)^2\sigma^2_{h_{cyl}}+\left(\frac{\delta V_{tab}}{\delta h_{pin}}\right)^2\sigma^2_{h_{pin}}+\left(\frac{\delta V_{tab}}{\delta r_{cyl}}\right)^2\sigma^2_{r_{cyl}}\\&+\left(\frac{\delta V_{tab}}{\delta r_{pin1}}\right)^2\sigma^2_{r_{pin1}}+\left(\frac{\delta V_{tab}}{\delta r_{pin2}}\right)^2\sigma_{r^2_{pin2}}\Bigg]^{1/2}\end{aligned} \tag{4.16}$$

In order to propagate the errors for any value calculated using Equation 4.7, the following derivations were calculated and applied to Equation 4.22.

$$\frac{\delta V_{tab}}{\delta h_{cyl}} = 2\pi {r_{cyl}}^2 \tag{4.17}$$

$$\frac{\delta V_{tab}}{\delta h_{pin}} = -\frac{1}{3}n\pi\left({r_{pin1}}^2+{r_{pin2}}^2+r_{pin1}r_{pin2}\right) \tag{4.18}$$

$$\frac{\delta V_{tab}}{\delta r_{cyl}} = 4\pi h_{cyl}r_{cyl} \tag{4.19}$$

$$\frac{\delta V_{tab}}{\delta r_{pin1}} = -\frac{1}{3}n\pi h_{pin}\left(2r_{pin1}+r_{pin2}\right) \tag{4.20}$$

$$\frac{\delta V_{tab}}{\delta r_{pin2}} = -\frac{1}{3}n\pi h_{pin}\left(2r_{pin2}+r_{pin1}\right) \tag{4.21}$$

$$\sigma_{V,tab} = \left[\left(\frac{\delta V_{tab}}{\delta h_{cyl}} \right)^2 \sigma_{h_{cyl}}^2 + \left(\frac{\delta V_{tab}}{\delta h_{pin}} \right)^2 \sigma_{h_{pin}}^2 + \left(\frac{\delta V_{tab}}{\delta r_{cyl}} \right)^2 \sigma_{r_{cyl}}^2 + \left(\frac{\delta V_{tab}}{\delta r_{pin1}} \right)^2 \sigma_{r_{pin1}}^2 + \left(\frac{\delta V_{tab}}{\delta r_{pin2}} \right)^2 \sigma_{r_{pin2}}^2 \right]^{1/2} \tag{4.22}$$

In order to propagate the errors for any value calculated using Equation 4.8, the following derivations were calculated and applied to Equation 4.25.

$$\frac{\delta SSA_{tab}}{\delta A_{tab}} = \frac{1}{V_{tab}} \tag{4.23}$$

$$\frac{\delta SSA_{tab}}{\delta V_{tab}} = \frac{A_{tab}}{{V_{tab}}^2} \tag{4.24}$$

$$\sigma_{SSA,tab} = \sqrt{\left(\frac{\delta SSA_{tab}}{\delta A_{tab}} \right)^2 \sigma_{A_{tab}}^2 + \left(\frac{\delta SSA_{tab}}{\delta V_{tab}} \right)^2 \sigma_{V_{tab}}^2} \tag{4.25}$$

Rapid Tooling Injection Moulding

The RTIM process couples SLA with IM. Mould inserts, produced via SLA, are housed within a metal mould casing (Figure 5.1). Also visible are a number of design features on the printed mould insert to make it suitable for use in the RTIM process. The tablet cavity is the section of the mould insert which will produce the tablet. The air cavity provides an overfill space for any excess injection material and offers a space for the air to compress upon moulding. The removal points can be found on each side of the mould, these aid in removing the mould inserts from the metal moulds. The separation point at the bottom of the mould inserts is used to separate the two halves of the mould insert.

The two halves of the metal mould were pieced together and placed into the HAAKE MiniJet Pro Piston Injection Moulding System (Thermo Fisher Scientific, USA) which is an upright air-pressurised injection moulder. The injection material is placed into the melt cylinder, the piston is attached and this is then placed into the injection moulder.

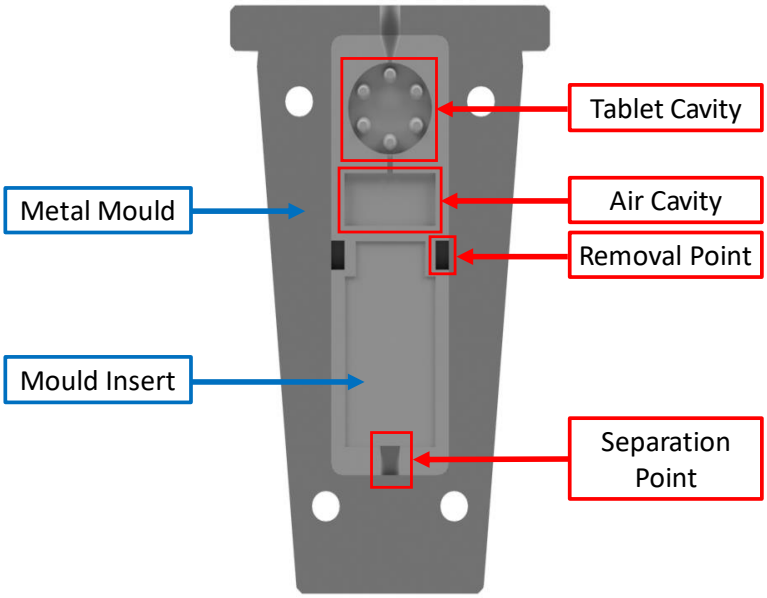

Figure 4.3: The mould insert for the 6 Pin Design inserted into the metal mould. This depiction represents one half of the full mould.

A number of processing parameters must be set:

- Cylinder temperature to which the injection material will be heated to.
- Mould temperature to which the mould will be heated to.
- Injection pressure which will be applied to the piston to move the injection material into the mould.
- Injection time is the length of time for which the injection pressure will be applied.
- Hold pressure which will be applied after the injection material has filled the mould.
- Hold time is the length of time for which the hold pressure will be applied.

These processing parameters vary for different injection materials (see Table 5.4). For all formulations the injection time, hold pressure and hold time were kept constant at 10 s, 50 bar and 10 s, respectively.

Table 4.4: RTIM process parameters used for each of the formulations. Formulations marked with * required the addition of an aerosol silicone-based lubricant to aid removal from the mould.

Formulation	**Cylinder Temp**	**Mould Temp**	**Injection Pressure**
AFF*	N/A	N/A	N/A
AFF/PEG 85/15*	200 °C	100 °C	150 bar
AFF/SA 85/15*	180 °C	100 °C	150 bar
AFF/PE 85/15*	180 °C	100 °C	150 bar
EPO/PEG 85/15*	N/A	N/A	N/A
KEF	140 °C	70 °C	150 bar
KELF	140 °C	70 °C	150 bar
KLF	140 °C	70 °C	150 bar
LDPE	150 °C	100 °C	150 bar
PVA*	200 °C	70 °C	200 bar
SOL/SOR 85/15*	N/A	N/A	N/A

A number of formulations (see formulations marked with * in Table 5.4) required the application of a silicone based lubricant onto the surface of the mould inserts to aid removal of the injected material. Upon completion of injection, the metal mould is removed from the injection moulder, the metal mould opened and the mould insert removed. When sufficiently cooled, the mould insert is opened and the tablet removed from the mould cavity.

Gravimetric Analysis

All tablets were weighed on a four decimal point balance (Entris II, Sartorius). The masses reported reflect the average of each batch produced. The mean and standard deviations reported are for $n = 60$ tablets (LDPE) or $n = 18$ (all other formulations).

Dimensional Analysis

The diameter and thickness of each tablet was measured using a digital calliper (Scienceware Digi-Max, Sigma Aldrich). A total of three diameter and three thickness measurements were taken for each tablet, the measurements shown are an average of

these replicates. The mean and standard deviations reported were $n = 60$ for LDPE and $n = 18$ for all other formulations.

Optical Coherence Tomography

A spectral-domain optical coherence tomography (OCT) system (GAN600 Series, Thorlabs, New Jersey, USA) equipped with a LK3-BB (focal length: 36 mm) was used to measure the actual pin dimensions. OCT produces cross-sectional images of a sample which can be used for depth measurements. The lateral resolution is ≈4 µm, the axial resolution in air is ≈3 µm and the image size is a 1024 x 1024 pixels with a x-axis pixel size of 5.86 µm and a y-axis pixel size of 1.95 µm. The OCT probe was focused over the pins on the tablet surface and a 2D cross-section image was acquired. The focus is adjusted to ensure a strong signal. The diameters (see Figure 4.2c) at both the top and bottom surfaces and the depth of the pins were measured. The mean and standard deviations are reported for 18 samples for all formulations.

4.4 Results

4.4.1 Gravimetric Analysis

The mass across the three designs was designed to be constant for a given formulation as the volume was constant across the three tablet geometries. Variations of the calculated volume across the three designs were <2.5% across all formulations (See Figure 4.4 and Table 7.1, 7.2 and 7.3 in Appendix A).

No data is shown for the AFF, EPO/PEG 85/15 and SOL/SOR 85/15 formulations as they were unprocessable via this RTIM process due to adhesion of the polymer to the mould surface. The average mass varied between formulations due to different true densities of the materials used (as can be observed in Figure 4.4). The variation in mass observed across all formulations and all designs was well within the pharmacopoeia standards (± 5% of the tablet core weight) for tablet mass variation (Figure 4.5a)(The International Pharmacopoeia, 2019). Figure 4.5b demonstrates the tablet to tablet variability within the LDPE tablets. A total of 60 tablets are displayed showing that

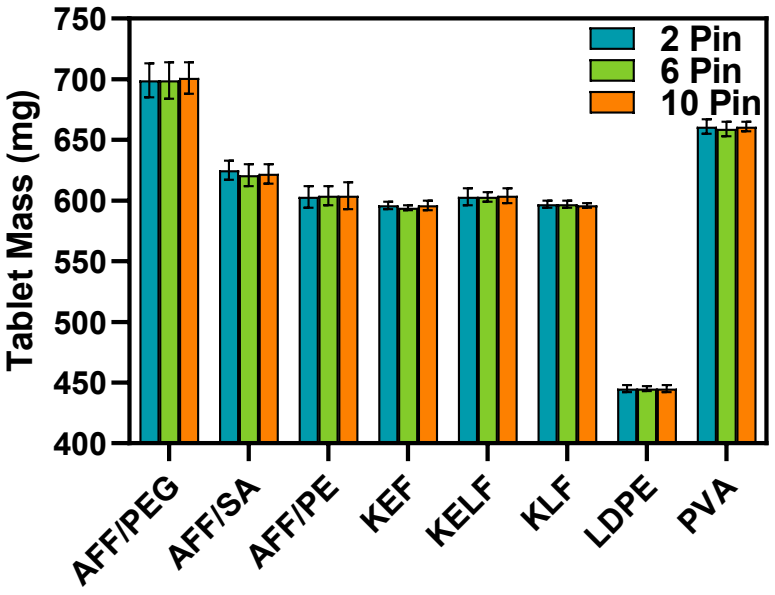

Figure 4.4: The average mass for all formulations. Error bars shown represent the standard deviation.

even within this larger batch size, the mass variation is low (±0.58%) and the RTIM process produces consistent and uniform tablets.

Generally, a higher degree of variation was observed for the Affinisol-based formulations (Figure 4.5c). This was attributed to the difficulty in processing these tablets. These formulations had a tendency to stick to the mould surface if not removed while warm leading to a reduced uniformity of mass compared to the other formulations tested. While the AFF/PEG formulation had the highest standard deviation across all formulations (±1.87%), the masses still fell within the pharmacopoeia limits (Figure 4.5c).

4.4.2 Dimensional Analysis

All formulations demonstrated high accuracy and precision to the digital designed thickness value of 3 mm, i.e. <99.84% of designed value with a standard deviation of ±0.88% across all formulations and geometries. The Affinisol-based formulations produced val-

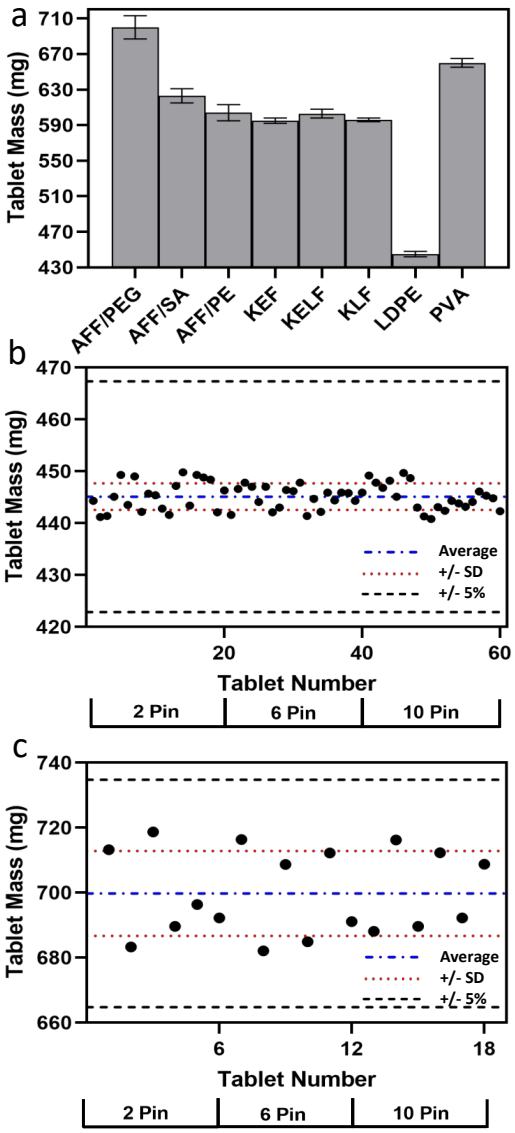

Figure 4.5: Tablet mass of RTIM tablets. a) The average mass of all tablets for each formulation. Error bars represent the standard deviation ($n = 60$ for LDPE, $n = 18$ for all other formulations). b) The mass of 60 LDPE tablets and c) the mass of 18 AFF/PEG tablets. For b) and c), the blue dotted lines represent the average tablet weight of this batch with the upper and lower red dotted lines being the average plus or minus the standard deviation respectively. The black dotted lines represents the upper and lower pharmacopoeia limit (in this case taken as tablet weight ±5%).

ues slightly higher than the design value (100.70% of design) and the measurements had a slightly higher standard deviation (±0.81%) than for non-AFF based formulations

(±0.30%) which is attributed to the difficulty associated with processing these formulations as previously discussed. As above, no data is shown for the AFF, EPO/PEG 85/15 and SOL/SOR 85/15 formulations.

With the exception of LDPE, all formulations demonstrated good accuracy and precision to the digital designed diameter values across all three tablet geometries (range from 98.68% ±0.42% to 99.71% ±0.23% of the intended values). The LDPE tablets were found to be consistently below the designed diameter values across all three designs (on average 96.61% of the designed values).

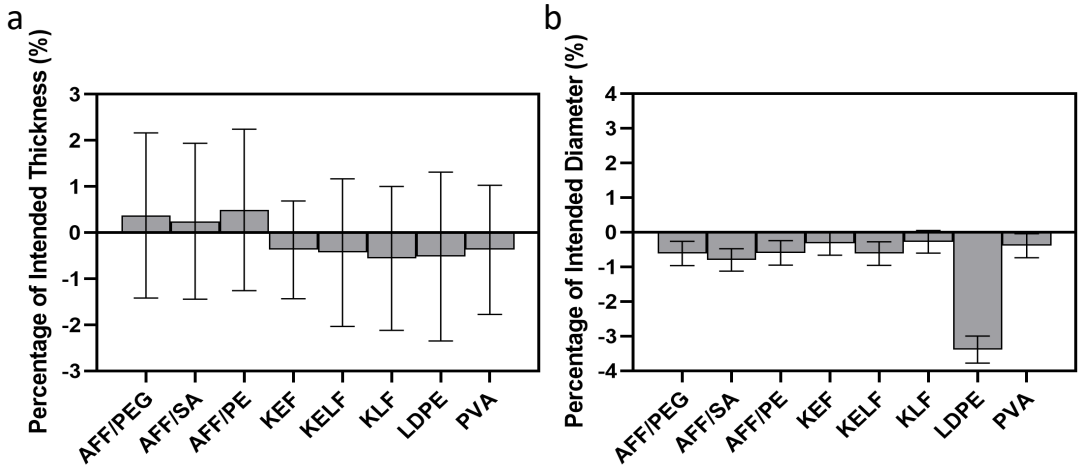

Figure 4.6: a) The average tablet thickness for all formulations b) The average tablet diameter for all formulations. a-b) Error bars shown represent the standard deviation.

The depth, top diameter and bottom diameter of the pins in all three geometries were measured using OCT. Both the depth of the pins and the bottom diameter (as seen in Figure 4.7a and c respectively) were below the expected values across all formulations. The top diameter of the pins (as seen in Figure 4.7b) was generally above the expected value of 3 mm across all formulations with the exception of LDPE. While the measured values deviated slightly from the designed values, the low values of the standard deviations across all measurements suggest that the variability within the batches was small.

Figure 4.8 displays the three tablet geometries for the LDPE, PVA, AFF/PEG and AFF/SA formulations. It is worth noting that for the AFF based formulations, the

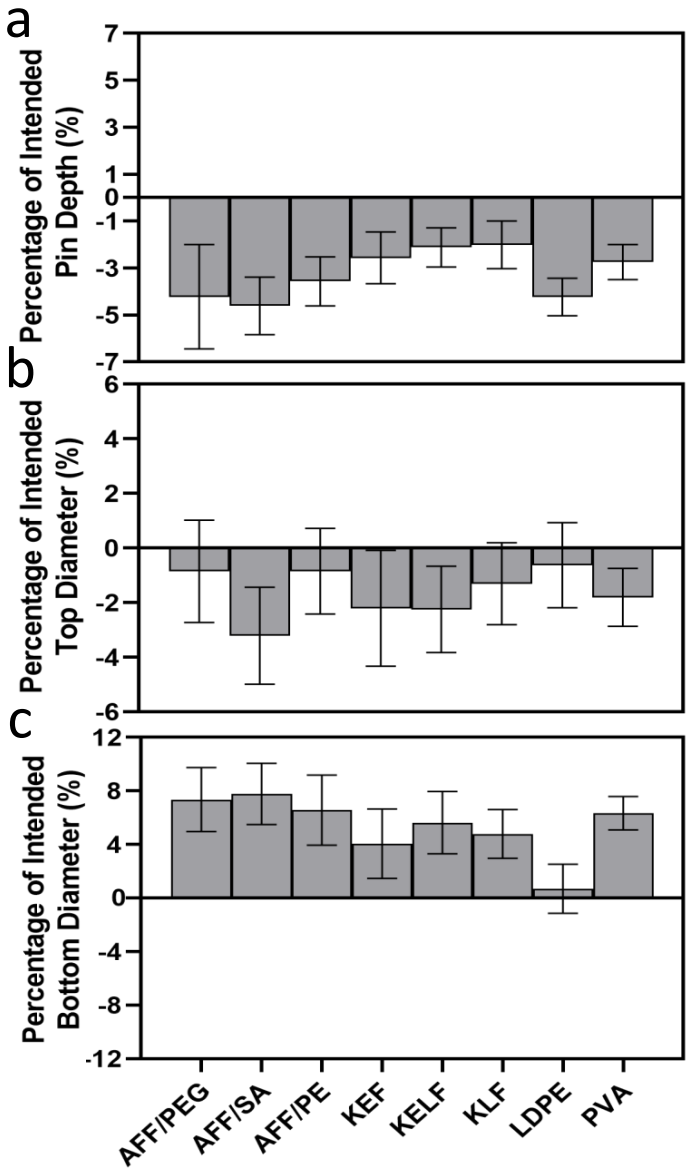

Figure 4.7: Tablet pin characteristics measured by OCT. a) The depth of the pins on the tablet surface (h_{pin} from Figure 4.2c) b) The top surface diameter of the pins on the tablet surface ($2 \times r_{\text{pin1}}$ from Figure 4.2c) c) The bottom surface diameter of the pins on the tablet surface ($2 \times r_{\text{pin2}}$ from Figure 4.2c). a-c: for each bar $n = 6$ measurements with the error bars representing the standard deviation.

RTIM process is not considered optimised and the colouration on the tablets produced is indicative of thermal degradation of the AFF polymer. Reduction of the processing temperatures would reduce this polymeric degradation and result in dosage forms

having a lighter colour.

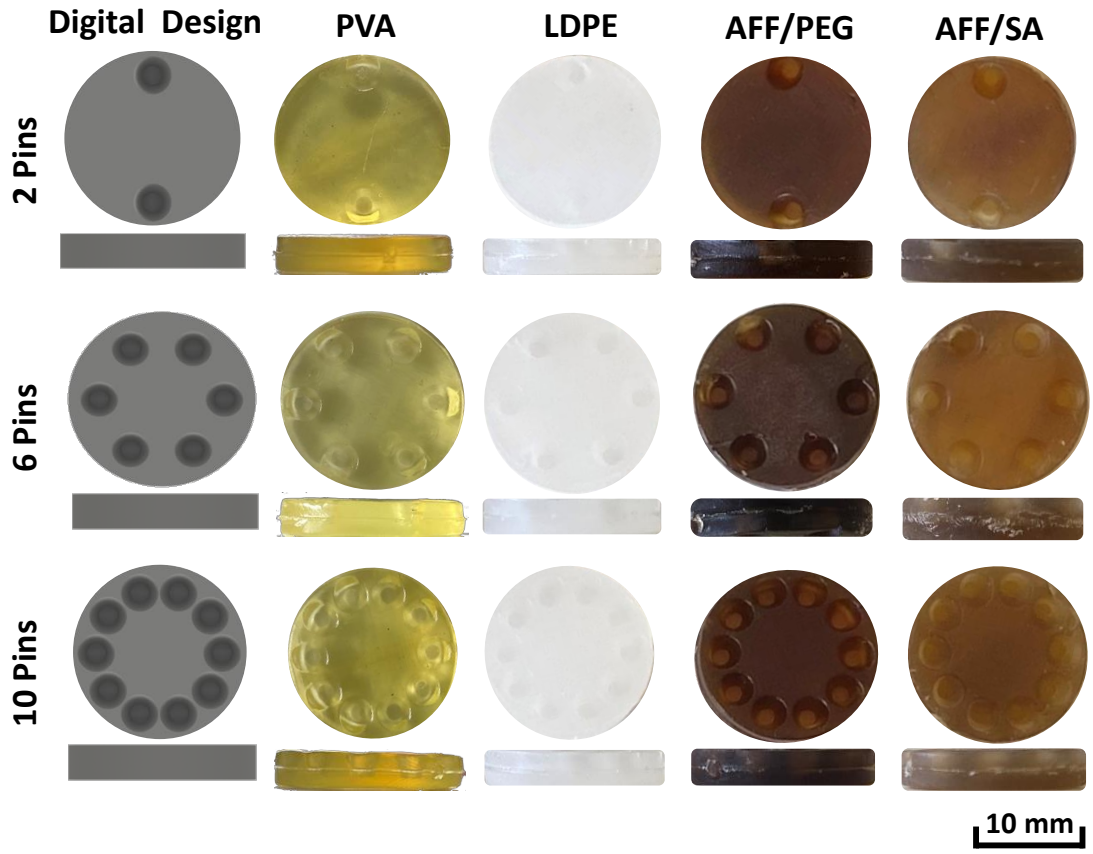

Figure 4.8: Physical tablets produced for four of the formulations trialled.

4.5 Discussion

4.5.1 Formulation Processability in RTIM

Three of the formulations trialled were deemed to be unprocessable: AFF, EPO/PEG 85/15 and SOL/SOR 85/15. For the AFF formulation, the main challenge was associated with the temperatures and pressures required to process the material. The temperatures and pressures required to achieve a workable viscosity of the formulation were too high for the mould materials to withstand, causing fracture of the plastic mould inserts and ultimately resulting in an unsuccessful RTIM process. EPO/PEG 85/15 and SOL/SOR 85/15, adhered strongly to the surface of the printed mould.

While this is an issue that was encountered with a number of other formulations (those marked with * in Table 5.4), the addition of the silicone-based lubricant was not able to overcome the issues for these formulations. For the EPO/PEG 85/15 and SOL/SOR 85/15 formulations a number of processing parameters were trialled including varying the temperatures for both the cylinder and the mould, reducing the injection pressure and the injection time. No successful processing conditions could be found for these materials in this specific RTIM process. The extent of the adhesion to the printed mould surface was such that the two mould halves were fused together. As such, removal of the tablets from these moulds was not possible and the formulations were deemed unprocessable.

4.5.2 Physical Parameters of the Tablets

Mechanical testing on the tablets produced was not possible as the maximum break force that could be applied by the available equipment was insufficient to break these tablets.

From the dimensional analysis (including OCT), the surface area, volume and specific surface area (Figure 4.9) were calculated using Equations 4.4, 4.7 and 4.8. A number of equations were combined to achieve these. Error propagation was also performed for these calculated values.

Theoretically, all formulations should produce physical parameters which match the digital design. The digitally designed volume was constant across the three geometries, while the surface area and specific surface area increased with the increased number of pins.

There are a number of factors which create uncertainty in these calculated values. Primarily, there is an inherent uncertainty that arises from the printing of the plastic mould inserts which was extensively studied in (Walsh et al., 2021b). Additionally, there are measurement errors associated with the different techniques used to measure the dimensions of the tablets. The uncertainty arising from the measurements alone attributes 22.79% of the uncertainty on volume, 24.11% for surface area and 22.82% for specific surface area. Finally, there are errors associated with the different formulations

used. This is most apparent when looking at the mass variability of the formulations, where some have significantly higher standard deviations than others. The only variable changed in that case is the formulation so it can be assumed that the difference in standard deviation is attributed solely to the formulation differences. These formulation differences are likely driven by varying polymer structures, rheology and interactions between polymer and plasticiser.

Figure 4.9a-c depicts the calculated values for surface area, volume and specific surface area for all formulations. With the exception of LDPE, both the surface area and volume data demonstrate a high degree of both accuracy and precision to the digital design. The LDPE formulation was found to have a lower surface area and volume than the digital design. The accuracy of the LDPE formulation was therefore lower than the others tested however the precision of the measurements remained high. As polyethylene (and therefore LDPE) is a semi-crystalline thermoplastic, this can be attributed to shrinkage on cooling which is characteristic of crystalline polymers (De Santis et al., 2010). While the shrinkage resulting in a reduced diameter was clear, there was some evidence of the thickness value also being lower than anticipated and lower than all other formulations tested. This shrinkage is expected to be highest on the longest axis which for these designs would be the diameter. This shrinkage is due to the crystallinity within the LDPE, which increases the packing of the polymer below its melting temperature. This increased packing results in the polymer occupying less space, and thus shrinkage is observed. The specific surface area demonstrated high accuracy and precision across all formulations trialled. Even in the case of LDPE, where reduced accuracy was observed for surface area and volume, the deficit to both was such that the specific surface area fell much closer to the digitally designed value.

The relationship between the number of pins featured in the design and the resultant specific surface area is highly linear producing an R^2 of 0.99 based on the data collected for all formulations trialled in this study (Figure 5.7). This indicates that further modification of the specific surface area could be achieved via this pin-based approach with a high degree of accuracy.

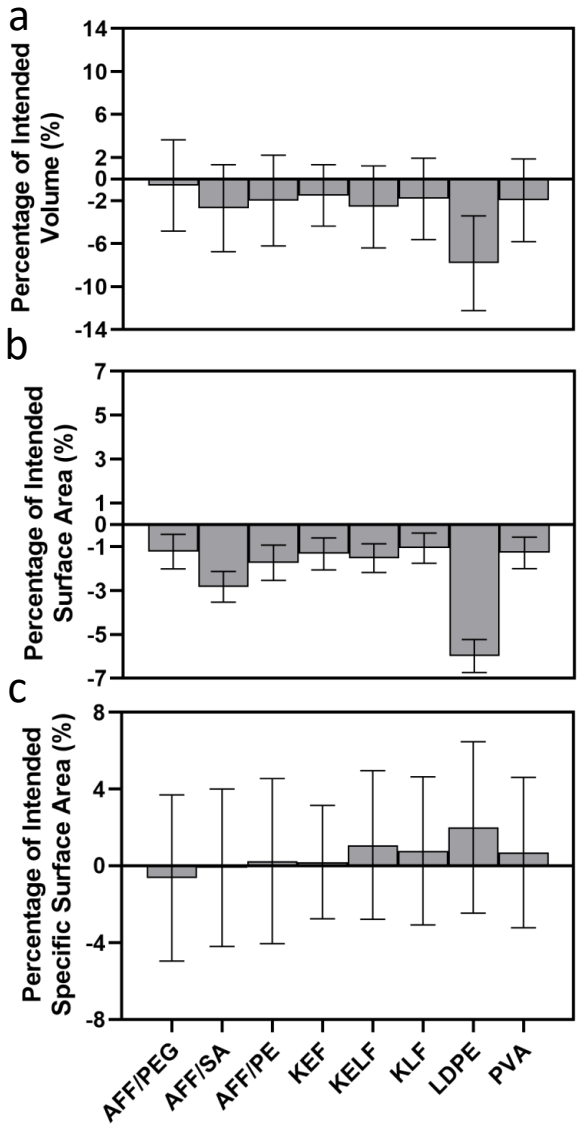

Figure 4.9: Analysis of the actual surface area, volume and specific surface area compared to the digital design. a) The average surface area for each formulation as calculated by Equation 4.4. b) The average volume for each formulation as calculated by Equation 4.7. c) The average specific surface area for each formulation as calculated by Equation 4.8. a-c: for each bar, $n = 18$ tablet with the error bars representing the propagated standard deviation.

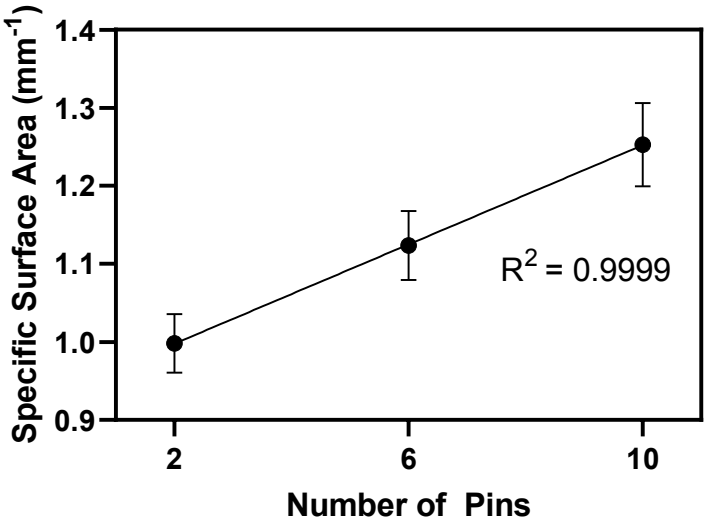

Figure 4.10: The average specific surface area for all formulations vs. the number of pins in the tablet geometry. Note that the R^2 is based on three data points.

4.5.3 Comparison to Similar Techniques

A number of publications have reported success in producing tablets via AM techniques such as fused deposition modelling (FDM) (Goyanes et al., 2014, 2015b, 2016; Ibrahim et al., 2019; Goyanes et al., 2015a) and stereolithography (SLA) (Robles Martinez et al., 2018).

The relative standard deviation reported in Figure 4.11 demonstrates that the tablets produced using the RTIM method as described in this work have a lower mass variability than other tablets produced via AM techniques (FDM or SLA). While both FDM and SLA are AM techniques based on a layer-by-layer building process, the associated resolutions can be quite different. Typically, FDM has a lower resolution than SLA, ultimately resulting in a less accurate and precise printing process particularly for small features or objects. The RTIM process is formative, producing the tablets via a mould insert created via SLA. As such, the actual formation of the tablet does not depend on a resolution limited additive manufacture process. These differences in manufacture process are also responsible for the differences in surface roughness that can be observed between tablets directly produced from FDM and those produced via

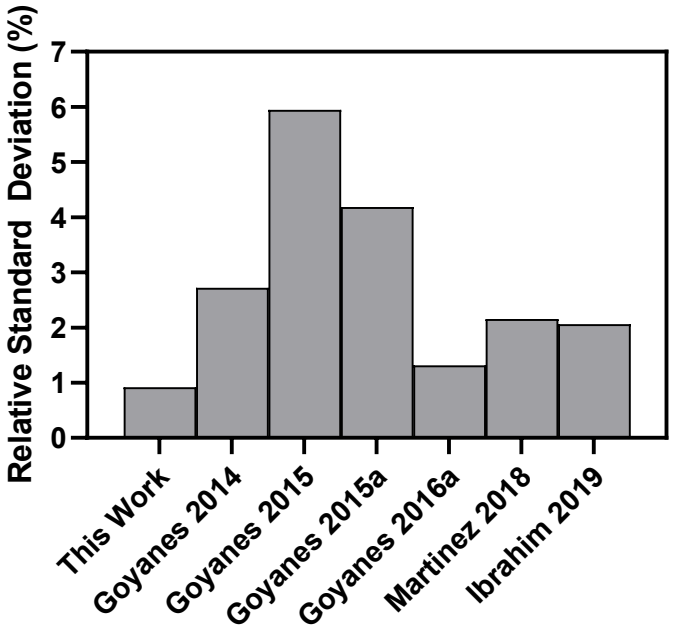

Figure 4.11: The relative standard deviation of tablet masses from this work and a number of similar manuscripts. From left to right, the manuscripts referenced are Goyanes et al. (2014), Goyanes et al. (2015b), Goyanes et al. (2015a), Goyanes et al. (2016), Robles Martinez et al. (2018) and Ibrahim et al. (2019).

RTIM. FDM tablets have significantly higher uncontrolled surface roughness and pore structure. Both surface roughness and pore structure variations makes the accuracy of surface area (and therefore specific surface area) for tablets produced via FDM much harder to achieve and very difficult to correctly measure in the tablets produced.

The accuracy and precision of the surface area of PVA based tablets produced via RTIM were higher than that of the tablets produced via FDM (Figure 4.12) (Goyanes et al., 2015a). There are slight formulatory differences, with the PVA formulation used by Goyanes et al. containing approximately 4% w/w paracetamol opposed to the pure PVA formulation used in this study. However, it is not expected that this was responsible for the difference in accuracy and precision. The difference observed was attributed to the techniques involved in producing the tablets. There will be limitations in terms of the accuracy in the FDM process, such as nozzle size and layer height, and the geometry printed can also diverge from the digital design as the printed material

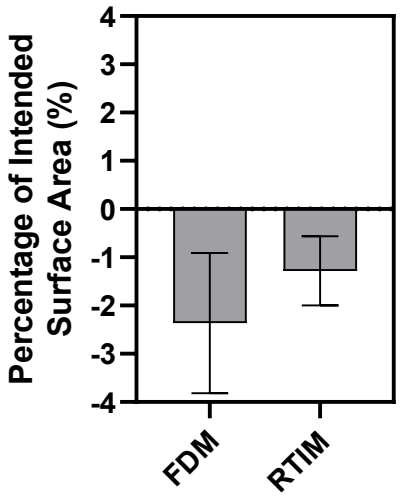

Figure 4.12: The percentage of the designed surface area of PVA based tablets (the cylindrical tablets based on similar surface area) from Goyanes et al. (2015a) and this study. The error bars represent the standard deviation for FDM and the propagated standard deviation for RTIM.

cools and solidifies. RTIM tablets on the other hand are produced via a fixed geometry mould cavity so the material is forced to adopt the desired geometry as it cools. This results in RTIM producing tablets which are truer to the digital design in terms of the physical properties than FDM. The precision of RTIM is also higher than the FDM process (Figure 4.12).

One of the major advantages to using RTIM is that the interparticle porosity within the dosage forms is extremely low and is far better controlled than dosage forms produced via FDM or compaction. The layer-by-layer process by which FDM operates introduces porosity within the dosage forms which is both unwanted and uncontrolled (Pires et al., 2020). This porosity will vary depending on a number of factors linked both to the formulation and the parameters by which the printer is operating (Markl et al., 2017, 2018a; Pires et al., 2020). RTIM on the other hand is a formative manufacture process so the variability in porosity that arises from the layer-printing is not present. As such, the control of the interparticle porosity is much higher and results in dosage forms with effectively 0% interparticle porosity due to the nature of the manufacture technique.

Additionally, in comparison to FDM, RTIM presents the potential for an increased formulation space. Typically, the drug loading that can be achieved for FDM printing is low due to the necessity for the print filament to possess the correct properties for successful printing (Zhang et al., 2018, 2017; Korte and Quodbach, 2018; Aho et al., 2019). There have however been cases where a higher drug loading has been achieved (Prasad et al., 2019). Additionally, these filament properties also limit which polymers can be used in conjunction with FDM, further reducing the formulation space available for FDM (Zhang et al., 2018). Further work on material development will be required to expand the formulation space of FDM (Gioumouxouzis et al., 2019). RTIM on the other hand is not dependent on the filament properties and thus higher drug loadings and a wider range of polymer carriers can be used without further research and development. This will greatly expand the formulation space and allow a greater variety of drugs, drug loadings and polymers to be utilised for more complex dosage form geometries.

It must be mentioned that the RTIM process is not without its limitations. The major limitation of this technique is the current throughput. Both the RTIM and FDM processes require material preparation via hot melt extrusion, however RTIM also requires the printing of the mould inserts which adds significant time. The actual production of the tablets however is typically faster for RTIM, with a single tablet able to be produced every 1-2 minutes while for FDM this is in the 4-5 minute range (Korte and Quodbach, 2018; Zhang et al., 2017). Both of these times quoted would be for a formulation considered to be favourable, an unfavourable formulation would extend these production times further. The throughput of RTIM could be improved by utilising it as a development tool for a more traditional μIM process using a tooled steel mould. This would allow for a far more efficient process and would allow for direct coupling with HME. While the structural flexibility for RTIM is considered high due to the ability to create accurate and precise surface micro-features, it must also be noted that internal features would be far more difficult to produce. Therefore, there are still structural and geometric limitations with the RTIM technique. Despite not having the constraints of the filament properties that FDM has, RTIM has additional limitations such as the material rheology and the tendency for some materials to stick

to the mould inserts. Even with these drawbacks, the RTIM process displays clear potential to produce dosage forms with highly accurate and precise physical structures.

4.6 Conclusion

The RTIM method produced tablets from of a variety of thermoplastic pharmaceutical grade polymers. These tablets were close to the digital designs in terms of their dimensions, surface area, volume and specific surface area. Shrinkage upon cooling was observed for LDPE, a semi-crystalline polymer, primarily in the tablet diameter measurements.

The mass variability of all tablets produced was low and well within the limits of the pharmacopoeia. The specific surface areas of the tablets produced were accurate to the digital designs suggesting that this RTIM process can be used to produce tablets of designed geometries for the purpose of fine-tuning drug release profiles.

RTIM has proven to be an accurate and precise method for the production of tablets with a desired specific surface area. It is well known that for many formulations, drug release kinetics are dependent on the specific surface area of the tablets (Goyanes et al., 2015a; Robles Martinez et al., 2018; Pires et al., 2020). As such, to refine the drug release behaviour, the control of the specific surface area must be accurate. This has been achieved through addition and modification of pins into the tablet geometry and subsequent altering of the overall tablet diameter. The decision as to whether the RTIM process is the most appropriate is application dependent. Consideration of the accuracy, precision, material requirements and throughput amongst other factors should be carefully examined when deciding the most appropriate manufacture technique for the desired application. These factors will directly influence the throughput, cost and overall quality and trueness to the digital design. Evidence suggests that RTIM can be used successfully for low production runs of <500 parts, and for larger batches it can be used as a development tool to obtain the desired tablet design prior to producing a traditional tooled steel mould for scaled up production (Rahmati and Dickens, 2007).

Authorship Declaration

Erin Walsh: Conceptualisation, Methodology, Validation, Formal analysis, Data curation, Writing - original draft, Writing - review and editing, Visualisation.

Elke Prasad: Material preparation, Writing - review and editing.

Gavin Halbert: Writing - review and editing.

Joop H. ter Horst: Conceptualisation, Writing - review and editing, Supervision.

Daniel Markl: Conceptualisation, Methodology, Resources, Writing - review and editing, Visualisation, Supervision, Project Administration, Funding acquisition.

Chapter 5

Modulation of Drug Release of Oral Solid Dosage Forms by Specific Surface Area Modification Using Rapid Tooling Injection Moulding

5.1 Chapter Summary

With the demand for micro-scale batch production in the pharmaceutical industry growing, the increase in demand for novel manufacturing processes continues. One major driver towards these micro-scale batches is the ability to produce pharmaceutical dosage forms with fine-tuned drug release profiles. This study demonstrates the use of rapid tooling injection moulding (RTIM) for the production of pharmaceutical dosage forms and as a process development tool. These dosage forms feature surface micro-features with the intention of altering the specific surface area (SSA) of the tablets. The impact of SSA modification on the resulting drug release profile is assessed, with significant differences observed for formulations based on the polymers polyvinyl alcohol

(PVA) and Klucel ELF. The polymer base of the formulation was found to be critical to the sensitivity of the drug release profile to SSA modification. A workflow was developed to fine-tune the drug release profile for formulations which demonstrate a linear response in drug release to SSA modification. All work and writing is my own unless stated otherwise.

5.2 Introduction

With the pharmaceutical market shifting in response to growing interest in the personalised and precision medicines sector, interest in novel manufacturing techniques elevates. Traditional pharmaceutical manufacture techniques are limited when it comes to small scale production, with major cost implications. This creates a barrier to progress within this sector of the pharmaceutical market and novel manufacturing techniques could provide a solution. These new technologies can be used to manufacture micro-scale batches of pharmaceuticals with less cost and in a more environmentally friendly and sustainable manner. This will allow the pharmaceutical industry to respond to changes in demand, and to manufacture medicines for smaller patient populations and clinical trials in a cost-effective manner.

Within the sector of personalised and precision medicines, the ability to execute better control over the drug release from a dosage form is one of the major research goals. A major advantage to some small scale batch manufacture techniques, such as additive manufacture (AM) and injection moulding (IM), is the greater flexibility to alter the performance parameters such as the drug release. Modified drug release is defined as being a drug release which differs from the traditional (Bruschi, 2015). This can take the form of time and/or spatial modification and typically is utilised to achieve therapeutic outcomes otherwise not achievable via the traditional delivery form. The field of controlled drug delivery is multidisciplinary, with major contributions across the fields of engineering and material sciences (Bruschi, 2015). These modifications are designed to improve therapeutic effect and patient compliance (Markl and Zeitler, 2017). There are a number of ways in which the drug release may be modified. Immediate-release formulations such as orally dispersible tablets designed to disintegrate in under a minute prior to the patient swallowing are designed to demonstrate rapid disintegration and dissolution on contact with the dissolution media (Markl and Zeitler, 2017). This is common in analgesic pharmaceutics where rapid onset of the therapeutic effect is required (Sheshala et al., 2011). This type of release-modification can also be effective at improving the bioavailability of drug molecules which are poorly soluble (Battu

et al., 2007). Other applications of drug release modification include sustained-release, where a gradual and slow release profile is desired to achieve a steady level of the drug in the blood plasma over an extended period of time (Bruschi, 2015).

With the fine-tuning of drug release profiles forming an important part of the move towards precision medicines, new manufacturing methods must be developed in order to meet this growing need. The ability to produce small-batch pharmaceuticals from a digital design, allowing for a far greater degree of flexibility in the tablet geometry, is one way in which this drug release modification could be achieved. One example of such a technique is AM which is commonly referred to as 3D printing. This technique can be utilised to produce oral solid dosage forms (OSDF) with a digitally designed geometry, which provides the freedom for formulators to adjust the drug dose and alter tablet geometry. Another manufacturing technology with potential to produce small scale batches in response to the demand is IM. IM has been recognised for its value to the pharmaceutical industry, for both packaging and more recently for the production of pharmaceutical dosage forms (Bartlett et al., 2017; Quinten et al., 2009b; Zema et al., 2012). A novel approach to producing pharmaceutical dosage forms arises from the combination of both additive manufacture and injection moulding techniques. This approach, known as rapid tooling injection moulding (RTIM) couples stereolithography (SLA) AM with micro-scale IM.

The combination of SLA AM, which has demonstrated its ability to produce accurate and precise micro-features on a mould surface (Walsh et al., 2021b), with µIM allows for the inclusion of micro-features on the surface of a pharmaceutical tablet. The RTIM process operates by the production of a mould insert via rapid tooling, i.e. the production of a mould via AM. This mould insert is placed inside a traditional steel mould used for IM. The IM process is considered to be in the micro-range due to the scale of the channels that feature in the mould insert design. A pharmaceutical formulation (typically pre-processed via hot melt extrusion to ensure molecular level mixing) is fed into the injection moulder where it undergoes heating and softens. A pressure is then applied to the softened material, and it is forced into the mould cavity and, upon cooling, adopts the shape defined by the mould insert. The application of SLA

in RTIM has been assessed in detail in Walsh et al. (2021b). Critical parameters of the material used for the production of the moulds, scaling factors applied to the printing and accuracy and precision of micro-features from this work must all be considered when utilising SLA in the RTIM manufacture process. The µIM process is heavily dependent on the melt characteristics of the pharmaceutical formulation (Zhang and Gilchrist, 2012). Typically, these formulations will be based on a thermoplastic polymer. The µIM process poses its own challenges and limitations. Zhang and Gilchrist (2012) demonstrated some evidence that the viscosity of molten thermoplastic materials was found to be lower in the micro-channels typical of the µIM process than would have been expected (based on measurement via a capillary rheometer). This highlights the highly sensitive nature of this manufacture process to the melt rheology of the injection material. Due to the rheological limitations, this technique is not suitable for all pharmaceutical formulations. A study by Walsh et al. (2021a) assessed a number of pharmaceutical polymer-based formulations for their suitability, accuracy and precision in an RTIM process. Success was achieved in processing a number of common pharmaceutical polymers via RTIM, with the resultant dosage forms being highly accurate to their digital designs (average of <1% variation for specific surface area (SSA) from the digital design). This study indicated the potential for this manufacture technique to be used for fine-tuning drug release profiles where accuracy and precision to the digital design is critical.

One way to alter the drug release profile is to modify the physical structure of the OSDF. The geometry of the tablet, particularly the SSA has been shown to influence the drug release profile (Goyanes et al., 2015b; Robles Martinez et al., 2018; Quinten et al., 2009b). Modification of the SSA of solid dosage forms can be achieved via altering the surface area while maintaining constant volume. This alteration of surface area can be realised by designing surface micro-features onto the tablet surface. While the aforementioned techniques (AM, IM and RTIM) all have the ability to produce tablets from a digital design, and therefore there is a degree of flexibility in the tablet geometry, the extent to this flexibility varies. A number of factors must be considered, such as the accuracy and precision of the techniques particularly in the production

of micro-features, the flexibility to alter tablet geometries and the consistency of the internal micro-structure of the dosage forms produced. Compared to the traditional manufacturing techniques for OSDFs such as powder compaction, both RTIM and AM provide a far greater degree of structural flexibility. There are however drawbacks to using these techniques, with the throughput being considerably lower for both AM and RTIM. Additionally, the limitations on the materials which can be processed via these manufacture methods results in a reduced formulation space for RTIM compared to powder compaction, with an even greater reduction when moving to AM.

As the pharmaceutical industry moves more towards smaller batch sizes, RTIM has potential to play an important role in the future of the manufacturing landscape. The principle objectives of this study are to assess the RTIM process for its suitability both to produce pharmaceutical dosage forms directly for the purpose of adjusting the drug release profiles and also as a development tool for achieving the required tablet design for a desired drug release. The drug release will be adjusted through changing the SSA of the tablets produced, achieved via the inclusion of surface micro-features. Three paracetamol-based formulations were trialled, with Affinisol (hydroxypropyl methylcellulose), Klucel ELF (hydroxypropyl cellulose) and Parteck MXP PVA 4-88 (polyvinyl alcohol) being the polymers investigated.

5.3 Materials and Methods

5.3.1 Materials

Stereolithography Additive Manufacture

The Clear v4 photoresin from Formlabs (Massachusetts, USA) was utilised in this work based on the findings from Walsh et al. (2021b). Isopropyl alcohol (Sigma Aldrich, USA) is used during the post-processing stages after printing.

Rapid Tooling Injection Moulding

The names, supplier details and acronyms for all raw materials used are detailed in Table 5.1. The acronym for each material will be used throughout this chapter to refer

to a particular material.

Table 5.1: List of raw materials, their supplier details and their acronyms which will be used in this chapter.

Material	Supplier	Acronym
Affinisol HPMC HME 15LV	The Dow Chemical Company, USA	AFF
Klucel ELF HPC	Ashland, USA	KELF
Parteck MXP PVA 4-88	Sigma Aldrich, USA	PVA
Paracetamol	Mallinckrodt, UK	PCM

The formulations used in this work required processing via hot melt extrusion (HME). The formulations are detailed in Table 5.2, where all formulation ratios are by weight.

Table 5.2: List of formulations and their acronyms that will be used in this chapter.

Formulation	Acronym
Affinisol HPMC HME 15LV(50%) + Paracetamol (50%)	AFF/PCM 50/50
Klucel ELF (90%) + Paracetamol (10%)	KELF/PCM 90/10
Parteck MXP PVA 4-88 (90%) + Paracetamol (10%)	PVA/PCM 90/10

The rationale for selecting the three polymers used in this chapter were to assess the impact that differing drug-release mechanisms would have on the relationship between SSA and drug release. The AFF/PCM 50/50 formulation is expected to be highly swelling, the hypothesis is that this swelling will occlude the pin structures on the surface of the tablets and no relationship between the SSA and the drug release will be observed. The KELF/PCM 90/10 formulation is expected to exhibit both swelling and erosion mechanisms for drug release. Due to the low molecular weight variety of the Klucel polymer used in this case, it is expected that the swelling will be minimised, with erosion being the primary release mechanism. Finally, the PVA/PCM 90/10 formulation is expected to exhibit drug release via the erosion mechanism. It is hypothesised that the erosion mechanism of drug release will be favourable for demonstrating a relationship between SSA and drug release.

Dissolution Testing

The following materials were used to produce buffer, stock and standard solutions for use in dissolution testing: monopotassium phosphate (KH_2PO_4) from VWR, USA; acetaminophen (PCM) from Mallinckrodt, UK and sodium hydroxide (NaOH) from Fluka, USA.

5.3.2 Methods

Stereolithography Additive Manufacture

The Form 2 (Formlabs, Massachusetts) SLA printer was used to produce rapid tooled mould inserts. The mould inserts were printed at an angle of 45° from the build platform. When the printing stage was complete, the mould inserts were washed in an agitated wash basin containing isopropyl alcohol for a period of 10 minutes before being left to dry. Following this, the moulds are removed from the build platform and placed in a UV oven for 60 minutes at 60°C. Supporting material was removed from the mould inserts and the rear of the mould surface was lightly sanded. Full detail on the method used in this work can be found in (Walsh et al., 2021b).

Design of Tablet Geometries

Three different mould insert designs were produced for this study to modify the SSA of the dosage forms (see Figure 5.1b for an example). The basis of the designs generated was to produce a step-wise increase in the SSA. The increase in SSA values between the designs were selected for this study based on data from the literature which demonstrated detectable differences in the drug release profile (Goyanes et al., 2015a). Conical frustum shaped 'pins' (Figure 5.1a) were added to the designs in increasing number ($n = 2, 6$ or 10 for the three tablet geometries) to adjust the SSA. In order to maintain the tablet mass across all three designs for a formulation, the volume of the three designs was kept constant. This was achieved by adjusting the diameter of the tablet to account for the reduction in volume resulting from the introduction of the pins. The thickness of each tablet is kept constant for all three designs as are the

dimensions of the pins.

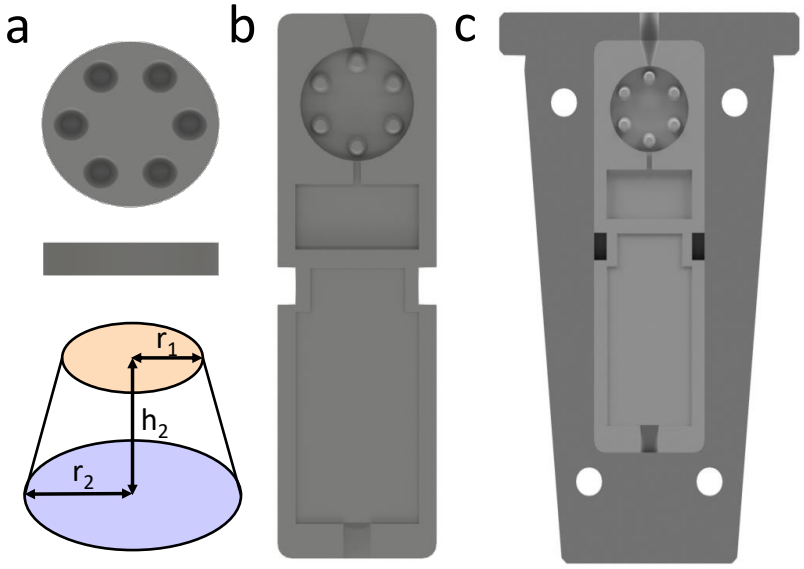

Figure 5.1: Schematic of the digital design of the tablet and the mould insert. a) Tablet design features top-bottom: Top view, side view and design of an individual pin. b) A rendering of the mould designed to produce 6 Pin tablets. c) The mould insert for the 6 Pin Design inserted into the metal mould. This depiction represents one half of the full mould.

The basic design of the tablet geometries comprised a cylindrical tablet with the conical frustum pins cut into the top surface (Figure 5.1a). Full details of the tablet dimensions produced from these designs can be found in Table 5.3. The volume, surface area and specific surface area of the tablets were calculated using the Equations detailed in Chapter 4.

Rapid Tooling Injection Moulding

The RTIM process couples SLA with IM. Mould inserts, produced via SLA, are housed within a metal mould casing (Figure 5.1c). There are a number of design features on the printed mould insert to make it suitable for its use in an RTIM process. Further details on this can be found in Walsh et al. (2021a).

The two halves of the metal mould were pieced together and placed into the HAAKE MiniJet Pro Piston Injection Moulding System (Thermo Fisher Scientific, USA) which

Table 5.3: Summary table of tablet dimensions.

Design Feature	**2 Pin Design**	**6 Pin Design**	**10 Pin Design**
Diameter (mm)	15.23	15.69	16.12
Thickness (mm)	3	3	3
Volume (mm^3)	530.03	529.82	529.80
Surface Area (mm^2)	527.48	592.76	658.08
Number of Pins	2	6	10
Pin Depth (mm)	2	2	2
Pin Radius 1 (mm)	1.5	1.5	1.5
Pin Radius 2 (mm)	0.75	0.75	0.75
Specific Surface Area (mm^{-1})	1.00	1.12	1.24

is an upright air-pressurised injection moulder. The injection material was placed into the melt cylinder, the piston was attached and this was then placed into the injection moulder. A number of processing parameters must be set, including the cylinder and mould temperatures, the injection and hold pressures and the injection and hold times. These processing parameters will vary for different injection materials (Table 5.4). For all formulations the injection time, hold pressure and hold time were kept constant at 10 s, 50 bar and 10 s, respectively.

Table 5.4: RTIM process parameters used for each of the formulations.

Formulation	**Cylinder Temp**	**Mould Temp**	**Injection Pressure**
AFF/PCM 50/50	130 °C	70 °C	150 bar
KELF/PCM 90/10	120 °C	70 °C	150 bar
PVA/PCM 90/10	180 °C	100 °C	200 bar

All formulations required the application of a silcone-based lubricant (WD-40, USA) onto the surface of the mould inserts to aid removal of the injected material.

Upon completion of injection, the metal mould was removed from the injection moulder. The metal mould was then opened and the mould insert removed. When sufficiently cooled, the mould insert was then opened and the tablet removed from the mould cavity.

Gravimetric Analysis

All tablets produced were weighed on a 4 decimal point balance (Entris II, Sartorius). The masses reported reflect the average of each batch produced. The mean and standard deviations reported are for $n = 18$ per formulation.

Dimensional Analysis

The diameter and thickness of each tablet were measured using a digital calliper (Scienceware Digi-Max, Sigma Aldrich). A total of three diameter and three thickness measurements were taken for each tablet, the measurements shown are an average of these replicates. The mean and standard deviations reported are for $n = 18$ per formulation.

A spectral-domain optical coherence tomography (OCT) system (GAN600 Series, Thorlabs, New Jersey, USA) equipped with a LK3-BB (focal length: 36 mm) was used to measure the pin dimensions. OCT produces cross-sectional images of a sample which can be used for depth measurements. The lateral resolution was ≈4 µm, the axial resolution in air was ≈3 µm and the image size was a 1024 x 1024 pixels with a x-axis pixel size of 5.86 µm and a y-axis pixel size of 1.95 µm. The OCT probe was focused over the pins on the tablet surface and a 2D cross-section image was acquired. The focus was adjusted to ensure a strong signal. The diameters (see Figure 4.2c) at both the top and bottom surfaces and the depth of the pins were measured. The mean and standard deviations are reported for 18 measurements per formulation.

Dissolution

54.44 g of KH_2PO_4 was weighed into a 1000 mL standard flask and dissolved in deionised water, making up to the graduation mark. This solution was rinsed three times into an 8 L vessel and 57.6 mL of 0.5M NaOH was added. Deionised water was added to make up to the total volume and the solution was stirred thoroughly. The pH was adjusted using 0.5M NaOH to ensure a final pH of 5.8.

PCM stock solutions were prepared by weighing 200 mg of PCM into a 50 mL standard flask. Phosphate buffer was added to the flask. The flask was then sonicated until the

PCM was completely dissolved. The solution was allowed to cool before being made up to the graduation mark with phosphate buffer and inverting 10 times to ensure adequate mixing. Using a Gibson pipette, 5 mL aliquots were transferred to a 100 mL standard flask. This was made up to volume with phosphate buffer and inverted 10 times to mix. This solution was used as the standard. This process was duplicated to produce two standards.

The dissolution apparatus used is the ADT8i Dissolution bath (USP I, basket) with a closed loop setting and a T70+ UV/Visible spectrophotometer (Automated Lab Systems, UK). The vessel volume was 1000 mL with a paddle speed was set to 50 rpm. The vessels were set to 37°C and samples were taken via an auto-sampling pump set to flush 20 mL at a speed of 20 mL/min. Samples were taken at the following intervals: 5 min, 10 min, 15 min, 30 min, 1 hr, 2 hr, 4 hr, 6 hr, 8 hr. The UV detection wavelength was set to 243 nm and 1 mm flow cell cuvettes were used. A 20 μm cannula filter (ALS, UHMW PE, Part No 50831) was fitted to the sampler heads.

All tablets were weighed and their weights recorded. A standard verification of both PCM standards produced was performed prior to the dissolution assay, with the absorbance values for both standards recorded.

5.4 Results

5.4.1 Gravimetric Analysis

The mass of all tablets produced indicated that the variability of <1% (inclusive of all formulations and tablet geometries) was well within the limits outlined by the The International Pharmacopoeia (2019). Mass variability between the different tablet geometries was also low at less than 1% variability across all three formulations (see Figure 5.2 and Table 7.8 in Appendix Section 7.2).

5.4.2 Dimensional Analysis

Both the thickness and diameter measurements obtained demonstrated high accuracy and precision to the digital designs across all three formulations. The average thickness

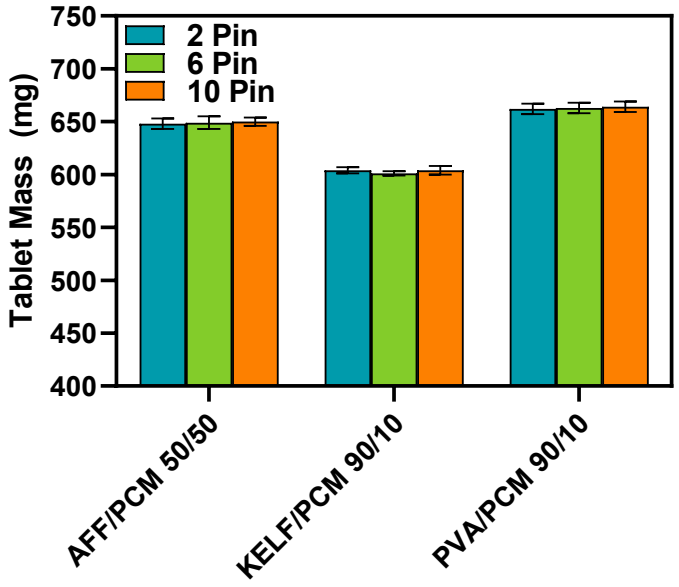

Figure 5.2: The average mass for all formulations. Error bars shown represent the standard deviation.

measurement across the three formulations was found to be 100.02% ±0.53 of the designed value with diameter being 99.44% ±0.37 of the designed values. This data can be seen in Appendix Section 7.2.

The pin depth, top diameter and bottom diameter of the pins were measured using OCT. The results from this study demonstrated that the pins are highly accurate and precise to the digital designs. The pin depth was found to be 97.14% ±0.42 of the designed value, the top diameter was 98.96% ±0.59 and the bottom diameter 100.89% ±0.94. This data can be seen in Figure 5.4.

From the dimensional measurements, the volume, surface area and specific surface area were calculated using the equations shared in Walsh et al. (2021a). The can be seen in Figure 5.5.

The accuracy and precision of the volume, surface area and SSA were high for the three formulation (volume was 99.26% ±1.53 of the intended value, while surface area was 98.71% ±0.59 and SSA was 99.46% ±1.00 based on the average of all tablets produced for this study). While the error bars look large in comparison to the absolute

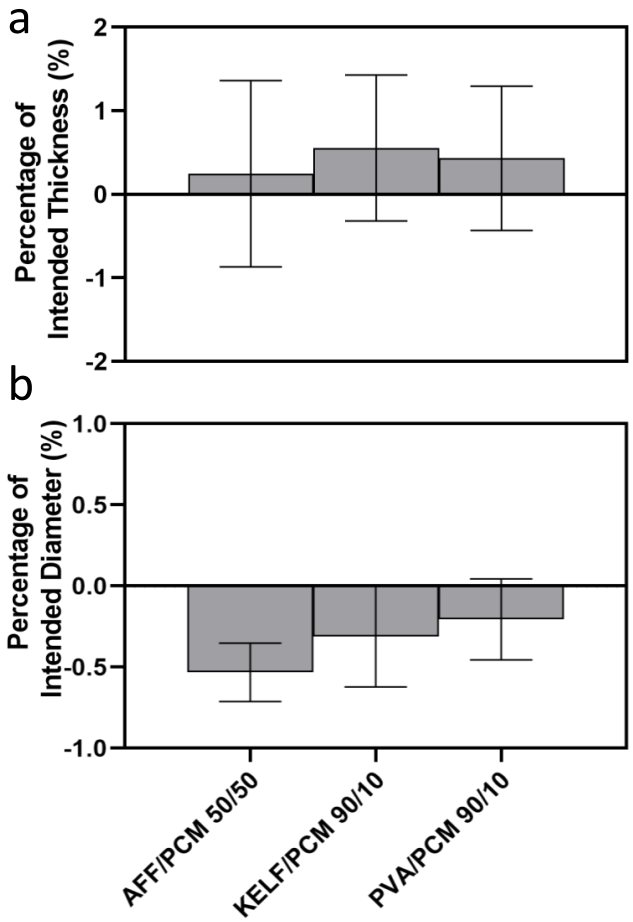

Figure 5.3: a) The average tablet thickness for all formulations b) The average tablet diameter for all formulations. a-b) Error bars shown represent the standard deviation.

deviation from the digital design, it should be noted that the errors displayed are calculated via error propagation.

5.4.3 Dissolution

Dissolution studies were conducted for each geometry on the three formulations (Figure 5.6). Data collection of AFF/PCM 50/50 formulations was terminated after the 240 min time point for the 6 Pin geometry due to errors with the dissolution apparatus. From this study, no significant differences in the drug release profiles could be detected from the three tablet geometries trialled. On the contrary, significant differ-

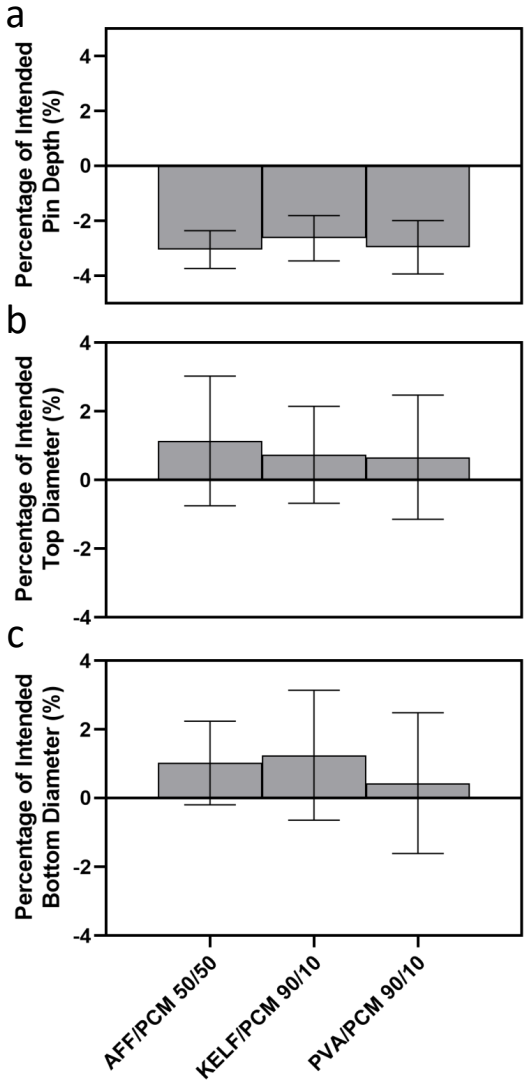

Figure 5.4: Tablet pin characteristics measured by OCT. a) The depth of the pins on the tablet surface (h_{pin} from Figure 4.2c) b) The top surface diameter of the pins on the tablet surface ($2 \times r_{\text{pin1}}$ from Figure 4.2c) c) The bottom surface diameter of the pins on the tablet surface ($2 \times r_{\text{pin2}}$ from Figure 4.2c). a-c: for each bar $n = 6$ measurements with the error bars representing the standard deviation.

ences in the rate of drug release were observed between the different tablet geometries for KELF/PCM 90/10 (Figure 5.6b) and PVA/PCM 90/10 (Figure 5.6c) formulations. The sample time points for the 6 Pin geometry differ to those of the 2 Pin and 10 Pin geometries due to running errors with the dissolution apparatus.

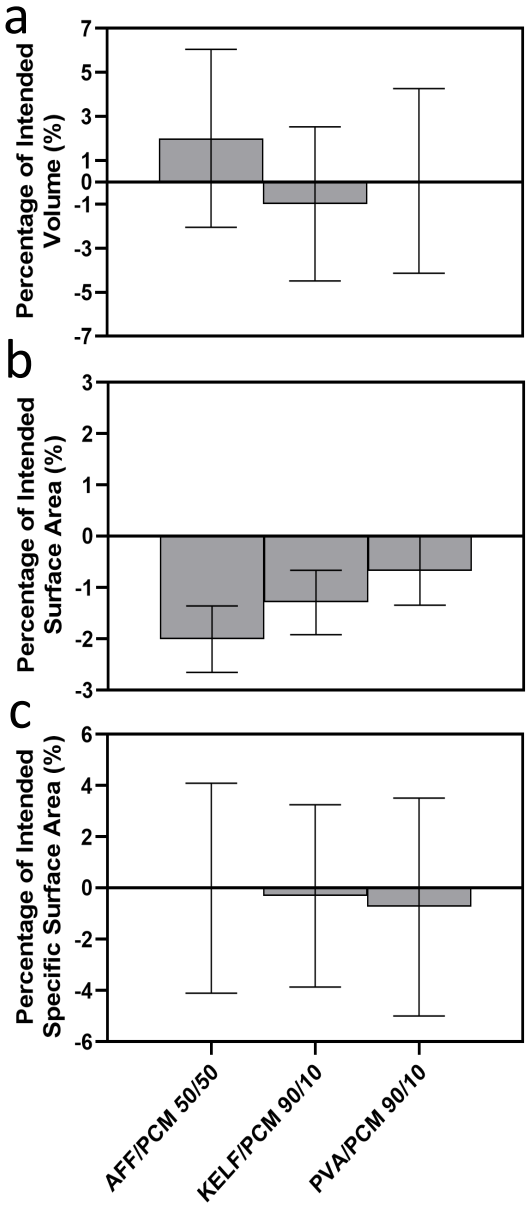

Figure 5.5: a) The calculated average volume of all tablets produced for each of the three formulations b) The calculated average surface area of all tablets produced for each of the three formulations c) The calculated average specific surface area of all tablets produced for each of the three formulations. Errors displayed are calculated via error propagation.

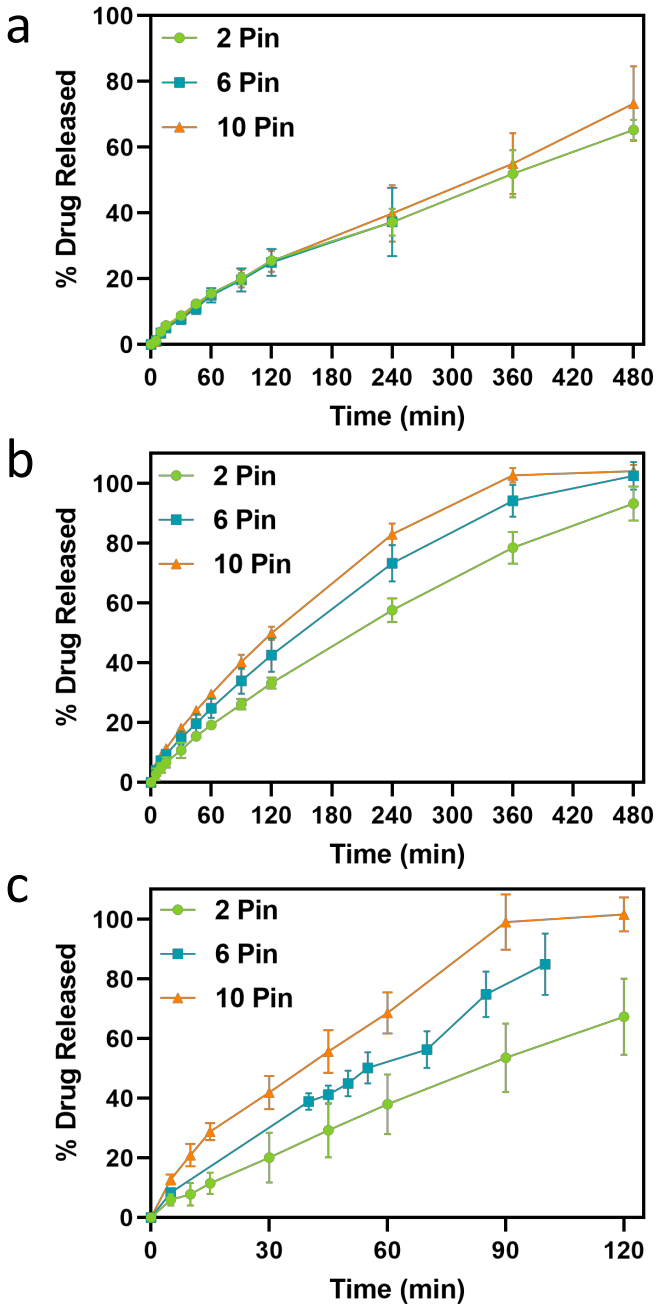

Figure 5.6: Drug release profiles for a) AFF/PCM 50/50, b) KELF/PCM 90/10 formulation and c) PVA/PCM 90/10 formulation. All: Symbols represent discrete data collection points with the connecting line acting as a guide for the eye. Error bars are the 95% confidence interval of the measurements.

5.5 Discussion

5.5.1 Physical Parameters of the Tablets

The mass variability for the three formulations trialled was found to be very low and was well within the pharmacopoeia limits. This low variability in mass supports the hypothesis that RTIM is able to produce dosage forms with high reproducibility with a very low uncontrolled porosity.

In theory, all of the formulations should produce physical parameters which match the digital design for their geometry. As per the digital design, volume is constant across the three geometries, while the surface area and specific surface area increases with the number of pins.

The error recorded is the summation of a number of sources of uncertainty. Primarily, there is uncertainty associated with the printing of the mould inserts. This has been studied in Walsh et al. (2021b). There will be also errors associated with the different measurements taken such as the calliper and OCT measurements. The uncertainty that arises from the measurements alone accounts for 22.79% of the errors for volume calculations, 24.11% for the surface area calculations and 22.82% for the specific surface area values. Lastly, there is uncertainty introduced from the different formulations used. The variability between the different formulations trialled in this study was low, however formulation composition is still an important consideration.

As can be observed in Figure 5.7 the relationship between the number of pins featured in the design and the resultant specific surface area is highly linear producing an R^2 of 1 based on the data collected for the three formulations trialled in this study. This indicates that further modification of the specific surface area could be achieved via this pin-based approach with a high degree of accuracy. The equation of the line provided in Figure 5.7 can therefore be used to determine the number of pins required to achieve a desired specific surface area.

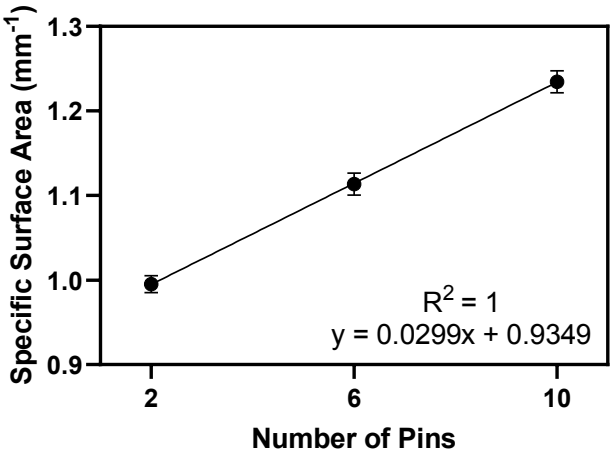

Figure 5.7: The average specific surface area for all formulations vs. the number of pins in the tablet geometry. Note the R^2 is based on 3 data points.

5.5.2 Drug Release Analysis

The AFF/PCM 50/50 formulation generally had a slow drug release, failing to reach 100% release after the 8 hour time period the dissolution test was conducted for. This is not unexpected as the polymer used in this formulation, Affinisol (which is a hydroxypropylmethyl cellulose (HPMC) polymer), is a slow release polymer. The release kinetics of the AFF based formulation are significantly impacted by the swelling behaviour exhibited by the polymer which occurs due to polymer chain relaxation (Fu and Kao, 2010). This limits the diffusion of the drug from the matrix before the swelling of the matrix which controls the drug release (Reynolds et al., 2002). Reynolds et al. (2002) conducted a study and observed that the brief initial period of drug release for AFF-based formulations prior to the matrix swelling is directly proportional to the designed SSA. This was not observed in this study, which is likely due to the formulation differences. The formulation used in the study by Reynolds et al. (2002) contained 2% w/w of promethazine HCl, 20% w/w of HPMC USP Type 2208, 77.5% w/w of dicalcium phosphate dihydrate and 0.5% w/w of magnesium stearate. The significant difference in both the drug loadings and the % w/w of the HPMC could account for the different observations made during this initial drug release phase. Additionally, the geometric differences between the RTIM tablets presented in this work and those

produced by Reynolds et al. (2002) are also likely to contribute to the differences in the drug release profiles observed. In the later phase of the drug release profile captured the 10 Pin geometry demonstrated slightly faster drug release than the 2 Pin geometry. The data captured for this formulation indicate a likely first order drug release profile. Future studies on this formulation would be required to determine if these differences would become significant in the final phase of drug release should the full dissolution profile be captured. Moreover, a more significant difference in the SSA of the geometries compared may be required to observe any significant impact on the drug release for this particular formulation.

Significant differences were observed for entirety of the drug release profile of KELF/PCM 90/10 and PVA/PCM 90/10 formulations. This finding is in agreement with other studies conducted where increasing the SSA results in a higher rate of drug release (Goyanes et al., 2015b; Reynolds et al., 2002). The KELF polymer used in this formulation is a hydroxypropylcellulose (HPC) polymer. This polymer controls drug release from a matrix via a swelling and erosion mechanism (Mohammed et al., 2012). The specific type of HPC used in this work is designed to exhibit a faster erosion process due to its lower molecular weight (Mohammed et al., 2012; Ashland Inc., 2017). As such, the KELF polymer is particularly useful in increasing the solubility of biopharmaceutical classification system class II drugs. The differences observed with the varying SSA for this formulation suggest that the release rate is controlled by the surface area rather than then swelling behaviour of the KELF polymer as it was the case for the AFF polymer discussed prior. While the KELF polymer was expected to demonstrate both swelling and erosion drug release mechanisms, the low molecular weight is expected to minimise swelling and favour erosion. Figure demonstrates that no significant swelling on the surface was visible for tablets of this formulation. The drug release curves for the KELF/PCM 90/10 formulations indicate first order drug release.

PVA is a hydrophilic polymer which absorbs water and swells as a result, however the swelling process can be obstructed by the presence of salts in the dissolution media (Morita et al., 2000; Mahon et al., 2020). As such, the PVA release curve obtained

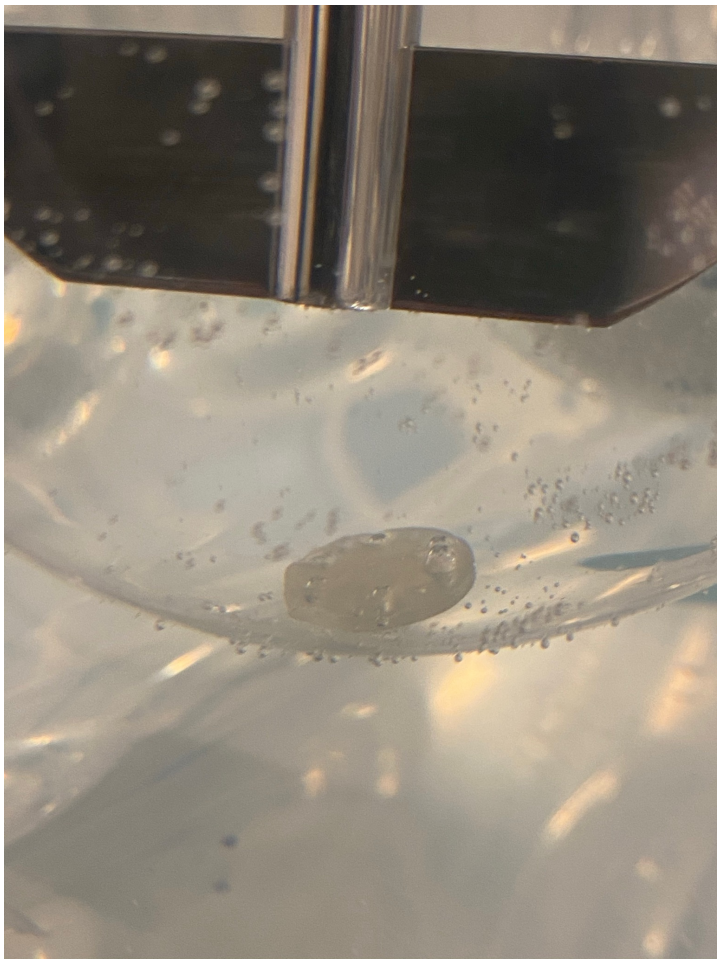

Figure 5.8: A photograph of a 6 pin KELF/PCM 90/10 tablet during the dissolution process.

in this study is mostly controlled by erosion of the polymer and diffusion of the drug from the matrix. This may explain the more linear shape of the drug release curves produced for this formulation, with this formulation displaying characteristics of a zero order drug release curve.

5.5.3 Power Law Fitting

From the drug release profiles obtained, a power law fitting (see Equation 5.1) was performed to allow comparison of the drug release profiles produced.

$$y = kx^m \tag{5.1}$$

The k and m parameters were derived from each data set obtained. Using these values the time to reach 50% drug release was determined and Figure 5.9 was produced. The obtained values of k and m are reported in the Appendix.

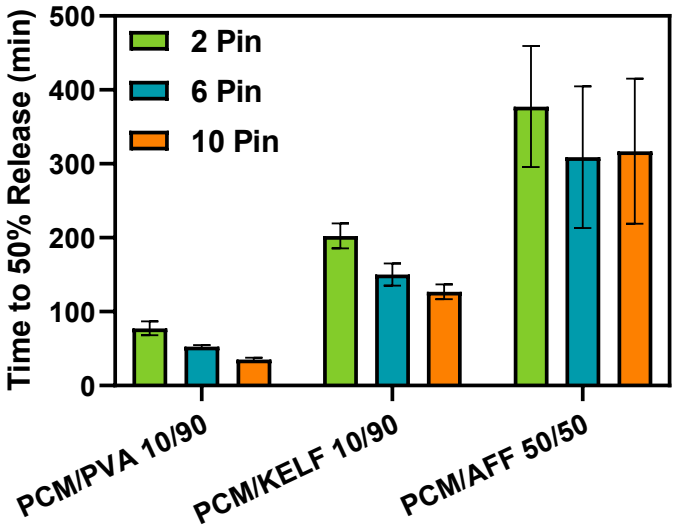

Figure 5.9: The time taken for formulations to reach 50% drug release (as calculated via the k and m parameters) for each formulation split by tablet geometry.

From Figure 5.9 it is clear that for both the PVA and KELF based formulations the increase in SSA results in a decrease in the length of time taken to release 50% of the drug in the dosage form. The AFF based formulation does not display this trend as discussed above. It is also clear that the polymer used in these formulations has a significant impact on both the sensitivity to the SSA modification but also to the absolute time for drug release. This is attributed to the differing mechanisms employed by these polymers in the drug release kinetics. As such, when utilising a technique such as RTIM for the fine-tuning of drug release profiles the polymer-base for the formulation and its drug release mechanisms must be careful considered.

Using the parameters determined using the Power Law (Eq. 5.1), Figure 5.10 was

produced. The time taken to achieve 50% drug release for the PVA formulations was calculated using these parameters for the 2, 6 and 10 Pin geometries that were produced. From this, the equation of the linear fit was then used to model what the time to achieve 50% drug release would be for tablet geometries with varying numbers of pins. This demonstrates that, for tablets of equal weight and drug loading, the drug release profile can be fine-tuned by altering the SSA via the inclusion of pins on the tablet surface.

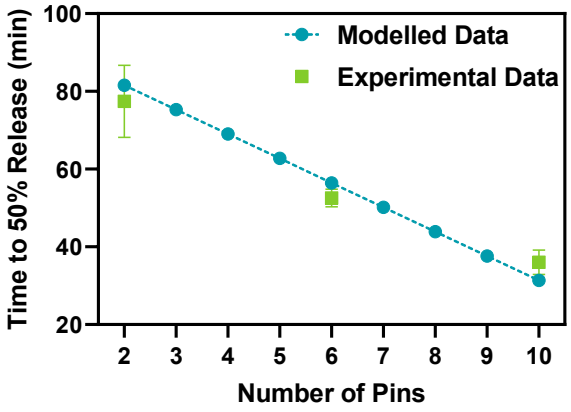

Figure 5.10: The modelled time to 50% drug release using the equation of the line obtained in from the PVA/PCM experimental data. The equation of the line is $y = -172.36x + 246.66$ with an R^2 of 0.9864.

5.5.4 Tablet Asymmetry

This differing presentation of the pin features on the tablet surface can be observed in Figure

Due to the asymmetric nature of the dosage forms produced in this work, there are two distinct faces. The first face is that which has the pins indented into the surface, and the second face is the flat cylindrical base. This asymmetry to the tablets presented some challenges during the dissolution studies. All of the tablets were positioned with the pin-face upwards when the dissolution studies were conducted. The system which was used for this work operates to drop the tablets into the dissolution vessels simultaneously. When the tablets fall, some come to rest in the base of

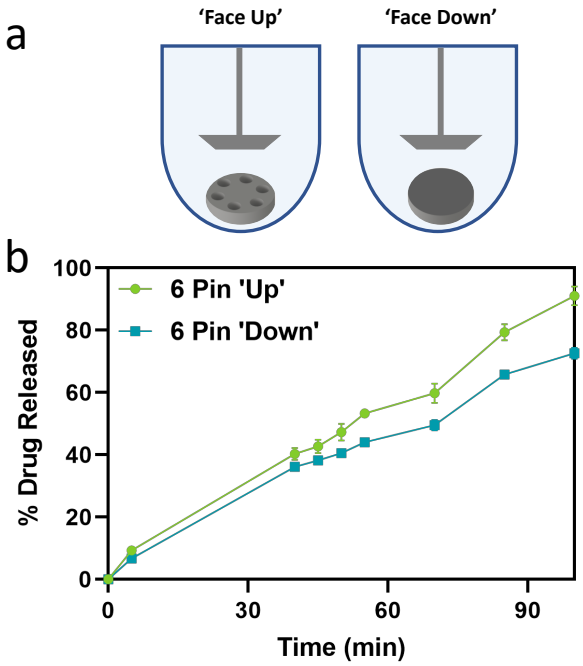

Figure 5.11: Impact of anisotropic tablet structure on drug release profiles of the PVA/PCM 90/10 formulation. a) A depiction of the 'Face Up' and 'Face Down' orientation that tablets may adopt in the dissolution vessels b) 6 Pin PVA/PCM 90/10 tablets split by 'Face up' and 'Face down'. Sample size for 'Face up' is 4 tablets and for 'Face down' is 2 tablets. Error bars represent the 95% confidence intervals.

the vessels with the pin-face upwards, and others with the pin-face downwards (see Figure 5.11a). The tablets which were pin-face downwards demonstrated slower drug release (see Figure 5.11b), which is attributed to the reduced access of the dissolution media to the surface micro-features and differing hydrodynamics on the two faces of the tablet. The impact of these downward facing tablets results in a higher error produced on the measurements as can be observed by comparing the error bars between Figure 5.13a and b.

It is accepted that *in-vitro* testing of the drug release profiles can be used to estimate *in-vivo* performance by establishing the correlations between the two. There are, however, a number of drawbacks to this approach (Markl and Zeitler, 2017; Costa et al., 2001; Wu et al., 2015). One major drawback is that the mass transport mechanisms which underpin the drug release cannot be fully understood from these studies (Markl

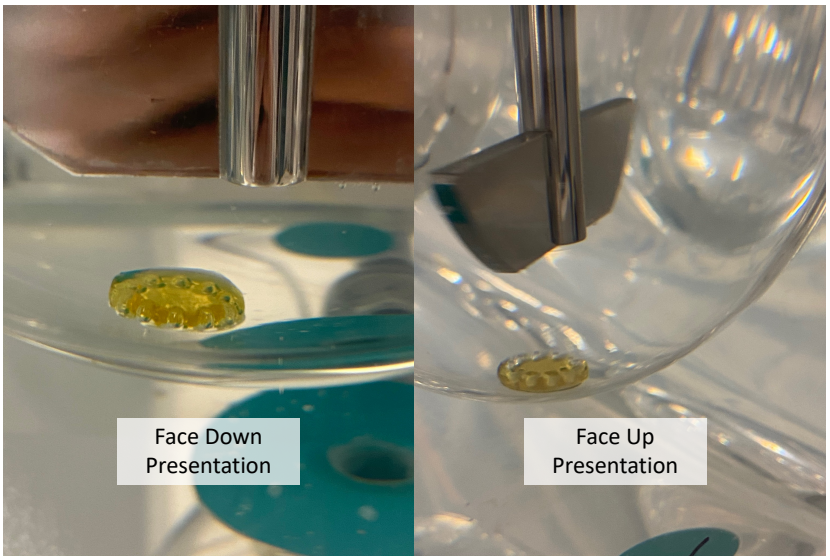

Figure 5.12: Photographs of two 10 pin PVA/PCM 90/10 tablets demonstrating both the 'Face up' and 'Face down' presentations within the dissolution set up.

and Zeitler, 2017). Additionally, the generalised nature of such empirical models results in limitations to their successful application (Markl and Zeitler, 2017). For future studies, the tablets could manually be placed into the dissolution vessels to avoid these inconsistencies. Putting micro-features on both faces of the tablet surface would likely reduce the errors associated with the asymmetry. However, the blocked face would still have limited liquid access and therefore the full impact of the increase in SSA would not be clear from such a set up. It is however worth stating that this issue is not an issue that would be encountered in vivo.

5.5.5 Drug Release Workflow

This suggests that, for formulations like the PVA/PCM 90/10 used in this work, a workflow could be developed which allows a desired drug release profile to be designed into a tablet through the SSA. The process for producing a tablet with a release-by-design basis is outlined in Figure 5.14.

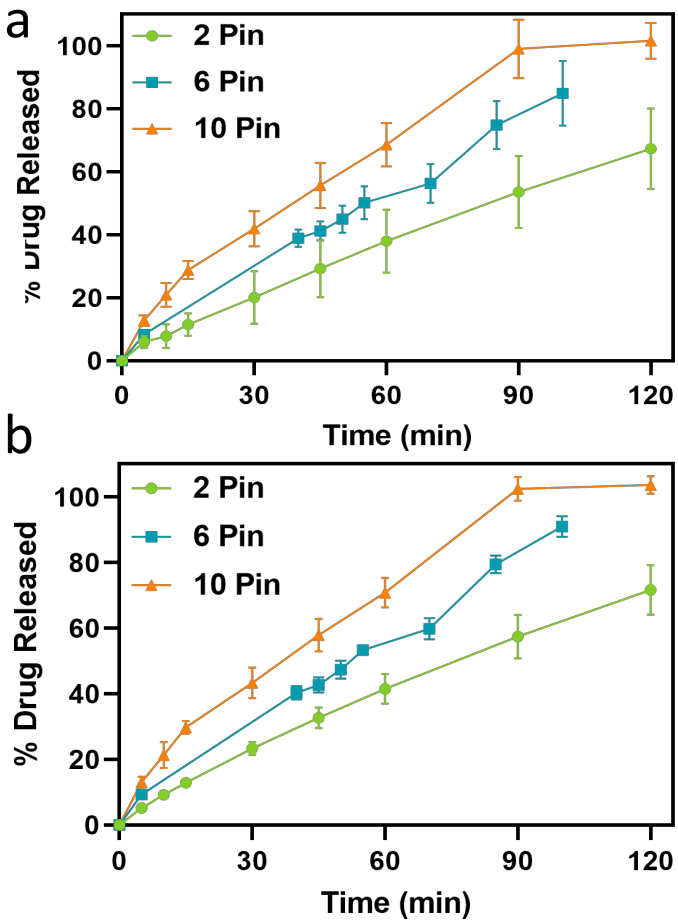

Figure 5.13: Impact of anisotropic tablet structure on drug release profiles of the PVA/PCM 90/10 formulation. a) Drug release profiles for all PVA/PCM 90/10 tablets produced b) Drug release profiles for only 'face up' PVA/PCM 90/10 tablets.

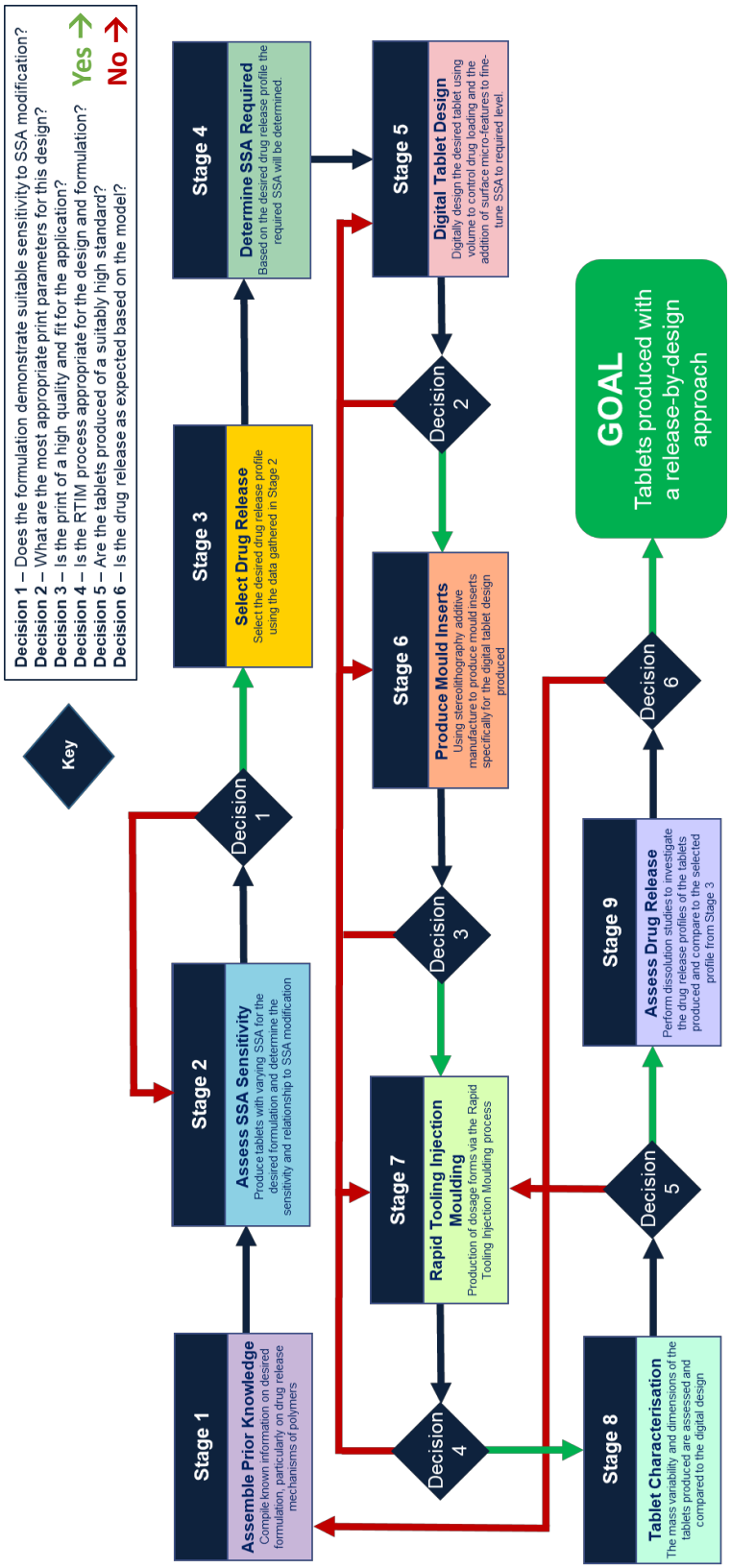

Figure 5.14: A workflow for the production of oral solid dosage forms on a release-by-design basis.

In Stage 1, information on the formulation must be gathered such as polymer rheology, drug release mechanisms (namely diffusion, swelling and erosion) and drug-polymer interactions. During Stage 2, initial studies are conducted by producing a number of dosage forms with varying SSA from the desired formulation to assess for the formulations sensitivity to SSA modification. This is determined by assessing the drug release rates of the tablets produced and comparing their release rates to the SSA. During Decision 1, we determine whether the formulation is suitable for this release-by-design approach. The relationship between SSA modification and drug release must be established. For the formulations used in this work, this is a linear relationship and therefore a linear model is appropriate. However, this can be a non-linear model depending on the identified relationship between SSA and release. During Stage 3, the desired drug release profile is selected. In Stage 4, we use the desired drug release profile to determine the SSA we would require to produce this. This is determined using the equation of the line of the data collected during Stage 2. Stage 5 involves the digital design of the tablet. The volume of the tablet will be determined by the required drug loading, and the required surface area will then be determined to ensure the desired SSA is achieved. The SSA can be modified through the addition of pins, as seen in this research. Figure 5.10b demonstrates how the release profile for PVA can be altered in a stepwise fashion by increasing the number of pins on the tablet surface. If the desired drug release profile falls between two of these points, the dimensions of

the pins themselves can be altered. The recommendation would be to select the pin number which falls directly below the desired release profile, and to then scale up the radii of the pin to increase the surface area that each pin provides. The diameter of the tablets is adjusted to account for any volumetric loss that results from the addition of the pins/alteration of the pin scale. During Decision 2, the print parameters required to produce the desired tablet design must be considered (details on what should be considered are covered in Walsh et al. (2021b)). Stage 6 involves the printing of mould inserts via SLA additive manufacture. Decision 3 is the point at which the printed mould inserts are assessed for quality and fit. Stage 7 is the RTIM process where the tablets are produced. Decision point 4 assess the success of the RTIM process and whether the tablets produced are of an appropriate standard. During Stage 8, the tablets produced are characterised in terms of their physical properties such as mass and dimensions. Decision 5 assesses whether these physical properties of the tablets are sufficiently close to the designed values. Stage 9 involves performing drug release studies with the tablets produced. The final decision point 6 evaluates whether the produced drug release profiles are as expected based on the selection from Stage 3 and the characterisation information from Stage 8.

At any decision point in the workflow there is potential to go back multiple steps - the determination of what is considered acceptable or unacceptable will be hugely variable and dependent on the specific formulation and application.

An example of the utilisation of the above workflow can be demonstrated using the PVA/PCM 90/10 formulation studied in this work. Stage 1 and 2 have been completed during the course of this study, with the relationship between SSA modification and drug release being established. If the desired drug release was to have 50% release by 43 minutes, the required SSA can be deduced using the equation of the line generated in Stage 2 (and demonstrated in Figure 5.15a).

In this case, the SSA required would be 1.18. From this, we can then design the digital tablet to achieve this SSA, in this case that would be a tablet with 8 pins on the surface as calculated using the relationship between number of pins and SSA (Figure 5.15b). Based on this pin number (and maintaining the pin dimensions stated

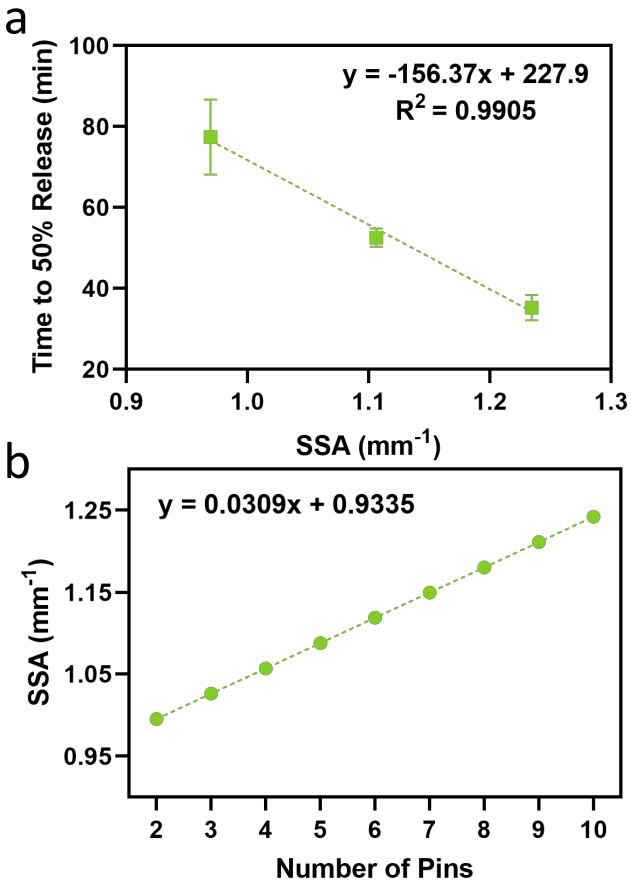

Figure 5.15: The relationship between SSA modification and drug release produced from Stage 2 of the workflow for the PVA/PCM 90/10 formulation.

before), and the fact that the volume of the dosage forms in this study is kept constant by adjusting the overall tablet radius, the required radius an also be calculated to be 7.95 mm. Following the remainder of the workflow would yield the desired dosage forms which, when analysed for drug release should provide a 50% drug release at 43 minutes. If the desired drug release requires an SSA not achievable by simply modifying the number of pins, the size of the pins can also be adjusted to produce the SSA required.

5.5.6 The Role of SLA Rapid Tooling in Manufacturing

The use of SLA as a rapid tooling technique for IM has shown its success, however the process does require careful selection of mould material, design and fabrication (Walsh et al., 2021b; Surace et al., 2021). Studies have found that SLA produced moulds

can be successfully used up to 500 times to produce plastic components as part of an RTIM process (Rahmati and Dickens, 2007). To achieve this, the production of the SLA mould must be fully optimised. In this work, the decision to use SLA as the manufacture method for the mould inserts is primarily driven through the ability to quickly produce iterative designs. The mould inserts must still have sufficient ability to withstand the temperatures and pressures of the IM process, however when the design optimisation work is complete and the final mould design has been determined, a traditional tooled steel mould can be produced for the scale up in tablet manufacture. These steel moulds are significantly more expensive to manufacture and have a commercial lead time of 6-12 weeks however they are far stronger and better able to withstand the repeated pressures and temperatures needed for production runs greater than 500 parts. Moving to a steel mould also offers benefits in terms of throughput for the process and allows for direct coupling to the HME stage, further optimising the manufacture process. The use of SLA for rapid tooling allows for a cyclic approach to mould design, with a design able to be produced, tested and any alterations made to the design within a much shorter time frame (as little as 1 day). The integration of SLA rapid tooling and injection moulding reduces the overall cost and the lead-time that comes with using traditional metal moulds (Formlabs, 2016a; Mendible et al., 2017) with the lead-time able to be reduced by as much as 50% (Levy et al., 1999). This coupling of technologies makes low production runs economically feasible and also allows for a more agile approach to research (Formlabs, 2016a; Mendible et al., 2017).

5.6 Conclusion

The RTIM method was capable of producing drug-loaded tablets from pharmaceutical polymer-based formulations.

The tablets produced demonstrated high accuracy and precision to the digital design and very low mass variability. The specific surface areas of the tablets produced were accurate to the digital designs and for two of the formulations trialled differences were observed in the drug release profiles.

RTIM allows for micro-scale features to be designed into the surface of a dosage form

and for these to be executed with a high degree of both accuracy and precision. The interparticle porosity of dosage forms produced via this technique is closely controlled. The formulation space available to RTIM is limited, particularly when compared to traditional manufacturing techniques such as powder compaction. RTIM offers advantages for low solubility drugs.

RTIM has demonstrated its capabilities to manufacture pharmaceutical dosage forms with designed surface micro-features to produce a tablet with a desired specific surface area. The results show that the drug release kinetics can be modified through the the adjustment of specific surface area of the tablets (formulation dependent), which is in line with previous studies (Goyanes et al., 2015a; Robles Martinez et al., 2018). For formulations which demonstrate a relationship in terms of drug release in response to SSA modification, a workflow has been developed to produce tablets via a release-by-design principle. While limitations do apply to this technique, RTIM has demonstrated promise as a manufacturing method which can play a role in the move to the producing smaller batch size of pharmaceuticals. The coupling of SLA and IM allows for a more nimble approach to the manufacturing process, making small batch production runs more economically feasible. By utilising RTIM as both a direct manufacture technology for low production runs of <500 parts and as a development tool for production runs above this level, a greater agility in the construction of a tablet manufacture process can be achieved. This dexterity will play a critical role in the future of pharmaceutical manufacturing, particularly in the fields of micro-batch production for precision medicines and clinical trials.

Authorship Declaration

Erin Walsh: Conceptualisation, Methodology, Validation, Formal analysis, Data curation, Writing - original draft, Writing - review and editing, Visualisation.

Alice Turner: Data curation, Writing - review and editing.

Moulham Alsuleman - Material preparation, Writing - review and editing.

Natalie Maclean - Methodology, Writing - review and editing.

Elke Prasad - Material preparation, Methodology, Writing - review and editing.

Chapter 5. Modulation of Drug Release of Oral Solid Dosage Forms by Specific Surface Area Modification Using Rapid Tooling Injection Moulding

Gavin Halbert - Writing - review and editing.

Joop H. ter Horst: Conceptualisation, Writing - review and editing, Supervision.

Daniel Markl: Conceptualisation, Methodology, Resources, Writing - review and editing, Visualisation, Supervision, Project Administration, Funding acquisition.

Chapter 6

General Conclusions and Future Work

6.1 Chapter Summary

This chapter concludes all the aforementioned research in this thesis. Additionally, some suggestions for future work are made and applications where the RTIM technique could be utilised briefly explored.

6.2 General Conclusions

In summary, through the course of this research, development in the rapid tooling injection moulding process for pharmaceutical applications has been advanced. A greater understanding of the critical parameters and assessment required for stereolithography resins was attained. A number of pharmaceutical-grade polymers were trialled within the system, with tablets successfully produced for the majority of materials. From this study, a deeper understanding of the limitations of the technique was obtained and this knowledge can be applied to the application of the technique with other pharmaceutical polymers. The accuracy and precision to the digital design of the tablets produced was assessed and was found to be high. The ability for this technique to produce dosage forms which were both accurate and precise to the digital designs indicated its suitability for modified drug release applications amongst others. In the final chapter of this thesis, tablets were produced from three paracetamol-based polymer formulations. Three tablet designs were produced for each formulation, with the specific surface area of the designed tablets increasing. For two of the trialled formulations, a clear relationship between increasing the specific surface area of the tablet and an increase in the rate of drug release was observed. This was not observed for the third formulation, where the highly swelling nature of the polymer carrier is believed to hinder any benefits from the increase in specific surface area.

From this research, the RTIM process has demonstrated its capability to produce pharmaceutical dosage forms to a highly accurate and precise standard from a digital design. This technique has demonstrated potential for the direct manufacture of such dosage forms where low production runs are required such as clinical trials and personalised medicines. In addition to this, the technique can also be used as a development tool for larger scale manufacture. With the evolution of the pharmaceutical manufacture landscape inevitable, RTIM could play a role in the future frontiers of medicines manufacturing.

6.3 Future Work

This technique has a number of potential future applications, both within the pharmaceutical industry and beyond. The focus of this section will be on future pharmaceutical applications.

6.3.1 Use of RTIM in Pharmaceutical Manufacturing

The use of SLA in pharmaceutical manufacturing is growing. There is now evidence of direct fabrication of dosage forms via SLA, and the implementation of RTIM using SLA further expands the applications that can be explored. The RTIM process can be used as a manufacturing method for the direct production of pharmaceutical dosage forms with a high degree of flexibility and agility which is not offered by traditional manufacturing approaches. This will become of increased importance as the industry inevitably shifts towards smaller scale production that comes with the rise in personalised and precision medicine. Additionally, this direct manufacture approach would be suitable for the production of dosage forms for clinical trials and would allow for a greater variety of drug dosages to be produced, ultimately allowing for the dosage selection process to be more accurate and better for patients. For larger production runs, the RTIM process can be implemented as a development tool to identify the optimal mould. The highly iterative nature of the RTIM process allows for a desired geometry for a dosage form to be determined in a far quicker, less expensive and more environmentally friendly manner. When the desired geometry has been determined, a traditional tooled steel mould can then be manufactured and used in place of the SLA printed mould inserts. This would increase the throughput of the process and would also allow direct coupling with techniques such as HME and post-production analysis and packaging. Both applications of the RTIM are summarised in Figure 6.1.

6.3.2 Drug Release by Design

With drug release being one of the most critical parameters to how effective our medicines are for patients, it is somewhat surprising that is is often an afterthought of

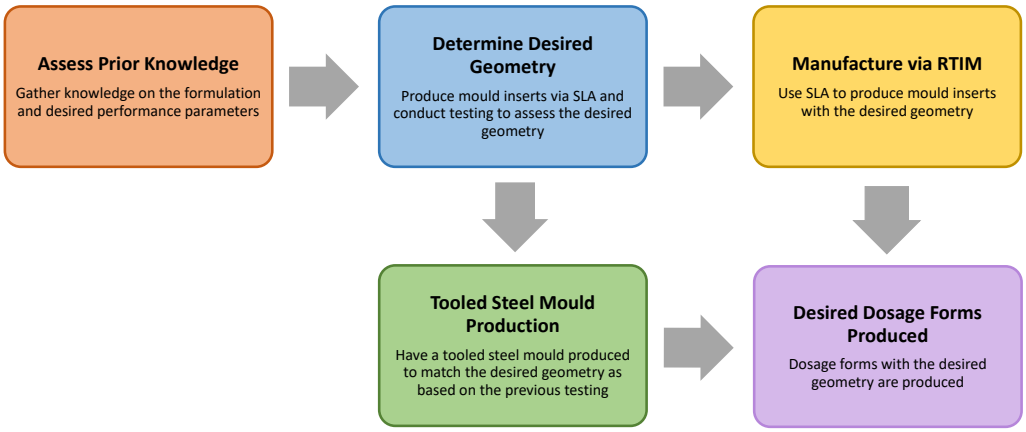

Figure 6.1: A schematic demonstrating the two avenues in which RTIM can be used for the manufacture of pharmaceutical dosage forms.

the formulation and manufacturing process. Typically, the drug release will be assessed after the formulation has been selected and a batch of tablets produced. At that point, if the drug release is found to be unsuitable, a change to either the formulation itself or to the manufacture process must be implemented. The drug release then must be assessed again, and this cycle can repeat multiple times in order to achieve a satisfactory release. This does raise some questions - with drug release being so critical, what is considered to be 'satisfactory'? Surely with such an important parameter, we should be aiming for the perfect release profile for that specific drug and patient. RTIM offers an alternative avenue for this, with the workflow shared in Chapter 5 demonstrating this.

6.3.3 Medical Device Manufacture

Medical devices are often very personal to the individual patient for whom they are designed. They will often require a specialised shape and fit for the patient, and when this is well achieved improvements in patient comfort and compliance can be expected. There has been some documented evidence on the employment of AM as a manufacture technique for medical devices (Gibson and Srinath, 2015; Chin et al., 2017; Ali et al., 2020). RTIM could also be used to manufacture such devices, with benefits in the

accuracy and precision of the device produced. The ability to produced mould inserts in place of producing a traditional mould would result in improved economics and sustainability for the production of such objects which are typically very low production runs, sometimes of only one part. The increased flexibility on the formulations and materials that can be used in conjunction with RTIM compared to direct fabrication from AM also offers benefits for the technique.

6.3.4 Engineered Pharmaceutical Particles

The RTIM method could be used to manufacture pharmaceutical particles with a defined size and shape. An example of a mould insert design to produce micro-scale particles is detailed in Figure 6.2. These particles could be used for a number of applications, such as the assessment of the impact of the particle size/shape on the measurements of process analytical technology (PAT) tools. This is a growing area of interest in the pharmaceutical industry as a greater understanding of particle and material attributes is developed. One example of how these engineered particles could be used to develop PAT tools are to improve the accuracy in particle sizing technologies to identify different aspect ratios in particles. With needle-shaped particles being increasingly common in drug molecules, a greater understanding of these extremes of aspect ratios would improve our ability to assess and understand the impact these particles have on the manufacturing process. RTIM could be used in this case to make a series of particles with differing aspect ratios to understand the current outputs from these technologies and to 'train' them to more accurately determine the size and shape of particles.

A further application of these particles is in compaction studies. The ability of RTIM to create particles with differing shapes and sizes would allow us to better understand the impact that a single particle being misshapen has on the resultant compact for example. It could also be used in the development of a model to allow formulators to better predict the outcomes of compaction when using a blend of materials with different particle shapes and sizes and in varying ratios. From these compaction studies, a better understanding of the resultant pore structures can also be developed.

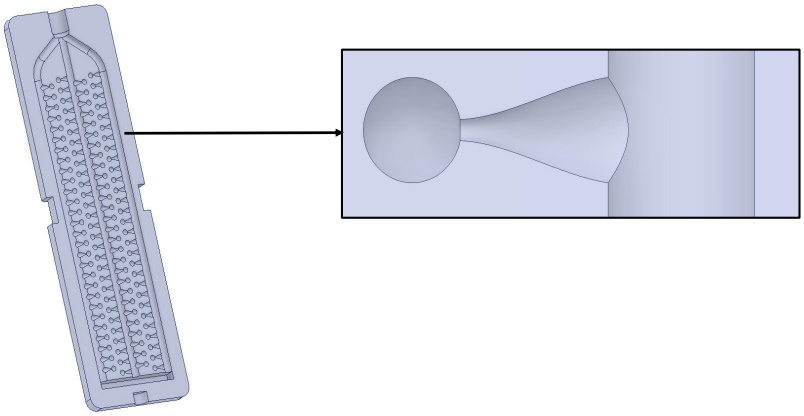

Figure 6.2: An example of a mould insert design for the production of spherical particles. A conical stem leading up to the particles is suggested to minimise the contact between the stem and the particle for ease of removal.

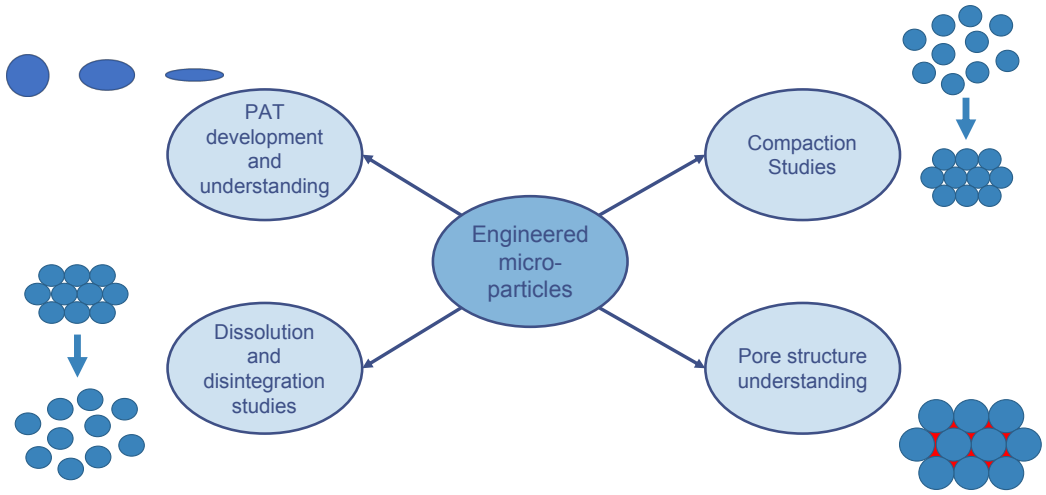

Figure 6.3: A schematic demonstrating some of the applications of pharmaceutical engineered micro-particles.

These compacts can also then be studied to look at the impact that these differing formulations have on the disintegration and dissolution behaviour. The particles themselves can also be used for capsular drug deliver where a specific blend of differing particle shapes, sizes and drug loadings can be used to achieve a desired drug release profile.

Chapter 7

Appendix

7.1 Manufacture of Oral Solid Dosage Forms with Micro-Structure Features via Rapid Tooling Injection Moulding

The data provided in this section is in support of Chapter 4. This appendix provides a data summary for all processable formulations across the three tablet designs.

Table 7.1: Comparison of tablet properties to the 2 Pin digital design for all processable formulations.

Formulation	**Digital Design**	**AFF/PEG**	**AFF/SA**	**AFF/PE**	**KEF**	**KELF**	**KLF**	**LDPE**	**PVA**
Tablet Diameter (mm)	15.23	15.14	15.14	15.11	15.14	15.15	15.16	14.77	15.16
Tablet Thickness (mm)	3.00	3.01	3.01	3.01	2.99	2.98	2.98	2.98	2.99
Pin Depth (mm)	2.00	1.91	1.89	1.94	1.95	1.95	1.97	1.91	1.96
Pin Top Diameter (mm)	1.50	1.48	1.44	1.49	1.47	1.47	1.48	1.49	1.47
Pin Bottom Diameter (mm)	3.00	3.23	3.27	3.19	3.17	3.19	3.13	3.01	3.18
Tablet Volume (mm^3)	530.10	533.24	526.47	519.18	517.40	518.84	518.99	495.11	523.24
Tablet Surface Area (mm^2)	527.54	524.39	519.56	519.56	518.14	519.70	519.87	499.34	522.40
Specific Surface Area (mm^{-1})	1.00	0.98	0.99	1.00	1.00	1.00	1.00	1.01	1.00

Table 7.2: Comparison of tablet properties to the 6 Pin digital design for all processable formulations.

Formulation	**Digital Design**	**AFF/PEG**	**AFF/SA**	**AFF/PE**	**KEF**	**KELF**	**KLF**	**LDPE**	**PVA**
Tablet Diameter (mm)	15.68	15.55	15.55	15.59	15.14	15.53	15.63	15.13	15.64
Tablet Thickness (mm)	3.00	3.01	3.00	3.02	2.99	2.99	2.99	2.99	2.98
Pin Depth (mm)	2.00	1.92	1.92	1.92	1.95	1.96	1.96	1.91	1.94
Pin Top Diameter (mm)	1.50	1.49	1.47	1.49	1.47	1.47	1.49	1.48	1.47
Pin Bottom Diameter (mm)	3.00	3.23	3.17	3.21	3.07	3.21	3.16	3.01	3.19
Tablet Volume (mm^3)	530.12	527.14	521.05	521.05	521.81	523.84	511.12	485.49	519.05
Tablet Surface Area (mm^2	593.00	585.05	575.31	584.08	585.62	583.56	587.48	554.35	585.19
Specific Surface Area (mm^{-1})	1.12	1.11	1.10	1.12	1.12	1.14	1.13	1.14	1.13

Table 7.3: Comparison of tablet properties to the 10 Pin digital design for all processable formulations.

Formulation	**Digital Design**	**AFF/PEG**	**AFF/SA**	**AFF/PE**	**KEF**	**KLF**	**KELF**	**LDPE**	**PVA**
Tablet Diameter (mm)	16.12	16.06	15.97	16.06	16.09	16.07	16.12	15.55	16.06
Tablet Thickness (mm)	3.00	3.02	3.01	3.02	2.99	3.00	2.98	2.99	2.99
Pin Depth (mm)	2.00	1.92	1.91	1.93	1.94	1.96	1.95	1.92	1.94
Pin Top Diameter (mm)	1.50	1.49	1.44	1.48	1.46	1.46	1.47	1.50	1.47
Pin Bottom Diameter (mm)	3.00	3.19	3.26	3.19	3.13	3.11	3.15	3.04	3.20
Tablet Volume (mm^3)	530.12	520.51	499.73	517.77	524.93	519.36	520.27	485.20	516.78
Tablet Surface Area (mm^2)	658.32	646.98	632.02	645.66	650.04	648.33	651.05	618.20	648.08
Specific Surface Area (mm^{-1})	1.24	1.24	1.26	1.25	1.24	1.25	1.25	1.27	1.25

Table 7.4: Summary table of tablet mass variations.

Formulation	**2 Pin Design**	**6 Pin Design**	**10 Pin Design**	**Average**
AFF/PEG 85/15	699±14 mg	699±15 mg	701±13 mg	700±13 mg
AFF/SA 85/15	625±8 mg	621±9 mg	622±8 mg	623±8 mg
AFF/PE 85/15	603±9 mg	604±8 mg	604±11 mg	604±9 mg
LDPE	445±3 mg	445±2 mg	445±3 mg	445±3 mg
KEF	596±3 mg	594±2 mg	596±4 mg	695±3 mg
KELF	603±7 mg	603±4 mg	604±6 mg	603±5 mg
KLF	597±3 mg	597±3 mg	596±2 mg	596±2 mg
PVA	661±6 mg	659±6 mg	661±4 mg	660±5 mg

7.2 Fine-tuning of Drug Release of Oral Solid Dosage Forms by Specific Surface Area Modification Using Rapid Tooling Injection Moulding

The data provided in this section is in support of Chapter 5. This appendix provides a data summary for all processable formulations across the three tablet designs, a summary of the tablet masses and the k and m parameters as calculated via the power law.

Table 7.5: Comparison of tablet properties to the 2 Pin digital design for all formulations.

Formulation	**Digital Design**	**AFF/PCM 50/50**	**KELF/PCM 90/10**	**PVA/PCM 90/10**
Tablet Diameter (mm)	15.23	15.08	15.11	15.14
Tablet Thickness (mm)	3.00	2.99	2.99	3.03
Pin Depth (mm)	2.00	1.93	1.95	1.93
Pin Top Diameter (mm)	1.50	1.48	1.48	1.50
Pin Bottom Diameter (mm)	3.00	3.08	3.02	3.04
Tablet Volume (mm^3)	530.10	518.66	519.86	528.80
Tablet Surface Area (mm^2)	527.54	517.71	519.42	522.60
Specific Surface Area (mm^{-1})	1.00	1.00	1.00	0.99

Table 7.6: Comparison of tablet properties to the 6 Pin digital design for all formulations.

Formulation	**Digital Design**	**AFF/PCM 50/50**	**KELF/PCM 90/10**	**PVA/PCM 90/10**
Tablet Diameter (mm)	15.68	15.56	15.61	15.63
Tablet Thickness (mm)	3.00	2.99	2.98	3.02
Pin Depth (mm)	2.00	1.94	1.95	1.94
Pin Top Diameter (mm)	1.50	1.48	1.48	1.48
Pin Bottom Diameter (mm)	3.00	2.98	3.02	3.02
Tablet Volume (mm^3)	530.12	521.65	522.49	531.80
Tablet Surface Area (mm^2	593.00	580.86	584.42	589.46
Specific Surface Area (mm^{-1})	1.12	1.11	1.12	1.11

Table 7.7: Comparison of tablet properties to the 10 Pin digital design for all formulations.

Formulation	**Digital Design**	**AFF/PCM 50/50**	**KELF/PCM 90/10**	**PVA/PCM 90/10**
Tablet Diameter (mm)	16.12	15.97	16.10	16.13
Tablet Thickness (mm)	3.00	2.99	3.01	2.99
Pin Depth (mm)	2.00	1.95	1.94	1.95
Pin Top Diameter (mm)	1.50	1.48	1.48	1.50
Pin Bottom Diameter (mm)	3.00	3.04	3.04	3.00
Tablet Volume (mm^3)	530.12	518.22	532.38	530.79
Tablet Surface Area (mm^2)	658.32	644.46	652.51	655.15
Specific Surface Area (mm^{-1})	1.24	1.24	1.23	1.23

Table 7.8: Summary table of tablet mass variations.

Formulation	**2 Pin Design**	**6 Pin Design**	**10 Pin Design**	**Average**
AFF/PCM 50/50	648±5 mg	649±6 mg	650±4 mg	649±5 mg
KELF/PCM 90/10	604±3 mg	601±2 mg	604±4 mg	603±3 mg
PVA/PCM 90/10	662±5 mg	663±5 mg	664±5 mg	663±5 mg

Table 7.9: Summary table of k and m parameters.

Formulation	**k**	**m**
AFF/PCM 50/50 2 Pin	1.168	0.848
AFF/PCM 50/50 6 Pin	1.459	0.880
AFF/PCM 50/50 10 Pin	3.696	0.732
KELF/PCM 90/10 2 Pin	0.770	0.786
KELF/PCM 90/10 6 Pin	1.243	0.738
KELF/PCM 90/10 10 Pin	1.513	0.730
PVA/PCM 90/10 2 Pin	0.890	0.689
PVA/PCM 90/10 6 Pin	0.783	0.710
PVA/PCM 90/10 10 Pin	0.723	0.736

7.3 Impact of the COVID-19 Pandemic

While the impact of the COVID-19 pandemic has been widespread and felt by all, I would like to take the opportunity to outline the direct impact that this has had on my research.

When the UK entered lock-down in March 2020, our research facilities based on campus at the University of Strathclyde closed. Access to the laboratory was not regained until August 2020. Whilst I utilised this time to the best of my ability, the implications of not being able to access the laboratory were significant. Practical research was critical to the progress of my research, and this loss of time resulted in reduced data output and progress.

When access to our research facilities was regained, I was fortunate to be the sole user of the majority of the equipment I required. Within our department, maximum occupancy limits were put in place across the laboratories. This, in turn with the implementation of activity planning forms which had to be submitted at least one week prior to the activity taking place, meant that although the facilities were open, my productivity was severely impaired.

While I have been very lucky to be able to submit my thesis without major delays, had I not encountered the aforementioned set-backs I believe I would have been able to conduct further research and expand both on my own knowledge and in sharing additional knowledge with the wider research community.

Bibliography

J. Aho, J. P. Bøtker, N. Genina, M. Edinger, L. Arnfast, and J. Rantanen. Roadmap to 3D-Printed Oral Pharmaceutical Dosage Forms: Feedstock Filament Properties and Characterization for Fused Deposition Modeling. *Journal of Pharmaceutical Sciences*, 108(1):26–35, 2019. ISSN 15206017. doi: 10.1016/j.xphs.2018.11.012.

M. A. Alhnan, T. C. Okwuosa, M. Sadia, K. W. Wan, W. Ahmed, and B. Arafat. Emergence of 3D Printed Dosage Forms: Opportunities and Challenges. *Pharmaceutical Research*, 33:1817–1832, 2016. ISSN 1573904X. doi: 10.1007/s11095-016-1933-1.

M. A. Ali, M. Rajabi, and S. Sudhir Sali. Additive manufacturing potential for medical devices and technology. *Current Opinion in Chemical Engineering*, 28:127–133, 2020. ISSN 22113398. doi: 10.1016/j.coche.2020.05.001.

M. Alomari, F. H. Mohamed, A. W. Basit, and S. Gaisford. Personalised dosing: Printing a dose of one's own medicine. *International Journal of Pharmaceutics*, 494 (2):568–577, 2015. ISSN 18733476. doi: 10.1016/j.ijpharm.2014.12.006.

D. Annicchiarico and J. R. Alcock. Review of factors that affect shrinkage of molded part in injection molding. *Materials and Manufacturing Processes*, 29:662–682, 2014. ISSN 15322475. doi: 10.1080/10426914.2014.880467.

N. S. Arden, A. C. Fisher, K. Tyner, L. X. Yu, S. L. Lee, and M. Kopcha. Industry 4.0 for pharmaceutical manufacturing: Preparing for the smart factories of the future. *International Journal of Pharmaceutics*, 602:120554, 2021. ISSN 03785173. doi: 10.1016/j.ijpharm.2021.120554.

Bibliography

Ashland Inc. Klucel hydroxypropylcellulose physical and chemical properties (Datasheet). Technical report, 2017. URL http://www.ashland.com/file_source/Ashland/Product/Documents/Pharmaceutical/PC_11229_Klucel_HPC.pdf.

ASTM International. Standard Test Method for Deflection Temperature of Plastics Under Flexural Load in the Edgewise Position, 2001. URL https://www.astm.org/Standards/D648.htm.

ASTM International. Standard Practice for Preparation of Metallographic Specimens, 2016. ISSN 21653992. URL http://www.astm.org/cgi-bin/resolver.cgi?E140%0Ahttp://www.astm.org/Standards/E8.htm.

F. D. Bähner and J. K. Huusom. A Debottlenecking Study of an Industrial Pharmaceutical Batch Plant. *Industrial and Engineering Chemistry Research*, 58(43): 20003–20013, 2019. ISSN 15205045. doi: 10.1021/acs.iecr.9b03134.

L. Bartlett. *A Preliminary Study of Using Plastic Molds in Injection Molding*. Master of science thesis, The Ohio State University, 2017. URL http://www.albayan.ae.

L. Bartlett, E. Grunden, R. Mulyana, and J. Castro. A Preliminary Study On The Performance Of Additive Manufacturing Tooling For Injection Moulding. In *SPE ANTEC*, pages 100–104, 2017.

S. K. Battu, M. A. Repka, S. Majumdar, and R. Y. Madhusudan. Formulation and evaluation of rapidly disintegrating fenoverine tablets: Effect of superdisintegrants. *Drug Development and Industrial Pharmacy*, 33(11):1225–1232, 2007. ISSN 03639045. doi: 10.1080/03639040701377888.

R. C. R. Beck, P. S. Chaves, A. Goyanes, B. Vukosavljevic, A. Buanz, M. Windbergs, A. W. Basit, and S. Gaisford. 3D printed tablets loaded with polymeric nanocapsules: An innovative approach to produce customized drug delivery systems. *International Journal of Pharmaceutics*, 528(1-2):268–279, 2017. ISSN 18733476. doi: 10.1016/j.ijpharm.2017.05.074.

D. Bould, J. Sienz, C. Arnold, M. Huszar, F. Belblidia, and H. M. Davies. Sustainable injection moulding: The impact of materials selection and gate location on part warpage and injection pressure. *Sustainable Materials and Technologies*, 5:1–8, 2015. ISSN 22149937. doi: 10.1016/j.susmat.2015.07.001.

M. L. Bruschi. *Strategies to Modifiy the Drug Release from Pharmaceutical Systems*. Elsevier, 2015. ISBN 9780081001127.

S. Y. Chin, Y. C. Poh, A. Kohler, J. T. Compton, L. L. Hsu, K. M. Lau, S. Kim, B. W. Lee, F. Y. Lee, and S. K. Sia. Additive manufacturing of hydrogel-based materials for next-generation implantable medical devices. *Science Robotics*, 2(2), 2017. doi: 10.1126/scirobotics.aah6451.Additive.

J. S. Cohen. Dose Discrepancies Between the Physicians' Desk Reference and the Medical Literature, and Their Possible Role in the High Incidence of Dose-Related Adverse Drug Events. *Archives of Internal Medicine*, 161(7):957–964, 2001. doi: doi:10.1001/archinte.161.7.957.

J. Colton and B. Blair. Experimental study of post-build cure of stereolithography polymers for injection molds. *Rapid Prototyping Journal*, 5(2):72–81, 1999. ISSN 13552546. doi: 10.1108/13552549910267452.

P. Costa, J. Manuel, and S. Lobo. Modeling and comparison of dissolution profiles. *European Journal of Pharmaceutical Sciences*, 13:123–133, 2001. ISSN 1521298X. doi: 10.14227/DT160209P41.

F. De Santis, R. Pantani, V. Speranza, and G. Titomanlio. Analysis of shrinkage development of a semicrystalline polymer during injection molding. *Industrial and Engineering Chemistry Research*, 49(5):2469–2476, 2010. ISSN 08885885. doi: 10.1021/ie901316p.

U.S. Food Department of Health and Human Services and Drug Administration. Pharmaceutical Quality for the 21st Century A Risk-Based Approach Progress Report. Technical report, 2007. URL `https:`

//www.fda.gov/about-fda/center-drug-evaluation-and-research-cder/pharmaceutical-quality-21st-century-risk-based-approach-progress-report.

K. Eggenreich, S. Windhab, S. Schrank, D. Treffer, H. Juster, G. Steinbichler, S. Laske, G. Koscher, E. Roblegg, and J. G. Khinast. Injection molding as a one-step process for the direct production of pharmaceutical dosage forms from primary powders. *International Journal of Pharmaceutics*, 2016. ISSN 18733476. doi: 10.1016/j.ijpharm.2016.03.034.

T. Finnes. High Definition 3D Printing – Comparing SLA and FDM Printing Technologies. *The Journal of Undergraduate Research*, 13(13), 2015. ISSN 0008-3976. doi: 10.1111/j.1744-7976.2005.00414.x.

C. Fischer, A. Seefried, B. Merle, M. Göken, and D. Drummer. Influencing hardness and wear during the dynamic tempered microinjection molding process by considering isothermal holding time. *Polymer Engineering and Science*, 57(2):121–128, 2017. ISSN 15482634. doi: 10.1002/pen.24394.

A. T. Florence and V. H. L. Lee. Personalised medicines: More tailored drugs, more tailored delivery. *International Journal of Pharmaceutics*, 415(1-2):29–33, 2011. ISSN 03785173. doi: 10.1016/j.ijpharm.2011.04.047.

Formlabs. Moldmaking with 3D Prints - Techniques for Prototyping and Production. Technical report, Formlabs, 2016a. URL https://3d.formlabs.com/moldmaking-with-3d-prints/.

Formlabs. Material Data Sheet - High Temp. Technical report, Massachusetts, 2016b. URL https://archive-media.formlabs.com/upload/XL-DataSheet.pdf.

Formlabs. Material Data Sheet - Standard. Technical report, Formlabs, Massachusetts, 2017. URL https://archive-media.formlabs.com/upload/Clear-DataSheet.pdf.

Y. Fu and W. J. Kao. Drug Release Kinetics and Transport Mechanisms of Non-

degradable and Degradable Polymeric Delivery Systems. *Expert Opinion on Drug Delivery*, 7(4):429–444, 2010. doi: 10.1517/17425241003602259.Drug.

N. Genina, J. Holländer, H. Jukarainen, E. Mäkilä, J. Salonen, and N. Sandler. Ethylene vinyl acetate (EVA) as a new drug carrier for 3D printed medical drug delivery devices. *European Journal of Pharmaceutical Sciences*, 90:53–63, 2016. ISSN 18790720. doi: 10.1016/j.ejps.2015.11.005.

J. Giboz, T. Copponnex, and P. Mélé. Microinjection molding of thermoplastic polymers: A review. *Journal of Micromechanics and Microengineering*, 17:96–109, 2007. ISSN 09601317. doi: 10.1088/0960-1317/17/6/R02.

I. Gibson and A. Srinath. Simplifying Medical Additive Manufacturing: Making the Surgeon the Designer. *Procedia Technology*, 20(July):237–242, 2015. doi: 10.1016/j.protcy.2015.07.038.

C. I. Gioumouxouzis, C. Karavasili, and D. G. Fatouros. Recent advances in pharmaceutical dosage forms and devices using additive manufacturing technologies. *Drug Discovery Today*, 24(2):636–643, 2019. ISSN 18785832. doi: 10.1016/j.drudis.2018.11.019.

A. Goyanes, A. B. M. Buanz, A. W. Basit, and S. Gaisford. Fused-filament 3D printing (3DP) for fabrication of tablets. *International Journal of Pharmaceutics*, 476(1):88–92, 2014. ISSN 18733476. doi: 10.1016/j.ijpharm.2014.09.044.

A. Goyanes, P. Robles Martinez, A. Buanz, A. W. Basit, and S. Gaisford. Effect of geometry on drug release from 3D printed tablets. *International Journal of Pharmaceutics*, 494(2):657–663, 2015a. ISSN 18733476. doi: 10.1016/j.ijpharm.2015.04.069.

A. Goyanes, J. Wang, A. Buanz, R. Martínez-Pacheco, R. Telford, S. Gaisford, and A. W. Basit. 3D Printing of Medicines: Engineering Novel Oral Devices with Unique Design and Drug Release Characteristics. *Molecular Pharmaceutics*, 12:4077–4084, 2015b. ISSN 15438392. doi: 10.1021/acs.molpharmaceut.5b00510.

A. Goyanes, M. Kobayashi, R. Martínez-Pacheco, S. Gaisford, and A. W. Basit. Fused-filament 3D printing of drug products: Microstructure analysis and drug release characteristics of PVA-based caplets. *International Journal of Pharmaceutics*, 514 (1):290–295, 2016. ISSN 18733476. doi: 10.1016/j.ijpharm.2016.06.021.

A. Goyanes, F. Fina, A. Martorana, D. Sedough, S. Gaisford, and A. W. Basit. Development of modified release 3D printed tablets (printlets) with pharmaceutical excipients using additive manufacturing. *International Journal of Pharmaceutics*, 527(1-2):21–30, 2017. ISSN 18733476. doi: 10.1016/j.ijpharm.2017.05.021.

Grand View Research. Pharmaceutical Manufacting Market Size, Share and Trends Analysis Report by Drug Development, By Formulation, By Route of Administration, By Therapy Area, By Prescription, By Age Group, And Segment Forecasts, 2020-2027. Technical report, Grand View Research, 2020.

A. Harvey, A. Brand, S. T. Holgate, L. V. Kristiansen, H. Lehrach, A. Palotie, and B. Prainsack. The future of technologies for personalised medicine. *New Biotechnology*, 29(6):625–633, 2012. ISSN 18716784. doi: 10.1016/j.nbt.2012.03.009.

M. Heckele and W. K. Schomburg. Review on micro molding of thermoplastic polymers. *Journal of Micromechanics and Microengineering*, 14, 2004. ISSN 09601317. doi: 10.1088/0960-1317/14/3/R01.

M. Ibrahim, M. Barnes, R. McMillin, D. W. Cook, S. Smith, M. Halquist, D. Wijesinghe, and T. D. Roper. 3D Printing of Metformin HCl PVA Tablets by Fused Deposition Modeling: Drug Loading, Tablet Design, and Dissolution Studies. *AAPS PharmSciTech*, 20(5):1–11, 2019. ISSN 15309932. doi: 10.1208/s12249-019-1400-5.

International Standards Organisation. International Standards Organisation ISO/ASTM 52900 Additive Manufacturing - General Principles. Technical report, International Standards Organisation, 2015. URL `https://www.iso.org/obp/ui/#iso:std:iso-astm:52900:ed-1:v1:en`.

Jacobs, P. F. *Rapid Prototyping and Manufacturing: Fundamentals of StereoLithography*. McGraw-Hill, Inc., New York, 1993. ISBN 0070324336.

W. Jamróz, M. Kurek, E. Łyszczarz, W. Brniak, and R. Jachowicz. Printing techniques: Recent developments in pharmaceutical technology. *Acta Poloniae Pharmaceutica - Drug Research*, 74(3):753–763, 2017. ISSN 00016837.

W. Jamróz, J. Szafraniec, M. Kurek, and R. Jachowicz. 3D Printing in Pharmaceutical and Medical Applications – Recent Achievements and Challenges. *Pharmaceutical Research*, 2018. ISSN 1573904X. doi: 10.1007/s11095-018-2454-x.

M. Jani, B. B. Yimer, T. Sheppard, M. Lunt, and W. G. Dixon. Time trends and prescribing patterns of opioid drugs in UK primary care patients with non-cancer pain: A retrospective cohort study. *PLoS Medicine*, 17(10):1–16, 2020. ISSN 15491676. doi: 10.1371/journal.pmed.1003270.

Y. Kapoor, R. F. Meyer, B. K. Meyer, J. C. DiNunzio, A. Bhambhani, J. Stanbro, K. J. M. Ploeger, E. N. Guidry, G. M. Troup, A. T. Procopio, and A. C. Templeton. Flexible Manufacturing: The Future State of Drug Product Development and Commercialization in the Pharmaceutical Industry. *Journal of Pharmaceutical Innovation*, 16(1):2–10, 2021. ISSN 19398042. doi: 10.1007/s12247-019-09426-z.

H. Y. Karasulu and G. Ertan. Different geometric shaped hydrogel theophylline tablets: Statistical approach for estimating drug release. *Farmaco*, 57(11):939–945, 2002. ISSN 0014827X. doi: 10.1016/S0014-827X(02)01297-1.

S. Kashyap and D. Datta. Process parameter optimization of plastic injection molding: a review. *International Journal of Plastics Technology*, 19:1–18, 2015. ISSN 0975072X. doi: 10.1007/s12588-015-9115-2.

S. A. Khaled, J. C. Burley, M. R. Alexander, J. Yang, and C. J. Roberts. 3D printing of five-in-one dose combination polypill with defined immediate and sustained release profiles. *Journal of Controlled Release*, 217:308–314, 2015. ISSN 18734995. doi: 10.1016/j.jconrel.2015.09.028.

I. Khanna. Drug discovery in pharmaceutical industry - productivity challenges and trends. *Drug Discovery Today*, 17(19-20):1088–1102, 2012. ISSN 1359-6446. doi: 10.1016/j.drudis.2012.05.007.

G. Kollamaram, D. M. Croker, G. M. Walker, A. Goyanes, A. W. Basit, and S. Gaisford. Low temperature fused deposition modeling (FDM) 3D printing of thermolabile drugs. *International Journal of Pharmaceutics*, 545(1-2):144–152, 2018. ISSN 18733476. doi: 10.1016/j.ijpharm.2018.04.055.

C. Korte and J. Quodbach. Formulation development and process analysis of drug-loaded filaments manufactured via hot-melt extrusion for 3D-printing of medicines. *Pharmaceutical Development and Technology*, 23(10):1117–1127, 2018. ISSN 10979867. doi: 10.1080/10837450.2018.1433208.

J. G. Kovács, F. Szabó, N. K. Kovács, A. Suplicz, B. Zink, T. Tábi, and H. Hargitai. Thermal simulations and measurements for rapid tool inserts in injection molding applications. *Applied Thermal Engineering*, 85:44–51, 2015. ISSN 13594311. doi: 10.1016/j.applthermaleng.2015.03.075.

S. L. Lee, T. F. O'Connor, X. Yang, C. N. Cruz, S. Chatterjee, R. D. Madurawe, C. M. V. Moore, L. X. Yu, and J. Woodcock. Modernizing Pharmaceutical Manufacturing: from Batch to Continuous Production. *Journal of Pharmaceutical Innovation*, 10(3):191–199, 2015. ISSN 19398042. doi: 10.1007/s12247-015-9215-8.

G. N. Levy, R. Schindel, and J. P. Kruth. Rapid Manufacturing and Rapid Tooling with Layer Manufacturing (LM) Technologies, State of the Art and Future Perspectives. *CIRP Annals - Manufacturing Technology*, 2, 1999.

C. Y. Liaw and M. Guvendiren. Current and emerging applications of 3D printing in medicine. *Biofabrication*, 9(2), 2017. ISSN 17585090. doi: 10.1088/1758-5090/aa7279.

S. C. Ligon, R. Liska, J. Stampfl, M. Gurr, and R. Mülhaupt. Polymers for 3D Printing and Customized Additive Manufacturing. *Chemical Reviews*, 117(15):10212–10290, 2017. ISSN 15206890. doi: 10.1021/acs.chemrev.7b00074.

Donald M. Lloyd-Jones, Eric P. Leip, Martin G. Larson, Ralph B. D'Agostino, Alexa Beiser, Peter W.F. Wilson, Philip A. Wolf, and Daniel Levy. Prediction of lifetime risk

for cardiovascular disease by risk factor burden at 50 years of age. *Circulation*, 113 (6):791–798, 2006. ISSN 00097322. doi: 10.1161/CIRCULATIONAHA.105.548206.

T. Loftsson and M. E. Brewster. Pharmaceutical applications of cyclodextrins: Basic science and product development. *Journal of Pharmacy and Pharmacology*, 62(11): 1607–1621, 2010. ISSN 00223573. doi: 10.1111/j.2042-7158.2010.01030.x.

G. Lucchetta, M. Sorgato, S. Carmignato, and E. Savio. Investigating the technological limits of micro-injection molding in replicating high aspect ratio micro-structured surfaces. *CIRP Annals - Manufacturing Technology*, 63(1):521–524, 2014. ISSN 17260604. doi: 10.1016/j.cirp.2014.03.049.

G. Lurcott. The Effects of the Genetic Absence and Inhibition of CYP2D6 on the Metabolism of Codeine and Its. *Anesthesia Progress: Journal of the American Dental Society of Anethesiology*, 3006(99):154–156, 1999.

R. Mahon, Y. Balogun, G. Oluyemi, and J. Njuguna. Swelling performance of sodium polyacrylate and poly(acrylamide-co-acrylic acid) potassium salt. *SN Applied Sciences*, 2(1):1–15, 2020. ISSN 25233971. doi: 10.1007/s42452-019-1874-5.

D. Markl and J. A. Zeitler. A Review of Disintegration Mechanisms and Measurement Techniques. *Pharmaceutical Research*, 34(5):890–917, 2017. ISSN 1573904X. doi: 10.1007/s11095-017-2129-z.

D. Markl, J. A. Zeitler, C. Rasch, M. H. Michaelsen, A. Müllertz, J. Rantanen, T. Rades, and J. Bøtker. Analysis of 3D Prints by X-ray Computed Microtomography and Terahertz Pulsed Imaging. *Pharmaceutical Research*, 34(5):1037–1052, December 2017.

D. Markl, A. Strobel, R. Schlossnikl, J. Bøtker, P. Bawuah, C. Ridgway, J. Rantanen, T. Rades, P. Gane, K. Peiponen, and J. A. Zeitler. Characterisation of pore structures of pharmaceutical tablets: A review. *International Journal of Pharmaceutics*, 538 (1-2):188–214, March 2018a.

D. Markl, A. Strobel, R. Schlossnikl, J. Bøtker, P. Bawuah, C. Ridgway, J. Rantanen, T. Rades, P. Gane, K. E. Peiponen, and J. A. Zeitler. Characterisation of pore structures of pharmaceutical tablets: A review. *International Journal of Pharmaceutics*, 2018b. ISSN 18733476. doi: 10.1016/j.ijpharm.2018.01.017.

F. P. W. Melchels, J. Feijen, and D. W. Grijpma. A review on stereolithography and its applications in biomedical engineering. *Biomaterials*, 31(24):6121–6130, 2010. ISSN 01429612. doi: 10.1016/j.biomaterials.2010.04.050.

A. Melocchi, G. Loreti, M. D. Del Curto, A. Maroni, A. Gazzaniga, and L. Zema. Evaluation of hot-melt extrusion and injection molding for continuous manufacturing of immediate-release tablets. *Journal of Pharmaceutical Sciences*, 104:1971–1980, 2015. ISSN 15206017. doi: 10.1002/jps.24419.

G. A. Mendible, J. A. Rulander, S. P. Johnston, G. A. Mendible, J. A. Rulander, and S. P. Johnston. Comparative study of rapid and conventional tooling for plastics injection molding. *Rapid Prototyping Journal*, 23(1):344–352, 2017. doi: 10.1108/RPJ-01-2016-0013.

M. Mikulic. Pharmaceutical Products and Market. Technical report, 2017.

M. Mikulic. Global Pharmaceutical Industry - Statistics and Facts. Technical report, Statista, 2020. URL `https://www.statista.com/topics/1764/global-pharmaceutical-industry/`.

M. Mikulic. Pharmaceutical Products and Market. Technical report, Statista, 2021. URL `https://www.statista.com/statistics/299694/world-pharmaceutical-sales-by-region-forecast/`.

N. N. Mohammed, S. Majumdar, A. Singh, W. Deng, N. S. Murthy, E. Pinto, D. Tewari, T. Durig, and M. A. Repka. Klucel™ EF and ELF polymers for immediate-release oral dosage forms prepared by melt extrusion technology. *AAPS PharmSciTech*, 13 (4):1158–1169, 2012. ISSN 15309932. doi: 10.1208/s12249-012-9834-z.

M. Mohan, M. N. M. Ansari, and R. A. Shanks. Review on the Effects of Process Parameters on Strength, Shrinkage, and Warpage of Injection Molding Plastic Component. *Polymer - Plastics Technology and Engineering*, 56(1), 2017. ISSN 15256111. doi: 10.1080/03602559.2015.1132466.

R. Morita, R. Honda, and Y. Takahashi. Development of oral controlled release preparations, a PVA swelling controlled release system (SCRS). I. Design of SCRS and its release controlling factor. *Journal of Controlled Release*, 63(3):297–304, 2000. ISSN 01683659. doi: 10.1016/S0168-3659(99)00203-5.

S. Nale and A. G. Kalbande. A review on 3D Printing. *International Journal of Innovative and Emerging Research in Engineering*, 5(7):2001–2004, 2016.

T. D. Ngo, A. Kashani, G. Imbalzano, K. T. Q. Nguyen, and D. Hui. Additive manufacturing (3D printing): A review of materials, methods, applications and challenges. *Composites Part B: Engineering*, 143(December 2017):172–196, 2018. ISSN 13598368. doi: 10.1016/j.compositesb.2018.02.012.

Office For National Statistics. Overview of the UK Population: January 2021, 2021. URL `https://www.ons.gov.uk/peoplepopulationandcommunity/populationandmigration/populationestimates/articles/overviewoftheukpopulation/january2021`.

M. Packianather, C. Griffiths, and W. Kadir. Micro injection moulding process parameter tuning. In *Procedia CIRP*, 2015. doi: 10.1016/j.procir.2015.06.093.

K. Pietrzak, A. Isreb, and M. A. Alhnan. A flexible-dose dispenser for immediate and extended release 3D printed tablets. *European Journal of Pharmaceutics and Biopharmaceutics*, 96:380–387, 2015. ISSN 18733441. doi: 10.1016/j.ejpb.2015.07.027.

F. Q. Pires, I. Alves-Silva, L. A. G. Pinho, J. A. Chaker, L. L. Sa-Barreto, G. M. Gelfuso, T. Gratieri, and M. Cunha-Filho. Predictive models of FDM 3D printing using experimental design based on pharmaceutical requirements for tablet

production. *International Journal of Pharmaceutics*, 588:119728, May 2020. doi: 10.1016/j.ijpharm.2020.119728.

S. N. Politis and D. M. Rekkas. The evolution of the manufacturing science and the pharmaceutical industry. *Pharmaceutical Research*, 28(7):1779–1781, 2011. ISSN 07248741. doi: 10.1007/s11095-011-0479-5.

Polymer Properties Database. Polyacrylates, 2020. URL `https://polymerdatabase.com/polymer%20classes/Polyacrylate%20type.html`.

E. Prasad, M. T. Islam, D. J. Goodwin, A. J. Megarry, G. W. Halbert, A. J. Florence, and J. Robertson. Development of a hot-melt extrusion (HME) process to produce drug loaded Affinisol™ 15LV filaments for fused filament fabrication (FFF) 3D printing. *Additive Manufacturing*, 29(July):100776, 2019. ISSN 22148604. doi: 10.1016/j.addma.2019.06.027.

L. K. Prasad and H. Smyth. 3D Printing technologies for drug delivery: a review. *Drug Development and Industrial Pharmacy*, 42(7):1019–1031, 2016. ISSN 15205762. doi: 10.3109/03639045.2015.1120743.

M. E. Prendergast and J. A. Burdick. Recent Advances in Enabling Technologies in 3D Printing for Precision Medicine. *Advanced Materials*, 32:1–14, 2020. doi: 10.1002/adma.201902516.

J. A. Qayyum, K. Altaf, A. M. Abdul Rani, F. Ahmad, and M. Jahanzaib. Performance of 3D printed polymer mold for metal injection molding process. *ARPN Journal of Engineering and Applied Sciences*, 12(22):6430–6434, 2017. ISSN 18196608. doi: 10.3390/met8060433.

T. Quinten, T. De Beer, Jt. P. Remon, and C. Vervaet. Overview of Injection Molding As a Manufacturing Technique for Pharmaceutical Applications. *Innovation*, pages 1–42, 2009a.

T. Quinten, T. De Beer, C. Vervaet, and J. P. Remon. Evaluation of injection moulding as a pharmaceutical technology to produce matrix tablets. *European Journal of*

Pharmaceutics and Biopharmaceutics, 71:145–154, 2009b. ISSN 09396411. doi: 10.1016/j.ejpb.2008.02.025.

T. Quinten, Y. Gonnissen, E. Adriaens, T. De Beer, V. Cnudde, B. Masschaele, L. Van Hoorebeke, J. Siepmann, J. P. Remon, and C. Vervaet. Development of injection moulded matrix tablets based on mixtures of ethylcellulose and low-substituted hydroxypropylcellulose. *European Journal of Pharmaceutical Sciences*, 37:207–216, 2009c. ISSN 09280987. doi: 10.1016/j.ejps.2009.02.006.

S. Rahmati and P. Dickens. Stereolithography for injection mould tooling. *Rapid Prototyping Journal*, 3(2):53–60, 1997. ISSN 13552546. doi: 10.1108/13552549710176671.

S. Rahmati and P. Dickens. Rapid tooling analysis of Stereolithography injection mould tooling. *International Journal of Machine Tools and Manufacture*, 47(5 SPEC. ISS.): 740–747, 2007. ISSN 08906955. doi: 10.1016/j.ijmachtools.2006.09.022.

A. Rani, A. Majdi, K. Altaf, F. Ahmad, and J. Ahmad. Enhanced Polymer Rapid Tooling for Metal Injection Moulding Process. In *3rd International Conference on Progress in Additive Manufacturing*, pages 656–661, 2018. doi: 10.25341/D4J014.

J. Rantanen and J. Khinast. The Future of Pharmaceutical Manufacturing Sciences. *Journal of Pharmaceutical Sciences*, 104(11):3612–3638, 2015. ISSN 15206017. doi: 10.1002/jps.24594.

Amir Rashid. *Additive Manufacturing Technologies*. CIRP Encyclopedia of Production Engineering, 2018. doi: 10.1007/978-3-642-35950-7_16866-1.

T. D. Reynolds, S. A. Mitchell, and K. M. Balwinski. Investigation of the effect of tablet surface area/volume on drug release from hydroxypropylmethylcellulose controlled-release matrix tablets. *Drug Development and Industrial Pharmacy*, 28(4):457–466, 2002. ISSN 03639045. doi: 10.1081/DDC-120003007.

A. S. Ribeiro, N. Hopkinson, and C. H. Ahrens. Thermal effects on stereolithography tools during injection moulding. *Rapid Prototyping Journal*, 10(3):176–180, 2004. ISSN 13552546. doi: 10.1108/13552540410538996.

P. Robles Martinez, A. Goyanes, A. W. Basit, and S. Gaisford. Influence of Geometry on the Drug Release Profiles of Stereolithographic (SLA) 3D-Printed Tablets. *AAPS PharmSciTech*, 19(8), 2018. doi: 10.1208/s12249-018-1075-3.

M. Sadia, A. Sośnicka, B. Arafat, A. Isreb, W. Ahmed, A. Kelarakis, and M. A. Alhnan. Adaptation of pharmaceutical excipients to FDM 3D printing for the fabrication of patient-tailored immediate release tablets. *International Journal of Pharmaceutics*, 513(1-2):659–668, 2016. ISSN 18733476. doi: 10.1016/j.ijpharm.2016.09.050.

G. V. Salmoria, C. H. Ahrens, M. Fredel, and A. T. N. Pires. Fractography and microstructural analysis of parts built by stereolithography. In *Congresso em Ciencia de Materiais do Mercosul*, 2002.

M. Sarkis, A. Bernardi, N. Shah, and M. M. Papathanasiou. Emerging challenges and opportunities in pharmaceutical manufacturing and distribution. *Processes*, 9(3): 1–16, 2021. ISSN 22279717. doi: 10.3390/pr9030457.

L. Satin and J. Bílik. Impact of Viscosity on Filling the Injection Mould Cavity. *Materials Science and Technology*, 24(38):113–121, 2016.

J. Segurola. Material Properties, 2019. URL `https://www.3dresyns.com/`.

B. Sha, S. Dimov, C. Griffiths, and M. S. Packianather. Investigation of micro-injection moulding: Factors affecting the replication quality. *Journal of Materials Processing Technology*, 183(2-3):284–296, 2007. ISSN 09240136. doi: 10.1016/j.jmatprotec.2006.10.019.

Y. K. Shen and W. Y. Wu. An analysis of the three-dimensional micro-injection molding. *International Communications in Heat and Mass Transfer*, 29(3):423–431, 2002. ISSN 07351933. doi: 10.1016/S0735-1933(02)00331-7.

Y. K. Shen, S. L. Yeh, and S. H. Chen. Three-dimensional non-Newtonian computations of micro-injection molding with the finite element method. *International Communications in Heat and Mass Transfer*, 29(5):643–652, 2002. ISSN 07351933. doi: 10.1016/S0735-1933(02)00383-4.

R. Sheshala, N. Khan, M. Chitneni, and Y. Darwis. Formulation and in vivo evaluation of ondansetron orally disintegrating tablets using different superdisintegrants. *Archives of Pharmacal Research*, 34(11):1945–1956, 2011. ISSN 02536269. doi: 10.1007/s12272-011-1115-y.

J. Siepmann, H. Kranz, N. A. Peppas, and R. Bodmeier. Calculation of the required size and shape of hydroxypropyl methylcellulose matrices to achieve desired drug release profiles. *International Journal of Pharmaceutics*, 201(2):151–164, 2000. ISSN 03785173. doi: 10.1016/S0378-5173(00)00390-2.

Maria Siiskonen, Johan Malmqvist, and Staffan Folestad. Integrated product and manufacturing system platforms supporting the design of personalized medicines. *Journal of Manufacturing Systems*, 56(March):281–295, 2020. ISSN 02786125. doi: 10.1016/j.jmsy.2020.06.016.

J. Skowyra, K. Pietrzak, and M. A. Alhnan. Fabrication of extended-release patient-tailored prednisolone tablets via fused deposition modelling (FDM) 3D printing. *European Journal of Pharmaceutical Sciences*, 68:11–17, 2015. ISSN 18790720. doi: 10.1016/j.ejps.2014.11.009.

S. Stegemann. The future of pharmaceutical manufacturing in the context of the scientific, social, technological and economic evolution. *European Journal of Pharmaceutical Sciences*, 90:8–13, 2016. ISSN 18790720. doi: 10.1016/j.ejps.2015.11.003.

R. Surace, V. Basile, V. Bellantone, F. Modica, and I. Fassi. Micro Injection Molding of Thin Cavities Using Stereolithography for Mold Fabrication. *Polymers*, 13(11), 2021.

The Association of the British Pharmaceutical Industry. Facts and figures, 2021. URL `abpi.org.uk`.

The International Pharmacopoeia. 5.2 Uniformity of mass for single-dose preparations. *World Health Organisation*, pages 1–2, 2019.

G. Tosello, A. Gava, H. N. Hansen, and G. Lucchetta. Study of process parameters effect on the filling phase of micro-injection moulding using weld lines as flow markers. *International Journal of Advanced Manufacturing Technology*, 47(1-4):81–97, 2010. ISSN 02683768. doi: 10.1007/s00170-009-2100-1.

M. Trivedi, J. Jee, S. Silva, C. Blomgren, V. M. Pontinha, D. L. Dixon, B. Van Tassel, M. J. Bortner, C. Williams, E. Gilmer, A. P. Haring, J. Halper, B. N. Johnson, Z. Kong, M. S. Halquist, P. F. Rocheleau, T. E. Long, and T. Roper. Additive manufacturing of pharmaceuticals for precision medicine applications - A review of the promises and perils in implementation. *Additive Manufacturing*, 23:319–328, May 2018. ISSN 2214-8604. doi: 10.1016/j.addma.2018.07.004.

O. Tuteski and A. Kočov. Mold design and production by using additive manufacturing (AM) - Present status and future perspectives. *International Scientific Journal "Industry 4.0*, 85(2):82–85, 2018.

United Nations. 17 Sustainable Development Goals, 2015. URL `https://sdgs.un.org/goals`.

S. Valette, M. Larochette, S. Benayoun, C. Mauclair, J. Vera, A. Brulez, E. Contraires, N. Trannoy-Orban, and M. Pignon. Factors influencing microinjection molding replication quality. *Journal of Micromechanics and Microengineering*, 28(1):015004, 2017. ISSN 0960-1317. doi: 10.1088/1361-6439/aa9a4e.

S. Van den Broeck. *Guidelines on the design and implementation of stereolithographic 3D printed moulds for low volume injection moulding.* Master of science thesis, Ghent University, 2017.

A. B. Varotsis. Introduction to FDM 3D Printing, 2019. URL `https://www.3dhubs.com/knowledge-base/introduction-fdm-3d-printing`.

G. Verstraete, P. Mertens, W. Grymonpré, P. J. Van Bockstal, T. De Beer, M. N. Boone, L. Van Hoorebeke, J. P. Remon, and C. Vervaet. A comparative study between melt granulation/compression and hot melt extrusion/injection molding for

the manufacturing of oral sustained release thermoplastic polyurethane matrices. *International Journal of Pharmaceutics*, 513(1-2):602–611, 2016a. ISSN 18733476. doi: 10.1016/j.ijpharm.2016.09.072.

G. Verstraete, J. Van Renterghem, P. J. Van Bockstal, S. Kasmi, B. G. De Geest, T. De Beer, J. P. Remon, and C. Vervaet. Hydrophilic thermoplastic polyurethanes for the manufacturing of highly dosed oral sustained release matrices via hot melt extrusion and injection molding. *International Journal of Pharmaceutics*, 506(1-2):214–221, 2016b. ISSN 18733476. doi: 10.1016/j.ijpharm.2016.04.057.

K. Vithani, A. Goyanes, V. Jannin, A. W. Basit, S. Gaisford, and B. J. Boyd. An Overview of 3D Printing Technologies for Soft Materials and Potential Opportunities for Lipid-based Drug Delivery Systems. *Pharmaceutical Research*, 36(1), 2019. ISSN 1573904X. doi: 10.1007/s11095-018-2531-1.

B. Wagner, T. Brinz, S. Otterbach, and J. Khinast. Rapid automated process development of a continous capsule-filling process. *International Journal of Pharmaceutics*, 546:154–165, 2018. doi: https://doi.org/10.1016/j.ijpharm.2018.05.009.

G. Walker and A. Albadarin. Cracking the Code for Continuous Processing and Personalised. Technical report, University of Limerick, 2018.

E. Walsh, E. Prasad, G. Halbert, J. H. ter Horst, and D. Markl. Manufacture of Solid Oral Dosage Forms with Micro-structure Features via Rapid Tooling Injection Moulding (In Preparation). *To be determined*, 2021a.

E. Walsh, J. H ter Horst, and D. Markl. Development of 3D Printed Rapid Tooling for Micro-Injection Moulding. *Chemical Engineering Science*, page 116498, 2021b. ISSN 0009-2509. doi: 10.1016/j.ces.2021.116498.

X. Wang, M. Jiang, Z. Zhou, J. Gou, and D. Hui. 3D printing of polymer matrix composites: A review and prospective. *Composites Part B: Engineering*, 110:442–458, 2017. ISSN 13598368. doi: 10.1016/j.compositesb.2016.11.034.

R. Wimberger-Friedl. Injection molding of sub-μm grating optical elements. *Journal of Injection Molding Technology*, 4(2):78–83, January 2000. ISSN 1553905X. doi: 10.1016/b978-188420791-4.50020-1.

H. Wu, R. C. Lyon, M. A. Khan, R. J. Voytilla, and J. K. Drennen. Integration of Near-Infrared Spectroscopy and Mechanistic Modeling for Predicting Film-Coating and Dissolution of Modified Release Tablets. *Industrial and Engineering Chemistry Research*, 54(22):6012–6023, 2015. ISSN 15205045. doi: 10.1021/ie504680m.

L. Zema, G. Loreti, A. Melocchi, A. Maroni, and A. Gazzaniga. Injection Molding and its application to drug delivery. *Journal of Controlled Release*, 159(3):324–331, 2012. ISSN 01683659. doi: 10.1016/j.jconrel.2012.01.001.

J. Zhang, X. Feng, H. Patil, R. V. Tiwari, and M. A. Repka. Coupling 3D printing with hot-melt extrusion to produce controlled-release tablets. *International Journal of Pharmaceutics*, 519(1-2):186–197, 2017. ISSN 18733476. doi: 10.1016/j.ijpharm.2016.12.049.

J. Zhang, A. Q. Vo, X. Feng, S. Bandari, and M. A. Repka. Pharmaceutical Additive Manufacturing: a Novel Tool for Complex and Personalized Drug Delivery Systems. *AAPS PharmSciTech*, 19(8):3388–3402, 2018. ISSN 15309932. doi: 10.1208/s12249-018-1097-x.

N. Zhang and M. D. Gilchrist. Characterization of thermo-rheological behavior of polymer melts during the micro injection moulding process. *Polymer Testing*, 31(6):748–758, 2012. ISSN 01429418. doi: 10.1016/j.polymertesting.2012.04.012.

J. Zhao, R. H. Mayes, G. Chen, H. Xie, and P. Sing Chan. Effects of Process Parameters on the Micro Molding Process. *Polymer Engineering and Science*, 43(9), 2003. doi: 10.1002/pen.10130.